Holocene Deglacial Geologic History of the Ravn River Valley, Northern Baffin Island, Nunavut.

Andrew C. Hilchey
Department of Earth Sciences
Dalhousie University

Advisor
John Gosse
Department of Earth Sciences
Dalhousie University

March 2004

DALHOUSIE
University

Department of Earth Sciences
Life Sciences Centre, Room 3006
Halifax, Nova Scotia
B3H 4J1
Tel: (902) 494-2358
Fax: (902) 494-6889
E-mail: earth.sciences@dal.ca
WWW: http://meguma.earthsciences.dal.ca

Date: April 30, 2004

Author: Andrew C. Hilchey
Title: Deglacial Geologic History of the Ravn River Valley, Northern Baffin Island, Nunavut

Degree: B. Sc.
Convocation: May 25, 2004

Abstract

The Ravn River Valley in Northern Baffin Island, Nunavut, contained a proglacial ice-damned lake during the Holocene recession of the Paleo-Barnes Ice Cap. The style of deglaciation was complicated. A series of sublacustrine cross-valley moraines and both lateral meltwater channels and delta foresets that dip up-valley, indicate that initial ice-marginal retreat was southward across the west-east trending valley. Raised deltas, kame-deltas, spillways and paleo-lake shorelines in the Ravn River Valley indicate that this ice-damned lake had two stillstand lake levels; ~268 m and ~300-320 m throughout its duration. Lake level elevations were controlled by a prominent spillway at the valley head and by contemporaneous glacial ice that was retreating downvalley to the south-southwest.

Eight raised deltas were sampled for cosmogenic exposure dating. A boulder was sampled on one of the surfaces and the remaining samples were topset sands. The results indicate that a tributary valley near the valley head spillway was deglaciated at 8.3 ± 0.3 ka (uncertainty is 1σ precision of measurement). Exposure ages from the other 7 samples, including the boulder, range from 37.1 ± 1.0 ka to 18.7 ± 0.7 ka. Based on the preservation of the glacial and glaciolacustrine features, the relative lack of soil development, and chronology of deglacial events elsewhere on Baffin Island, these 7 ages are considered to be too old by a factor of 3 to 6. The probable explanations for this disparity are (1) that the samples all contained a concentration of ^{10}Be that was inherited from exposure prior to final deposition in the deltas, or (2) that there was a systematic error in the chemistry during sample preparation. If the former case is correct, the inheritance would indicate that the long-term average steady state erosion rate of the upland plateaus (the source of the deltaic sands) ranged from 38 to 91 m/Myr. This erosion rate is reasonable for bedrock that is affected by zones of wet-based (erosive) and cold based (non-erosive) ice as has been well established for Baffin Island. Using the tributary delta exposure age, the minimum rate of spillway incision was 5.5 m/ka.

Table of Contents

List of Figures

List of Tables

6

Acknowledgments:

Chapter 1: Introduction

Evidence suggests that anthropogenic activity is partially responsible for the present Arctic warming trend and models predict that if this continues the Arctic Ocean may be ice-free during the final summers of the 21st Century (Johannessan et al., 2002). Within the next 50 years, the temperature in the central Arctic may increase by 3-4 °C (ICPP, 2002 in Johannessan et al., 2002). This will have catastrophic effects on everything from ecosystems through to thermohaline circulation, including anthropogenic infrastructure that is susceptible to thawing hazards.

The Barnes and the Penny Ice Caps are believed to be two of the last known remnants of the extensive Laurentide Ice Sheet that once covered a large portion of the North American continent during the Late-Wisconsinan glaciation. Global warming has caused limited to extensive retreat for the majority of glaciers on Baffin Island during the early to mid 20th Century. However beginning in 1963, summer weather had become harsher and by 1983 it seemed as though some of the tidewater glaciers were advancing (Andrews, 1989). The Barnes Ice Cap is located in north-central Baffin Island and rests upon the Baffin Uplands Region. It has a surface area of approximately 5900 km^2, an average length of 150 km and is between 22 and 62 km wide (Andrews and Barnett, 1979). The Barnes Ice Cap has a central ice thickness of 600-700 m and has a series of proglacial lakes pooled against its northern, western and eastern margins (Andrews and Barnett, 1979).

Many glaciological and morphological studies have been conducted on the Barnes Ice Cap and its proximal margins since the 1950's. The study area for this project is

8

located approximately 85 kilometers from the northwest margin of the Barnes in the

North Baffin region (Fig. 1).
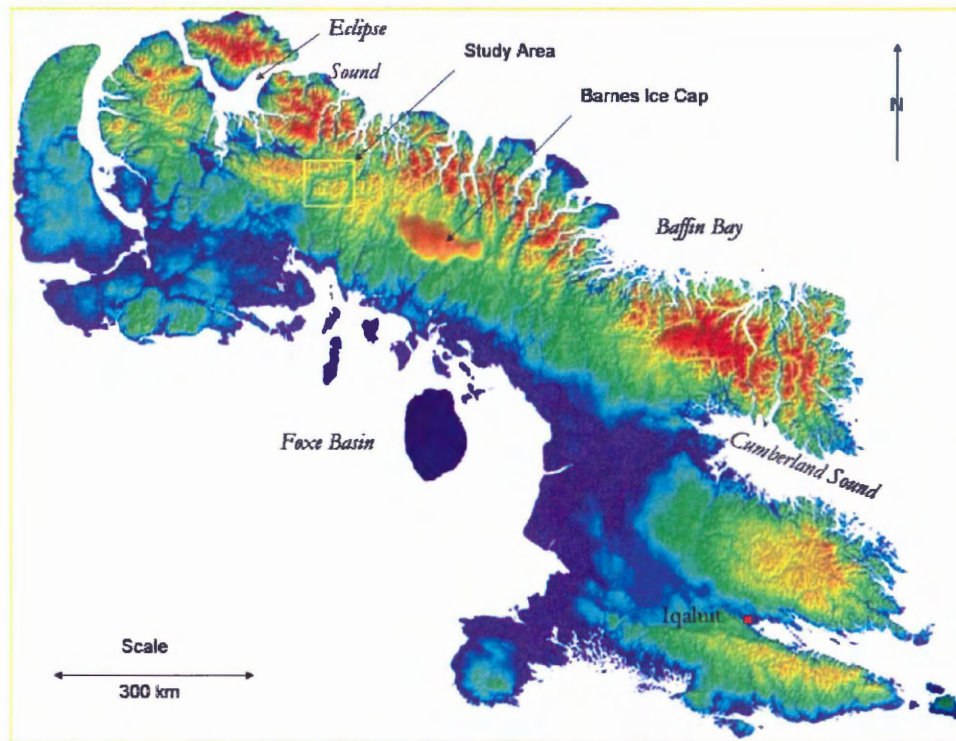
Figure 1: Digital elevation model for Baffin Island. Elevation decreases from red to blue. The study area is located in the Baffin Uplands, approximately 85 km to the northwest of the Barnes Ice Cap. The Ravn River Valley study area is indicated. Figure adapted from Institute of Arctic and Alpine Research (INSTAAR: http://instaar.colorado. edu/cosmolab/BI_CE_database /maps/map.html).

Two glacial geological studies have been carried out in the study area hitherto but only at a regional reconnaissance scale. The first surficial mapping study was engineered by Ives and Andrews (1963), who through detailed air photo interpretation and selective ground truthing, compiled the Cockburn Land Map Sheet portraying specific glacial features and landforms. Andrews (1963) attempted to determine the origin of cross-valley morainal features in the Ravn Valley by studying similar features in the Rimrock and Isortoq Valleys to the southeast. Subsequently, a reconnaissance glacial geological survey was conducted by Hodgson and Haselton (1974) who constructed a surficial

9

geological map for the northeastern Baffin and Bylot Island areas using aerial observation, selective ground truthing and air photo interpretation. They also produced a separate map showing features such as glacial lake shorelines, meltwater spillways and ice-marginal drainage channels.

Access by helicopter was provided to the Ravn River Valley during the summer of 2003 by helicopter through the Canada- Nunavut Geoscience Office's (C-NGO) North Baffin Project. The Ravn River Valley shows many typical landforms of a formerly glaciated valley that contained an ice-damned lake, namely ice-contact deltas, glaciolacustrine valley deltas, strandlines, kame terraces and glacial lake spillways. At least two prominent paleo-lake levels are evident from the lake morphosequences, providing an excellent opportunity to attempt to narrow down the chronology for each of them to interpret the history of the lake. The broad, well exposed nature of the Ravn River Valley make many of its delta surfaces ideal candidates for terrestrial cosmogenic nuclide (TCN) exposure dating. The Ravn is also thought to be a good test site for a new attempt to date unconsolidated deltaic sediments using cosmogenic exposure dating in the Arctic.

This study is comprised of two separate but integrated parts. The first includes the mapping of abundant surficial features in the Ravn River Valley and its tributaries and was conducted mostly from detailed air-photo interpretation, several foot traverses, aerial observations and background research. The second part involves a geochronological study attempting to constrain the timing of the lake levels. Because the lake levels are in part controlled by the position of the ice-margin, it is possible to

10

combine the surficial maps and lake chronology to elucidate the deglacial history of the

Ravn River Valley area.

Chapter 2: Quaternary Geological Background

2.1 Aims of Chapter

This chapter consists of a literature review describing the Late-Wisconsinan glacial maximum for Baffin Island followed by the description of the Holocene deglacial retreat from the North Baffin area, detailing the Ravn River Valley region. This section is intended to give the reader an understanding of the Late-Quaternary history of the area from the last glacial maximum to the present.

2.2 Physiography of the North Baffin Region

The physiography of the study area and surrounding region (Fig. 2) is typical for most of Baffin Island. It includes the Davis Highlands in the north, which is an elevated plateau, deeply incised by southwest-northeast trending fiords and valleys (Little et al., 2004). The Davis Highlands are bordered in the southwest by the Baffin Uplands, beginning at the heads of the longer fiords. The Baffin Uplands mainly comprises broad convex hills with elevations of up to 915 m in the northeast to elevations below 305 m in the southwest (Ives and Andrews, 1963). The regional watershed divide is slightly northeast of the central axis of the uplands region. Wide, deep (>300 m) river valleys run through this region, including the Ravn River Valley, which flows in a westerly direction onto the lower Lancaster Plateau (Fig. 2). The Lancaster Plateau is a graben whose northern border with the Baffin Uplands is marked by the Central Baffin Fault. The plateau is composed of lakes, bogs, flat rolling till plains, and subdued bedrock ridges (Little et al., 2004). In the south the Lancaster Plateau is bordered by the Foxe Plain in the south which dip gently towards the Foxe Basin.

12
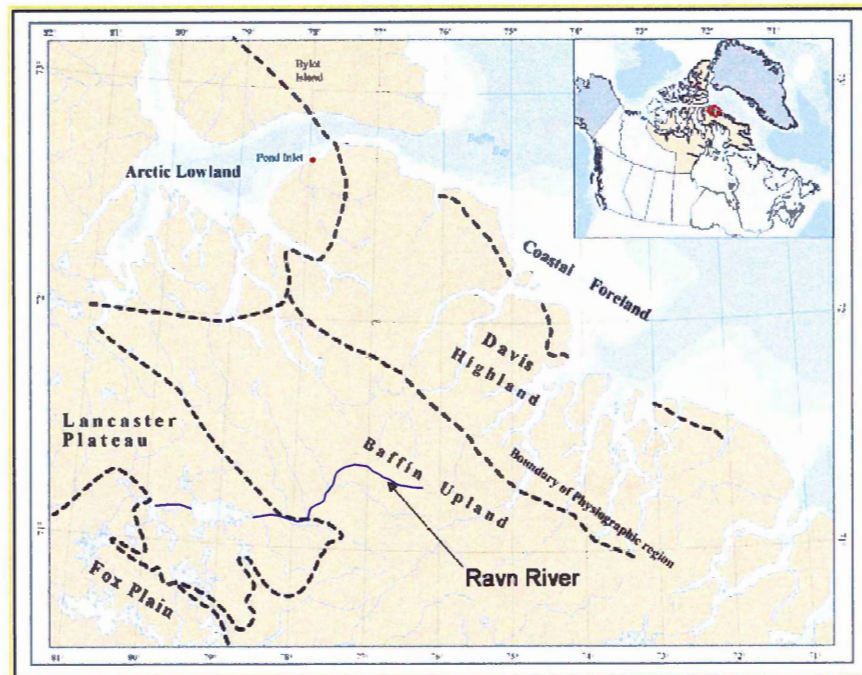
Figure 2: Physiography of Northern Baffin Island. The Baffin Uplands is separated from the Lancaster Plateau by the Central-Baffin Fault. The Ravn River dissects the Baffin Uplands and flows onto the flatter Lancaster Plateau along a fault escarpment and into Angajurjualuk Lake. Adapted from Little et al. (2004, In-Press)

2.3 Description of the last Glacial Maximum for North Baffin Island

Over the past half century there has been continuing controversy over the extent of the northeastern margin of the Laurentide Ice Sheet (LIS) on Baffin Island during the Late-Wisconsinan. Evidence suggests that active Laurentide ice on Baffin Island emanated from a dispersal centre in the middle of the Foxe Basin (Dyke et al., 2002; Ives and Andrews, 1963) and inundated the majority of southern Baffin Island (Miller et al., 2002). Flint (1943) proposed that the LIS submerged the fiord and interfiord areas, extending onto the continental shelf and far into Baffin Bay, possibly coalescing with the Greenland Ice Sheet. This later became known as the "Flint Paradigm" (Miller et al., 2002). After a couple of decades, workers such as Dyke and Prest (1987) suggested that

13

Laurentide ice only extended as far as the fiord heads. Glacial features found farther out in the fiords were thought to have been from an earlier Wisconsinan ice sheet. This became later known as the "Minimalist Paradigm" (Miller et al., 2002).

With refinements in cosmogenic nucide exposure dating, initiatives were taken to obtain ages on glacial features exposed along the fiords and sounds of eastern Baffin Island, mostly on the Cumberland Peninsula. Exposure ages obtained from the Duval Moraines in Pangnirtung Fiord by Marsella et al. (2000) established that they were Late-Wisconsinan, younger than was previously believed. Similarly, Miller et al. (2002) confirmed this in the Sunneshine Fiord of the Cape Dyer Peninsula and work by Bierman et al. (1999), Kaplan et al. (2001) and Briner et al. (2003) elsewhere in Eastern Baffin is in agreement with these results. Further investigation of seismic statigraphy (Maclean et al., 1986 and Praeg et al., 1986 in Miller et al., 2002) in fiords and sounds as well as the study of cores in the inter-fiord/sound areas (Wolfe and King, 1999 and Miller et al., 1999 in Miller et al., 2002), and Cumberland Sound (Jennings, 1993, Jennings et al., 1996 in Miller et al., 2002), in conjunction with cosmogenic exposure dating, allowed a new theory to be developed. The "Goldilocks Paradigm", advanced by Miller et al. (2002) summarizes that active, low gradient, fast moving outlet glaciers were sliding on deformable sediments extending along the lengths of the fiords (Kaplan et al., 2001) while the interfiord and highland areas were covered by a cold-based ice frozen to its bed. Throughout this thesis, "cold-based" is used to refer to ice conditions that either (i) are lacking basal water due to a highly efficient subglacial drainage, or (ii) are truly below the ice pressure melting temperature at the base and therefore inhibit sliding at the ice-substrate interface. Meanwhile, the outlet glaciers were connected to the LIS *via* the

heads of the fiords. According to Miller et al. (2002), outlet glaciers occupying fiords

north of the Hall Peninsula either terminated at the coastline or on the continental shelf.

Andrews (1989) indicated that there was a transition from warm to cold-based ice at an

altitude of approximately 400 m.

Briner et al. (2003) confirmed the presence of a large outlet ice stream in Clyde

Inlet using cosmogenic exposure dating. However, the results varied significantly from

those of ice-streams described farther to the southeast in that they were thicker and

terminated out on the continental shelf.

Navy Board Inlet, separating North Baffin from Bylot Island, was proposed by to

have been filled by Laurentide ice during its maximal Late-Wisconsinan extent (Dyke et

al. (2000) and Dyke and Hooper (2001)). The northeastern margin of the LIS is currently

thought to have reached its maximum extent just beyond the mouths of the fiords by

approximately 23-24 ^{14}C ka BP (Dyke et al., 2002) (Inset box in Fig. 3).
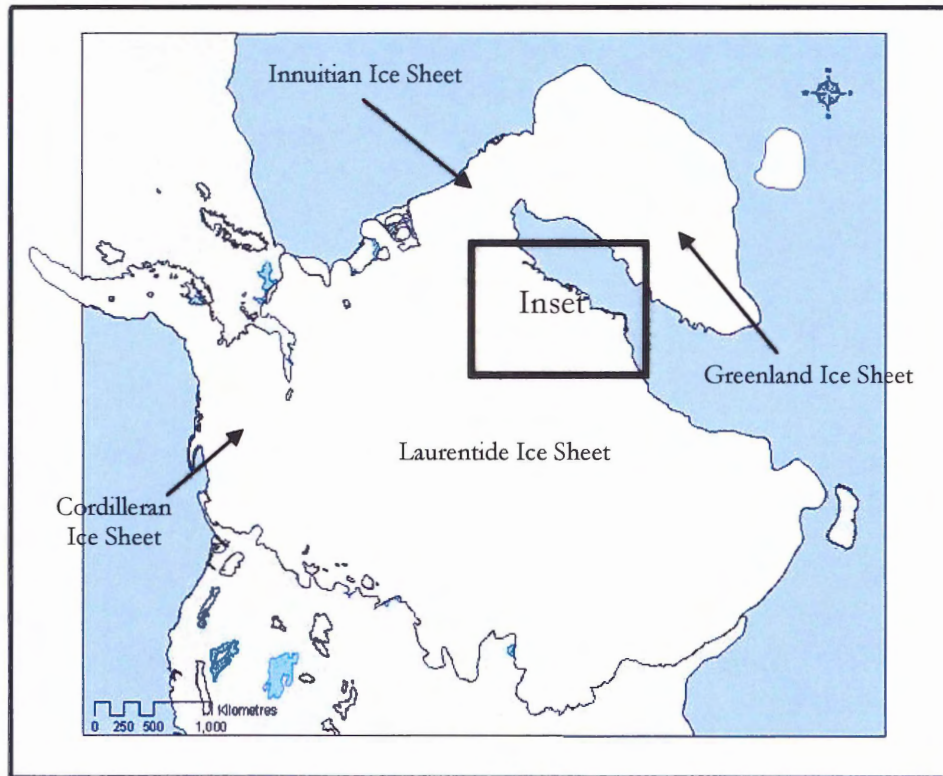
Figure 3: Maximum extent of the Laurentide Ice Sheet at the time of the Last Glacial Maximum (21.4 cal ka BP) according to Dyke et al., 2003. North of Baffin Island, the Laurentide Ice Sheet is shown to be coalescent with the Innuitian Ice Sheet which is coalescent with the Greenland Ice Sheet further to the northeast. Baffin Island comprises the northeast margin of the Ice Sheet. Ice streams are extending to the mouths of the fiords and cold based ice is present on the fiord heads and higher terrain. The northeastern margin of the LIS overlying Baffin Island is shown in the inset box.

2.4 Holocene Deglacial History of Baffin Island

2.4.1 Deglacial History of Baffin Island

Significant ice recession along the northeastern margin of the LIS is not evident until the end of the Younger Dryas (Dyke et al., 2003) (Fig. 4). Dyke (1974) described the deglacial history for the Baffin Island region by constructing an isochrone map based on finite radiocarbon dates, lichen diameter isophyses and glacial morphological feature interpolation.

16
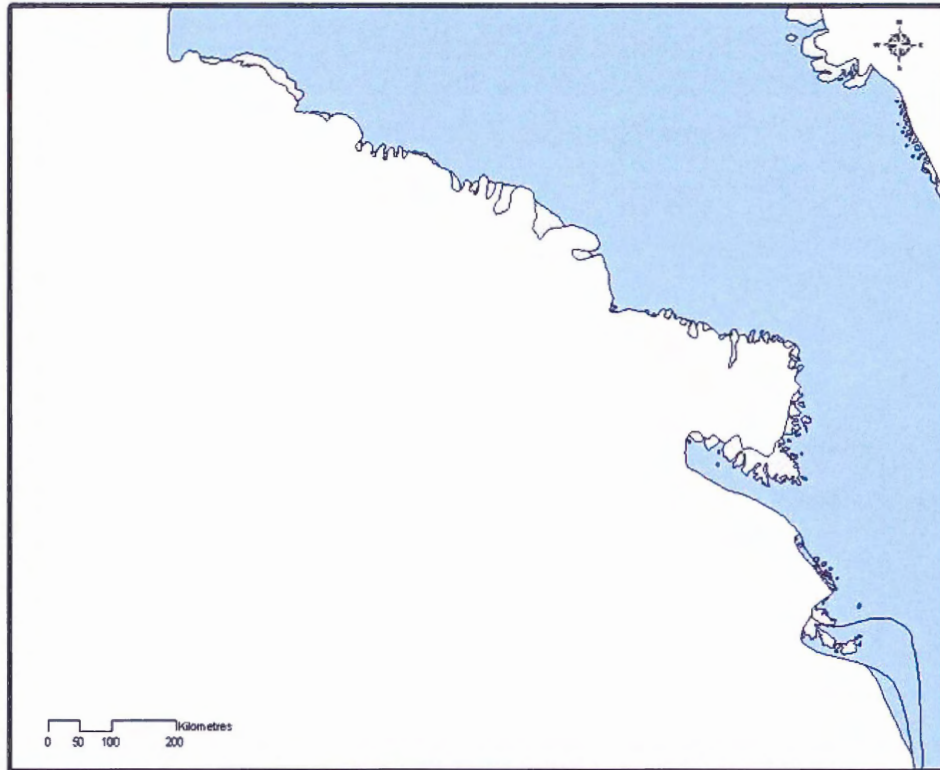
Figure 4: The Northeastern Laurentide Margin at 11.35-11.55 ka according to Dyke et al., 2003. Little ice recession had occurred along the northeastern margin of the Laurentide Ice Sheet until this time although significant retreat had already occurred elsewhere in North America.

Ice recession from the Hudson Strait began approximately 8.8 ^{14}C ka BP (Blake, 1966 in Dyke, 1974) (Fig. 5), and along with Hudson Bay, it was nearly completely deglaciated by 7.5 ^{14}C ka BP. A marine transgression had penetrated the majority of the Foxe Basin by 7 to 6.8 ^{14}C ka BP and it was simultaneously deglaciated. The strait separating the Melville Peninsula and Baffin Island became completely ice-free by 7 ^{14}C ka BP turning the now detached ice caps on Baffin Island into distinct entities from the shrinking LIS on the mainland. Dyke (1974) proposed that during the early stages of the ocean transgression into the Foxe Basin (~7 ^{14}C ka BP) the sea transgressed from the Foxe Basin up to the head of Cumberland Sound, creating a large calving bay where the

newly created Northern Baffin Island Ice Cap became separated from the Southern Baffin

Island Ice Cap (Fig. 6). This division was nearly complete by 4.55 ± 0.22 ^{14}C ka BP

(Dyke, 1974). On eastern Baffin Island, ice retreat had begun by 8 to 8.5 ^{14}C ka BP and

the Penny Ice Cap likely separated from the Northern Baffin Ice Cap 1000 yrs later.

After its inception, the North Baffin Island Ice Cap receded to the current position of the

Barnes Ice Cap.
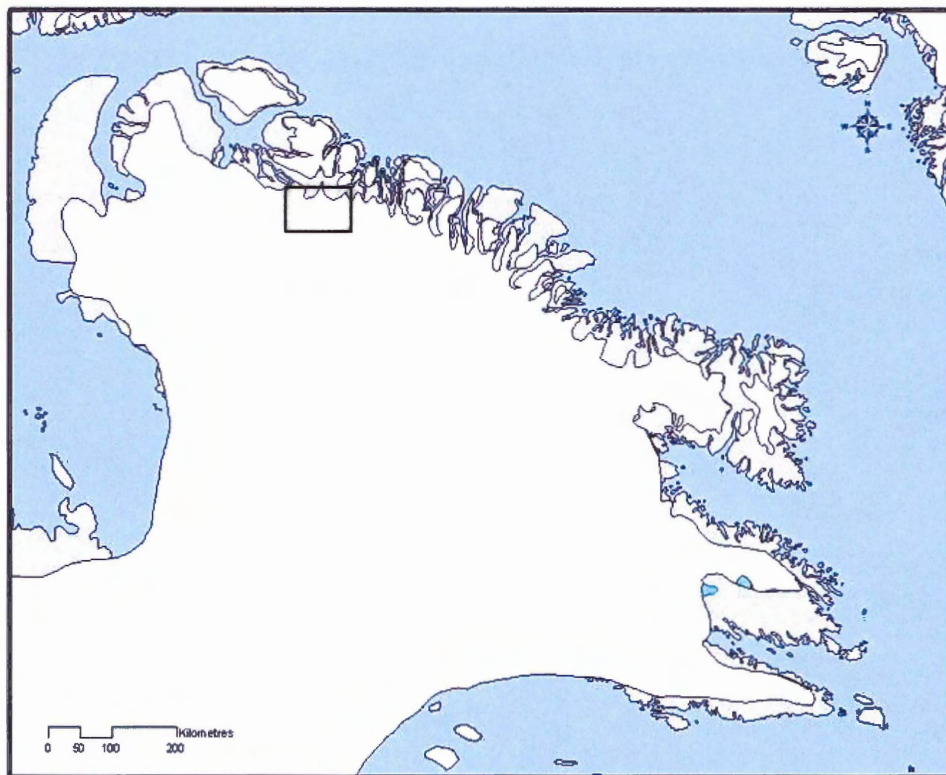
Figure 5: The northeastern margin of the Laurentide Ice Sheet approximately 8.98 cal ka BP according to Dyke et al., 2003. The approximate position of the Ravn River Valley is outlined in black. The ice margin had receded to the heads of the northeastern fiords and the Hudson Strait was almost completely ice-free. Meanwhile, ice joining Baffin Ice to the Mainland Ice in the Foxe Basin, was actively calving. Study area is shown in the box.
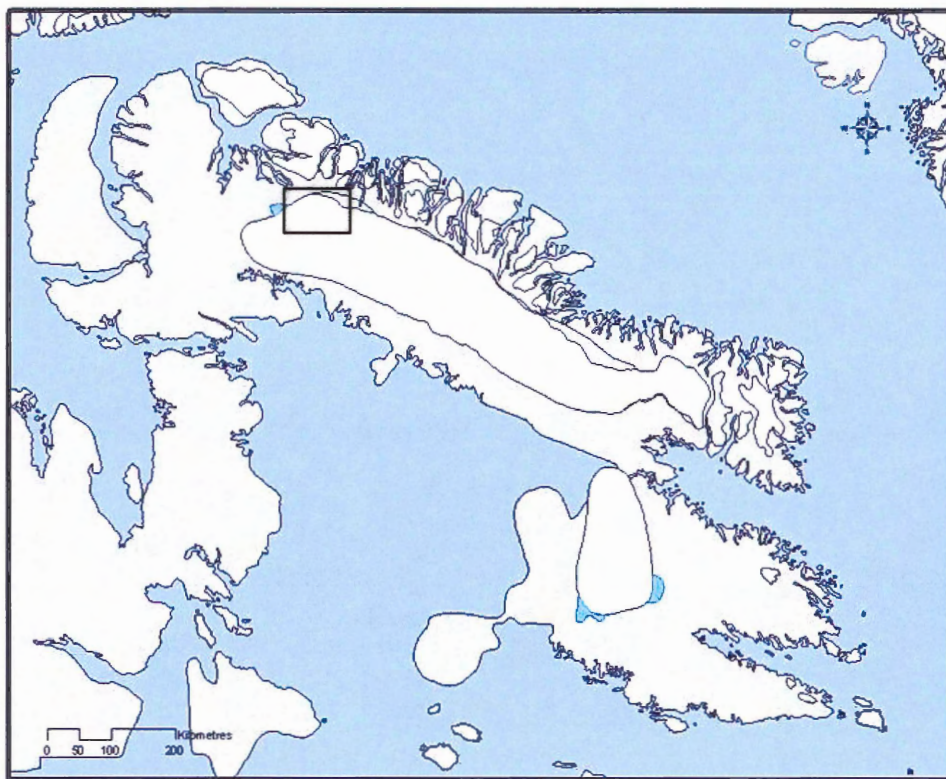
Figure 6: The positions of the Northern and Southern Baffin Island Ice Caps approximately 5.75 ka cal BP according to Dyke et al., 2003. The ice caps on Baffin Island were now distinct entities from the now nearly non-existent Laurentide Ice Sheet on the mainland. The Foxe Basin had transgressed to the head of Cumberland Sound creating a calving bay and caused the two ice caps to separate. Ice had nearly retreated to a position within the Ravn River Valley, shown in black. The Northern Baffin Ice Cap (Paleo-Barnes) then receded to the present-day location of the Barnes Ice Cap.

2.4.2 Deglacial History of Northern Baffin Island

A surficial geological reconnaissance survey carried out by Ives and Andrews (1963) attempted to elucidate the deglacial history of north-central Baffin Island. They recognized 6 phases of deglaciation. Lateral moraines on the fiords walls of northeastern Baffin were interpreted to have been deposited during the earliest glacial phase of the

19

Late-Wisconsinan which they called the Clyde phase. Clyde ice was believed to have inundated the entire inland area of Baffin Island and to have emanated from a dispersal center over the Foxe Basin. The northeastern fiords acted as conduits for outlet glaciers of the main ice sheet and extended out into Baffin Bay.

A prominent series of moraines, called the Cockburn Moraines, marked the next glacial stage named, the "Cockburn I phase". This system of moraines is continuous for over 400 miles along the heads of the Baffin Bay fiords. Ives and Andrews (1963) indicated that the Cockburn moraines represent an important stillstand or re-advance of inland ice approximately 10 ^{14}C ka B.P. when outlet glaciers were calving into the heads of the fiords. During this period, the main ice divide was estimated to have shifted northward from a position over the Foxe Basin during the Late-Wisconsinan, to one above the southwestern coast of Baffin Island. The Cockburn I phase was then followed by the "Cockburn II phase" (~7 ^{14}C ka B.P. - Ives and Andrews, 1963), which marks the time when the inland ice margin was resting at the position of the innermost set of end-moraines.

The next proposed phase of deglaciation was the "Atlantic phase", occurring approximately 5 ^{14}C ka when there was a major period of inland ice thinning and when the main ice margin had receded south over the regional watershed of the eastern mountain rim. This period, the Paleo-Barnes phase, was interpreted to represent an important change in the mode of deglaciation, as the inland ice developed similar glaciological properties to the present-day Barnes Ice Cap. During glacial recession, ice-dammed lakes developed within the valleys of the major westerly flowing rivers and their northern tributaries south of the watershed, marking the time when deglacierization

consisted of glaciofluvial and glaciolacustrine activity. Once over the watershed divide, the Paleo-Barnes receded to the southeast in a relatively consistent manner.

The next period was termed the "Sub-boreal" phase and was thought to have occurred roughly 3 ^{14}C ka BP. Large ice masses were hypothesized to have been detached from the retreating ice-margin that stagnated *in situ,* within the confines of the Ravn and Rowley River Valleys. The Paleo-Barnes Ice Cap then retreated to near its present position and underwent several readvances in neoglacial times.

According to Andrews (1989), between 5 and 8 ^{14}C ka BP, the recession of ice from the fiords of eastern Baffin Island was slow (Andrews (1982b) in Andrews, 1989). During this time period, temperatures were as warm as present and ablation rates should have exceeded the accumulation rates (Andrews (1982b) in Andrews 1989). It was proposed that increased snowfall from seasonal open ice may have compensated for this by increasing the rates of precipitation. During this period of deglaciation, there were several glacial readvances and by 5 ^{14}C ka BP, the only remaining remnants of the Laurentide Ice Sheet were lingering on Baffin Island.

Little et al. (2004-In press) proposed that once the LIS margin had receded to the southeast, away from the Cockburn moraine system, it thinned and detached itself from a large body of ice that remained as the Baffin ice sheet (equivalent to North Baffin Ice Cap, Dyke 1974). When the ice divide was displaced farther to the southeast, the ice sheet developed glaciological properties similar to those of the present day Barnes Ice Cap. Preliminary evidence showed that the Paleo-Barnes remained warm-based until it receded farther east where portions of it may have changed basal thermal regimes and become cold-based. In the retreating wake of the northern Barnes ice margin, a series of

21

cold-based local ice caps were left remaining in the Davis Highlands and Baffin Uplands. A prolonged presence of the Paleo-Barnes Ice Cap in the Lancaster Plateau may have prevented these local upland ice caps from flowing southwest onto the Lancaster Plain. Little et al. (2004-In press) suggested that meanwhile, a series of proglacial lakes formed in the uplands region. Throughout the next phase of deglaciation, ice on the Baffin Uplands was predominantly cold based while on the Lancaster Plateau it may have been warm and cold based (alternating spatially and temporally). The neoglacial period that followed is characterised by alpine-like glaciation occurring in some of the large upland valleys, in places damming rivers to form large lakes.

2.4.3 Deglacial History of the Ravn River Valley Region

The Ravn River Valley was estimated to have been deglaciated between 5.5 and 4.5 ^{14}C ka BP (Dyke, 1974). Ives and Andrews (1963) observed that kame terraces, formed in the northbank tributaries of the valley, converged at cols connecting adjacent valleys. These landforms were interpreted to represent meltwater overflow deposits that were emplaced when the main inland ice margin had thinned and receded south or southwest over the regional watershed divide. Tongues of ice resting in the northern tributary valleys then stagnated, creating pooled lakes, raised deltas, delta kame terraces and glacial lake shorelines. Meltwater then drained from the heads of these valleys into Eclipse Sound and Baffin Bay.

Relatively few kame terraces were noted in the south bank tributary valleys but there were an abundance of glacial drainage channels that ran down north facing slopes, dissecting valley terraces. These features were interpreted to have formed when the

Paleo-Barnes Ice Cap margin receded in a south-southwesterly direction and retreated slowly up the south bank slopes and tributary valleys. The northward sloping surface of the ice cap had a low surface gradient and when it receded up the steeply dipping northerly facing valley slopes, its movement was restricted and it became detached from the main ice margin in the valley bottom and stagnated in place. Evidence indicating stagnating blocks of ice in the main valley bottom included paired kame terraces on both sides of the main valley, raised deltas and pitted outwash deposits. During this phase of deglaciation, a glacial lake was generated in the Ravn River Valley, whose shoreline was primarily preserved in the southern facing valley walls and northern tributaries. Glacial drainage channels that descended down the southern valley walls, incising main valley kame terraces originated from the tops of the broad surrounding rounded hills and were interpreted to indicate that separate ice masses on the hilltops may have become detached from the Paleo-Barnes and stagnated as well.

Hodgson and Haselton (1974) interpreted sand and gravel terrace deposits in the Ravn Valley bottom to represent time-transgressive lacustrine ice-contact deltas that were deposited in front of westerly retreating ice that were later reworked by waves and altered by the further deposition of glaciolacustrine valley deltas. A major glacial lake spillway (Quernbiter spillway) was identified in the most northeasterly portion of the valley and once drained the lake into the Quernbiter River. Hodgson and Haselton (1974) suggested that the entire Baffin Uplands segment of the Ravn Valley was ice-free and contained an ice-dammed lake that was approximately 60 km long and 100 m deep at its western end. The lake was subsequently drained after the ice retreated from the Lancaster Plateau and the westernmost uplands portion of the Ravn Valley.

23

2.5 Morainal Features on Ravn River Valley Bottom

Andrews (1963) conducted a detailed air photo survey on cross-valley morainal features found on Baffin Island that were previously identified as sublacustrine moraines (Goldthwait, 1951 in Andrews, 1963). Several of these landforms were identified in the Ravn River Valley and some of its north bank tributaries. The majority of the air-photo work and field observations were carried out on cross-valley moraines found within the Isortoq and Rimrock River Valleys to the southeast where the moraine-like landforms were best developed. The lack of cross-valley moraines found within the Ravn and Rowley River Valleys was interpreted by Andrews (1963) to represent a difference in the deglacial conditions. The moraines were found in the upper valleys of upland westerly flowing rivers and were pinned between both the watershed divide in the northeast and a paleo-ice divide to the southwest. They had asymmetrical profiles, linear to bifurcating-arcuate forms, were comprised of basal till with a fabric and had a series of stratified central kames scattered upon their surfaces. They were all associated with paleo-ice dammed lakes and most were formed in a sublacustrine environment. The most likely theory proposed by Andrews (1963) was that they were formed from basal till being squeezed into frontal crevasses in a sublacustrine setting. Another plausible theory was that they were push moraines, however, their branching patterns made this unlikely.

Andrews and Smithson (1966) studied till fabrics in cross-valley moraines of the Isortoq River Valley. None of the moraines extended above the highest paleo-lake shoreline elevation so they were either formed in a sublacustrine or subglacial environment. The till fabric patterns did not seem to resemble anything like a shear or push moraine pattern. Andrews and Smithson concluded that the moraines had not

formed through the infilling of frontal crevasses because some of the moraines were highly oblique to the cross-valley orientation and that the crevasses were probably not present as sub-glacial cracks. For the linear-shaped moraines and associated central kames, it was hypothesized that they were formed during the ablation season. When the ice was undergoing seasonal large-scale melting events, some of the englacial meltwater was discharged subglacially, supported by the presence of central kames, liquefying the underlying till, causing the ice cliff to sink into the till pushing it up. Several moraines may then have been partially overridden by the ice cliff during colder periods, imparting a newer fabric and introducing a complicated pattern. S-shaped moraines may have been formed from semi-liquid till being injected into sub-glacial meltwater channels (Andrews and Smithson, 1966).

Barnett and Holdsworth (1974) studied sublacustrine moraines in Generator Lake impounded against the southeast corner of the Barnes Ice Cap. A series of paleo-lake shorelines extended back to 4.5 ^{14}C ka B.P. based on radiocarbon dates in organic material within raised delta foresets. A couple of prominent shorelines were observed, indicating stability, while shorter-lived shorelines represented times of only temporary stability. If a stream's input to the lake was assumed to be relatively constant, then the volume of sediment within each delta would have been representative of the duration for a particular glacial lake shoreline. Sublacustrine moraines were thought to have been formed through the development of an ice ramp above the base of the calving frontal ice cliff. An ice ramp would leave a gap between the base of the ice and the bottom of the lake that was eventually filled up with till during ice-recession, as long as lake level stability allowed the ramp to persist. The size of each moraine was interpreted to be

dependant on the ice flow rates and the volume of debris entrained within the glacier (Barnett and Holdsworth, 1974). The central kames were probably moulin deposits from the frontal crevasse system. The morainal patterns were formed though the movement of the glacial grounding line and were rotated by detached frontal ice blocks. The stability of the basal ice ramps was compromised when the lake depth fell below 30 m due to the higher ice cliffs above water level. Smaller sublacustrine moraines could have formed in shallower depths through basal ice melting cutting gaps in the bottom of the ice cliff. A valley with a lack of sublacustrine moraines such as the Ravn suggests that the retreat rates may have been more rapid (Barnett and Holdsworth, 1974).

2.6 Contribution of Project

The primary goal of this project is for the detailed mapping of limited surficial features within the Ravn River Valley and its tributaries to interpret its Holocene deglacial history. The results and interpretations will be compiled by the author in a digital form appropriate to be integrated into ongoing studies by the Canada-Nunavut Geoscience Office and other researchers.

A secondary goal of this project is to test cosmogenic nuclide exposure dating on unconsolidated deltaic sediments in the Arctic. This may fill a gap in the deglacial chronological record of the Holocene retreat of the Paleo-Barnes Ice Cap from northeast Baffin Island. No ages for ice-recession are available for the northeastern Baffin Uplands area. Extensive dating has been done along the coast where there is abundant datable marine radiocarbon material, and near the present margins of the Barnes Ice Cap, but interpolation is required for the interior areas (Dyke, 1974). However, the exposure

dating aspect of this project will be deemphasized since the results at present, are not

clearly understood.

Chapter 3: Methods

3.1 Methods Overview

Several methods were used to interpret the deglacial history of the Ravn River Valley. Detailed air-photo interpretation was carried out within and adjacent to the valley to locate and correlate former lake level indicators. The field component of the study was comprised of mapping, the measurement of paleo-lake level elevations and the sampling of eight deltas for cosmogenic nuclide exposure dating. The cosmogenic nuclide exposure ages were to provide timing for lake levels and a chronology for deglaciation. However, six of the eight samples had large cosmogenic exposure ages (discussed Chapter 4 and 5) and were interpreted to indicate upland erosion rates instead of in situ exposure ages.

3.1.1 Air Photo Interpretation

The black and white aerial photographs studied were taken in 1961 by the RCAF. Their scale was approximately 1: 60000 and the photos were not significantly obscured by snow or cloud cover. A pair of mirror stereo-glasses were used to view the images in detail. Only air photos of the Ravn River Valley and its tributaries were interpreted. Canada-Nunavut Geoscience Office-supported fieldwork conducted by the author in the summer of 2003 elsewhere on northern Baffin Island afforded the opportunity to gain invaluable experience in ground truthing, airphoto interpretations depicting a variety of glacial and periglacial landscapes. Paleo-lake level indicators such as deltas, strandlines and spillways were identified and distinguished from alluvial fans, colluvium and bedrock structure that may resemble paleoshorelines. These features were correlated to

28

determine the areal extent of each paleo-lake level. Non-glaciolacustrine morphometric features found within the immediate vicinity of the Ravn River Valley such as moraines kettles, col gullies, kame terraces, and meltwater channels were also mapped.

3.1.2 Field Work

Field logistics and resources for this portion of the project were provided by the Canada-Nunavut Geoscience Office (C-NGO). The Ravn Valley work was conducted for a period of 5 days during the summer of 2003 as a portion of the C-NGO's ongoing North Baffin Project whose primary 2003 mandate was surficial mapping and the interpretation of the glacial history of the North Baffin Region.

All transportation to and around the study area was accomplished on foot traverses or by a Bell 206 Long Ranger helicopter. A helicopter was needed due to the large extent of the field area (~ 638 km^2), high relief, absence of roads, and short time available for the research. A total of 56 sites were visited along the entire extent of the Ravn River Valley to obtain elevations from landforms associated with former lake levels. All measurements and observations were done from inside the helicopter to minimize the time spent at each site and eliminating the need for helicopter shutdown. The information recorded at each location included the GPS coordinates (UTM and elevation), altimetry and details identifying the landform feature and associated features. Each site was then ranked on its potential suitability as a candidate for cosmogenic nuclide exposure dating.

Of the 56 places surveyed, 8 delta sites were later sampled for cosmogenic exposure dating. The helicopter was shut down at each stop, permitting detailed field

notes to be taken in both field notebooks and palm pilots provided by the C-NGO. Observations were noted from sample pits dug at each site as well as the description of any associated and/or surrounding features such as lateral meltwater channels and bedrock washed surfaces.

The main constraint on fieldwork was time. Only a finite amount of helicopter and man hours could be allocated to this particular study. Not every paleo-lake level indicator site could be visited and those that were, required rapid field measurements, observations recording and sampling. This meant that other interesting deglacial features unrelated to paleo-lake levels could not be visited and were mapped inflight or from air photo interpretation.

3.1.3 Elevation Measurements

In order to determine the elevation at each site, two hand-held altimeters, a helicopter altimeter and a wrist computer were used. The altimeters were tuned each morning at base camp. Corrections to the altimetry for changes in barometric pressure throughout the day were conducted by (i) calibration, and (ii) "closing the loop" methods. The altitude was first recorded at the calibration site and then a number of different locations were visited. The helicopter would then revisit the calibration site (to close the loop) and record the elevation. Delta #17 and delta #48 were used as calibration sites during the day. The difference in elevation at the calibration site was divided by the time period between calibrations to determine the rate of barometric changes. At most sites the coefficients of variation among the different altimeters were within 3% which is sufficient for our purposes. A more precise survey would be necessary, for example, to

use the paleo-lake record for isostasy measurements. Unfortunately, a more precise

altimeter or GPS was unavailable at the time of the Ravn River Valley fieldwork.

3.2 Cosmogenic Exposure Dating of Deltas

3.2.1 Principles and Methods

The cosmogenic nuclide dating method was first applied to date surface exposure

durations in the early 1980's with the development of the accelerator mass spectrometer

(AMS) that allowed isotopic ratios as low as 10^{-15} to be measured (Gosse and Phillips,

2001). Since then it has been used to solve a broad range of geological and

geochronological problems primarily using boulders and bedrock surfaces as media for

sampling. In the early 1990's reliable ages of several allochthonous sedimentary

landforms were determined using the TCN dating method (eg. Gosse et al., 1995). The

TCN exposure dating method has been used to determine timing of deglaciation, glacial

advance, surface exposure durations, erosion and incision rates to name a few. This

study is the first known attempt to directly date deltas of unknown age using deltaic

sediments.

For a brief background summary description of cosmogenic nuclide exposure

dating applications and theory the reader is referred to Gosse and Phillips (2001). A

review of the principles of the method is given in Appendix 2. The following discussion

involves aspects of the method that are specific to the Baffin Island study area or to the

particular procedure used in this study.

The amount of TCN generated on Northern Baffin Island will be higher than areas

to the south. Due to the primarily dipole geometry of the geomagnetic field, the flux of

primary cosmic rays entering the atmosphere increases with geomagnetic latitude, creating higher TCN production rates (Gosse and Phillips, 2001). As in the case of radiocarbon dating, variations in the paleointensity of the earth's magnetic field may alter TCN production rates. Fortunately, at the latitude that the Ravn Valley samples were collected (71°) this effect is negligible because the rigidity of particles permitted to penetrate the field at this latitude is always lower than the average particle energy needed to produce TCN from spallogenic interactions (the vertical cutoff rigidity for the current field strength is approximately 58°). This is a significant advantage over lower latitude sites when attempting to measure short exposure durations (Holocene).

In sedimentary deltaic deposits, as with bedrock, the concentration of TCN typically decreases with depth. The concentration of a nuclide produced through spallation reactions and thermal neutron capture exponentially decreases with depth. The proportion of nuclides produced from muonic interactions increases with depth because muons penetrate deeper than neutrons (Gosse and Phillips, 2001). The concentration of a spallogenic TCN may remain relatively constant with depth if the landform has been continuously aggrading. If the sediment for a given catchment has had inheritance from previous exposures either before or during transport then nuclide concentrations will exponentially decrease with depth to its inheritance value instead of 0. Assuming that the aggradation of a given stratified sedimentary deposit occurred over a negligible amount of time, the layers below the surface being dated (beyond the attenuation length of fast neutrons) will contain the average amount of inheritance for that catchment basin. In order to calculate the time that the sand was exposed since deltaic deposition, the amount of inherited TCN is subtracted from the total (measured) concentration. Another way to

calculate inheritance, if there is a possibility an underlying surface may have been exposed for a long period of time, is to construct a sample depth profile. This can be done by measuring the concentrations for a given TCN over a range of depths in a vertical sequence (Anderson et al., 1996). Bulk density of the sample and covering sediment and soil is an important factor when calculating production for a given layer of sediment. If significant erosion has occurred, then the ^{10}Be concentration will decrease at all depths. One of the main problems in sampling sedimentary autochthonous and allochthonous landforms is that they may have been subject to vertical disturbances through cryturbation and/or bioturbation, mixing the grains of different horizons and concentrations of cosmogenic ^{10}Be (Gosse and Phillips, 2001).

The amount of inheritance for a particular sample depends upon several factors that control catchment erosion rate, including climate (annual rainfall and distribution of rainfall, temperature and freeze thaw cycles), rock resistance to erosion, and fracture density, (Gosse and Phillips, 2001). Zentmire et al. (1999) examined glacigenic sediments derived from the Alaskan Matanuska Glacier and found that they had zero inheritance. This is thought to have been due to the high degree of glacial erosion to a depth below the attenuation of cosmic ray flux. The ice cover also shields the sediment from further in situ production until deglaciation. These factors are important in this study because the deltaic sediments sampled were deposited in an ice-proximal environment and may have been eroded from an uplands that had spatially and temporally variable rates of erosion. Glacigenic sediment is also less likely to have multiple TCN ages due to its having been deeply eroded and rapidly deposited. The deltas in the Ravn Valley are believed to have been deposited over a short period of time.

3.3 Field Methods for Cosmogenic Nuclide Exposure Dating of Deltas

Eight raised deltas within the Ravn River Valley were sampled for TCN exposure dating. The goal of the sampling program was to excavate pits into the delta surfaces and sample only undisturbed horizontally stratified topset beds. If inheritance is negligible or known and accounted for, the exposure age of the topset layers will represent the time that the delta surface was deposited and hence, the age of the paleo-lake level at that elevation. Samples were taken only from delta surfaces that were flat to insure that no alluvial fans were sampled and to ensure that the topsets were dating a lake level age and not subsequent fluvial deposition. Alluvial fans pose a problem for cosmogenic exposure dating because it is difficult to associate sediment on the fan with a particular paleo-lake level. Fan sloped surfaces also make exposure age calculations more complicated. The 8 deltas sampled had minimal or no eolian cover on their surfaces sufficiently far from a valley wall to preclude the influence of colluvium and on surfaces that showed little or no evidence of erosion (although slight erosion of the deltas would have a negligible influence on the calculated age). Abundant lichen cover on the sampled delta surfaces was indicative of long term stability. If the sample location had less than $10°$ shielding above the horizon from the surrounding valley walls then topographic shielding was considered negligible and disregarded. This saved time at each cosmogenic sample site.

The sampled sediments were predominantly pebbly-granule sands but the majority of the deltas within the Ravn River Valley were composed of cobble gravel, and deemed difficult to sample. Also, if a larger grain size is sampled, then fewer clasts will be obtained and the chances for one of those clasts to add considerable amounts of

34

unrepresentative inheritance to the overall sample, is greater. A mixed zone was encountered below the delta surface that was typically 20-25 cm thick. These sediments were both bioturbated and cryoturbated, destroying all evidence of topset bedding. The vertical mixing of these sediments would have homogenized the sand grains (and hence, the ^{10}Be) within that zone, giving inaccurate ages if sampled. Samples were therefore taken from underneath this zone in identifiably undisturbed topset layers. Sample depths averaged 30 cm. Approximately 2 kg of amalgamated sand was collected with a trowel and paint scraper from a horizon that ranged in thickness from between 3 and 5 cm. Such large samples were collected because the deltas were expected to have young ages (<5 ka) and because the samples were not at the surface (i.e. lower ^{10}Be concentration at depth). It was ensured that no sand slumped down from the overlying layers to contaminate the sample. Each sample was then labeled and packaged into 2 plastic ziplock bags. In all instances, samples were from beds exhibiting primary sedimentary structures (cross bedding, laminations, imbrications) indicating the sediment was preserved intact and had not been subsequently disturbed.

Intermittent snow cover has certainly reduced the cosmic flux to these samples. The probable effects on the exposure dates for a range of thicknesses and densities of snow cover is likely minimal (less than 5%, Gosse and Phillips, 2001) and will not likely contribute a significant random error among the dates.

Cold-based ice occurs when the base of a glacier is below its pressure melting point and in therefore frozen to its bed (Benn and Evans, 1998). The possible presence of cold-based ice in the Baffin Uplands area means that boulders may have been left on delta surfaces without any further evidence of glacial disturbance. The boulders left by

the ice could have had high inherited concentrations from previous exposures. A significant variation in the total concentration may exist for individual particles on a deposited landform. Using numerous sand-sized particles of an ice-contact delta helps to bypass this problem. At one delta, a large boulder of quartz-rich granite gneiss was sampled to compare to the dates obtained from the amalgamated sand samples taken at other delta sites. The boulder was not thought to have been delivered to the delta from mass wasting because it was more than 30 m from the nearest colluvial apron. A rapid (>50 km within 1 kyr) retreat history was envisioned for the glacier that was within the Ravn River Valley and accordingly, it was believed that the glacially fed deltas were constructed over very short periods of time. These ideas helped guide our sampling strategy: it was not necessary to sample more deltas because their ages should be within 1σ. The ages of the boulder and subsurface sand samples should therefore provide close estimate for the timing of ice-marginal retreat.

3.4 Laboratory Methods

3.4.1 Physical and Chemical Separation

For details on the laboratory procedure the reader is referred to Appendix 2. The goal of this procedure is to obtain approximately 100 g (more if possible) of quartz concentrate with less than 150 ppm Al for each sample (see chemical worksheets in appendix). This large mass (about 5 times greater than most samples processed at Dal-CNEF) was required to attain the desired AMS precision (2-4%). The majority of the physical sample preparation was done in the Crystal Isolation Facility located in the

basement of the Dunn Building, Dalhousie University where the samples were crushed and milled using standard procedures (see Appendix 3).

The chemical pretreatment was done in the Cosmogenic Nuclide Extraction Facility (CNEF) in LSC Room 4617, Dalhousie University. The 355-500 μm grain size fraction after sieving was regarded as the optimal grain size (Dal-CNEF Lab Procedure) and if the amount was not adequate then the 250-355 μm fraction was utilized. Each sample was then placed in 2 separate teflon beakers, keeping the different grain sizes apart.

3.4.2 Accelerator Mass Spectometry (AMS)

The BeO powder from each sample (1 mg) was then packed in special target holders with niobium powder and sent to a laboratory at Lawrence Livermore University for mass spectral analysis. The mass spectrometer measures ^{10}Be / ^{9}Be and sends the results back to the CNEF to calculate the exposure ages. The amount of ^{10}Be in the sample is calculated with the following equation from Gosse and Phillips (2001):

$$^{10}Be = R_{\left[\frac{10}{9}\right]} \, m^c \left[N_A / A_{Be}\right] / m_{qtz}$$

Where:

^{10}Be = atoms g^{-1}

$R_{\left[\frac{10}{9}\right]}$ = measured ratio of $\dfrac{^{10}Be}{^{9}Be}$

N_A = Avogadro's number

A_{Be} = Atomic weight of Be

m_{qtz} = Mass of quartz

m^c = Mass of carrier added to the sample in grams

3.5 Uncertainties and Errors

According to Gosse and Phillips (2001) errors can be grouped into random and systematic errors. Random errors include measurement uncertainties and precision related errors. For example, the average Poisson error in the counts of ^{10}Be nuclides by the accelerator at Lawrence Livermore National Lab is 2-5 %. Random error about a mean age of a landform can also be caused by variations in individual sample characteristics such as erosion rates, and adjustments for burial durations, or thicknesses of the sample and topographic shielding. Systematic errors influence the accuracy of the calculations and include errors from mainly production rate estimates as well as temporal variations, stable element measurements as well as carrier and standards. The uncertainty for an exposure age can be calculated with the following equation (Gosse and Phillips, 2001):

$(\Sigma random^2 + \Sigma systematic^2)^{1/2}$

Overall, the expected random uncertainty for ages in the deltas should be 5% (1σ) and the total uncertainty in the age (when comparing to other chronometers) is 15% (1σ).

3.6 Erosion Rates

Erosion rates may be calculated using the formula:

$$\varepsilon = \frac{\overline{P}\left(\Lambda/\rho\right)}{\overline{N}}$$

where: ϵ = erosion rate in cm yr^{-1}
P = production rate in atoms g^{-1} yr^{-1}
Λ = attenuation (160 g cm^{-2})
ρ = density (2.6 g cm^{-3})
N = measured concentration of ^{10}Be in quartz (atoms g^{-1})

Chapter 4: Results

4.1 Surficial Deposits

The Holocene deglacial record for Baffin Island is well preserved in both marine and terrestrial depositional environments. The glacioterrestrial systems tract includes deposits that were formed in one of the following several types of glacially related settings (Eyles and Eyles in Walker and James, 1992):

1) Subglacial Deposits: If the ice is warm-based (above the pressure melting point at its base) then significant subglacial erosion will occur at its base and typically deposit a variety of poorly sorted diamictons, also known as a glacial tills. Other deposits associated with this type of environment are eskers, comprised of meltwater derived sediments being deposited as either subglacial or englacial channel fills.

2) Supraglacial Deposits: Are deposited when the ice-margin of a glacier stagnates, leaving behind hummocky melt-out material from the surface of the ice. Any deposit, on the surface of the glacier, such as meltwater deposits, supraglacial lakes and moulins will settle to the ground as the glacier wastes away. Subglacial and englacial debris may also be deposited in this manner. Sediment being supplied to the surface of a glacier surface is typically derived from areas of higher relief.

3) Glaciolacustrine Deposits: These deposits typically result from the damming of a large basin by ice. The main diagnostic feature of a glaciolacustrine environment is the presence of varves. Varves are annually accumulated layers of sediment of alternating grain size that show seasonal variations in sedimentation. Ice rafted debris falling from calved icebergs often fall into these sediments as dropstones. Deltas are also frequently deposited into this type of environment.

4) Glaciofluvial Deposits: Sediments are lain down by meltwater rivers. The deposition may be rapid, burying blocks of ice that later melt to form lakes with no input or output sources, known as kettle lakes. Glacial outwash plains (sandur) are typically deposited in a proglacial setting, infront of an ice-margin. Wind blown loess deposits may also be associated with the outwash in the absence of vegetation.

These facies models will be used to interpret the deglacial history for the Ravn River Valley.

Kame terraces are gently sloping features perched on valley sides that are deposited by meltwater between the glacier margin and the valley walls. They are usually composed of sands and gravels but may also contain debris that has fallen off the glacier surface (Benn and Evans, 1998). Gilbert –type deltas are most commonly found in glaciolacustrine settings and comprise: topsets, consisting of fluvial sediment deposited on the subaerial tops of the delta surfaces; foresets, which are beds comprised of sand and gravel deposited on the delta foreslope; and bottomsets deposited at the base of the pro-delta slope. The majority of the glaciolacustrine deltas found within the Ravn River Valley were Gilbert-Type. According to Benn and Evans (1998), kame deltas, also known as ice-contact deltas are deposited into marine, supraglacial or ice-marginal lakes and are similar in structure to glacial meltwater fed deltas. Ice-contact deltas, however, do not emanate from tributary basins that typically feed glaciolacustrine deltas with outwash and they typically show a former ice contact position. They are also found in topographically high areas where the only possible sediment source was from ice marginal meltwater.

Ice-marginal drainage channels, also known as lateral meltwater channels are capable of incising deeply into both sediment and bedrock, dependent on the properties of the media that they are incising, the annual discharge and the duration of channel use. They are mostly found around the margins of cold-based ice but also around warm based ice that is cold-based around its periphery. In many cases, each channel may represent a season of melting, allowing the ice recession rates for that season to be determined (Benn and Evans, 1998).

4.2 Summary of the Surficial Geology:

The reader is directed to see Fig. 7 for the remainder of the results section to view the milemarker map of the Ravn River Valley. The five most important features found within the Ravn River Valley and its tributaries include: 1) Lateral meltwater channels that are deeply incised into bedrock dipping in an up-valley direction that are almost exclusively confined to the northbank of the Upper Ravn; 2) Descending flights of kame terraces that are associated with the ice-marginal channels and are also primarily confined to the northbank in the Upper Ravn; 3) The presence of a large glacial lake spillway in the northeast that is incised at least 46 m into bedrock and whose strath and base closely correspond to glacial lake shoreline and delta elevations within the Ravn Valley; 4) The presence of a prominent glaciolacustrine shoreline at 300-320 m that is primarily confined to the northbank of the Upper Ravn Valley. It is also found in the Lower Ravn but is confined to the westbank; 5) Well preserved kame deltas are absent above the 41 km mark but are found on both valley sides below it. Raised glaciolacustrine deltas are found thoughout the Ravn River Valley but the ones eminating from southbank

42

tributaries are larger and more abundant. Both lacustrine and kame deltas record the

presence of two prominent shorelines, one at 300-320 m and one at 268 m.
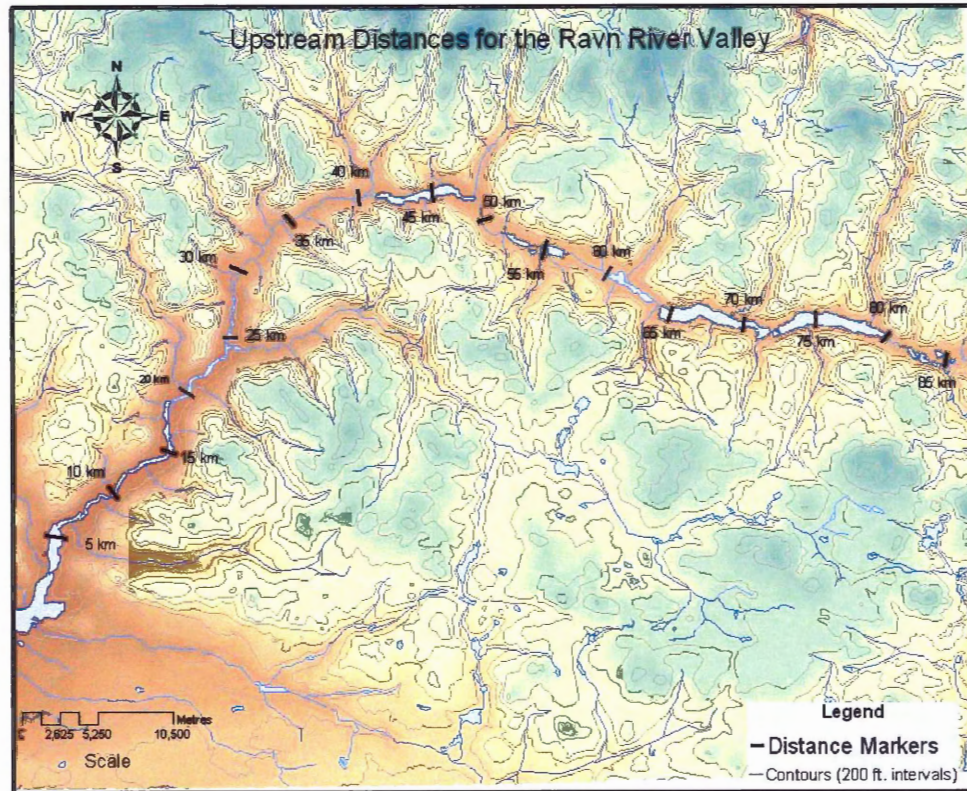
Figure 7: Upstream distance reference map for the Ravn River Valley.

4.3 Mapping Results for the Ravn River Valley

4.3.1 Spillways

In the most northeasterly part of the study area, approximately 86 km upstream,

there is a large paleo-lake spillway that was deeply incised into Archean granite gneiss.

The Ravn-Quernbiter spillway is only 100 m east of the modern Ravn-Quernbiter

drainage divide. The paleo-lake spillway sloped from west to east and an underfit stream

now runs through it (Figs. 8 and 9). One large strath is clearly visible on both sides of the

43

spillway at 301 m. The spillway has incised 46 m to 255 m at its base. The spillway

served as an outlet for an ice-dammed lake to the west for a long period of time and was

noted by both Ives and Andrews (1963) and Hodgson and Haselton (1974). The most

prominent paleo-lake level of 300-320 m and 268 m closely correspond to the elevations

of the spillway strath and bottom, attesting to a negligible differential isostatic uplift

along the entire Ravn paleo-lake system.
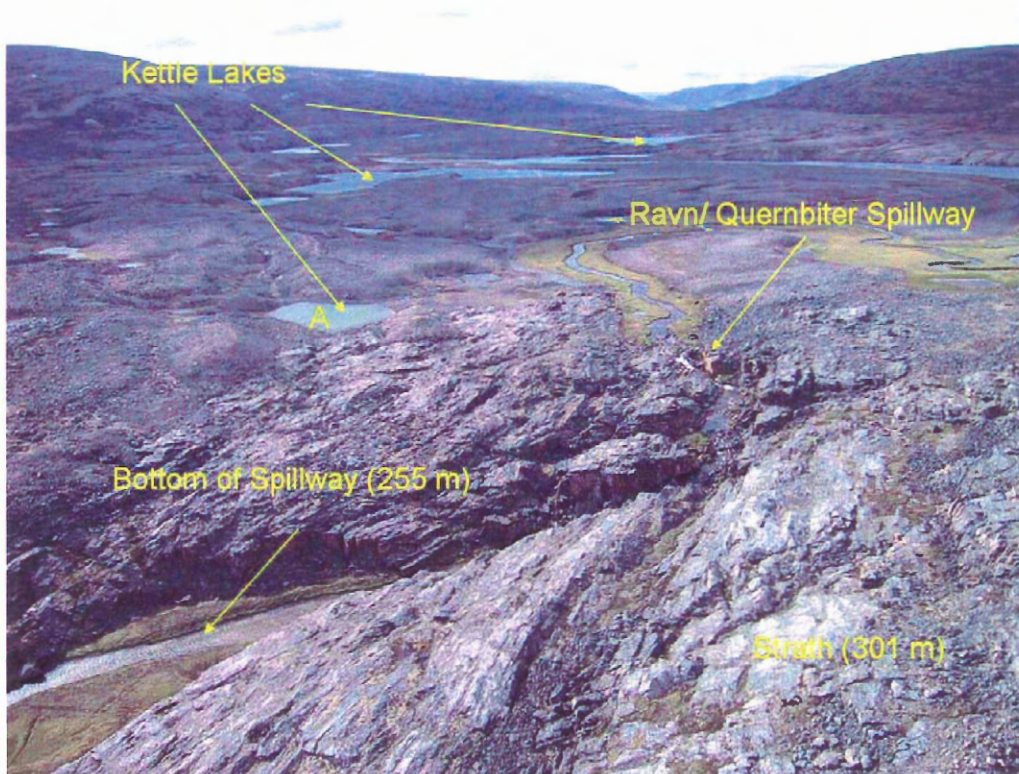
Figure 8: View looking west down the Ravn River Valley from the near the Ravn-Quernbiter drainage divide at km 86. Lake A is ~60 m wide. The spillway, seen in the foreground, was incised into Archean granite gneiss. The spillway began at an upper strath at 301 m a.s.l., and incised over the lake period and subsequent time to a depth of 255 m a.s.l. In the background, a large plain of kettled outwash is visible.

Figure 9: View from the bottom of the Ravn/Quernbiter spillway looking east, downstream at ~ km 86. The spillway was incised approximately 46 m, mostly during the period of Glacial Lake Ravn occupancy throughout the duration of Glacial Lake Ravn.

In the southwest, near the uplands mouth of the Ravn River Valley at km 2.5, there appears to be another spillway on the eastern side of the river at an elevation of 200 to 245 m. The spillway is deeply incised into bedrock and dips from east to west, into the Ravn Valley bottom. Washed bedrock surfaces are present on the 301 m strath surface on both sides of the spillway channel. Ice must have been damming the lake immediately to the west of the spillway, in order for it to have been an active outlet. This spillway is a convenient place for a lower lake outlet since the higher northeastern spillway was abandoned once the lake level fell below 268 m.

4.3.2 Kettled Outwash and Ice-Stagnation Deposits

Kettled outwash occurs when blocks of ice, detached from either a retreating glacier snout or transported *via* a catastrophic flood (jokulhlaups), are rapidly buried by glacial outwash (Benn and Evans, 2001). Immediately to the west of the Quernbiter spillway there is a long stretch of kettled outwash in the valley bottom (Ives and Andrews, 1963) between km's 80 and 86. There are many large kettle holes in the valley bottom, some larger than 300 m in diameter.

In the Upper Ravn Valley, there are also several kettled glaciolacustrine deltas eminating from southern tributary valleys. Delta surfaces 49 and 50 (322 m), 77 and 78 km upstream respectively, both contain kettle holes and occupy the southbank of the northeasternmost lake. Delta 48 (306 m), 72 km upstream, once fed by ice retreating south down its respective tributary valley, divides the two most northeasterly lakes and contains large kettle holes. The deposition of the delta was certainly obstructed by a large ice block deposited in the valley bottom, whose flow east was likely blocked by narrowing valley walls. Further to the west, south bank glacial lacustrine deltas 47 (308 m) and 42 (306 m), 64 and 55 km upstream respectively, also contain large kettle holes that appear to have been occupied by ice throughout their duration. The kettling was probably caused from the detachment of ice blocks from receding glacier snouts eminating from southern valleys.

Ice-stagnation features are clearly visible further to the west in the area where the Ravn River bends to flow to the southwest, between delta 31 (km 40) in the east and delta 27 (km 34.5) in the west. The stagnation landforms and sediments are primarily confined to the southern valley walls and southbank valley bottom. Delta 31 (311 m) appears to

have been fed from two main southern drainages and its curved shape (inside of curve facing down-valley) suggests that meltwater and sediment were being diverted around either a valley glacier or stagnating ice block, hugging the valley wall, and flowing east ultimately to a kame delta at the lobe terminus. To the west, the valley bottom contains kettles and large hummocky piles of sandy sediment. This kettled topography may represent the ice-contact position of a valley glacier or where an isolated large block of ice (>1 km^3) stagnated against the southern valley wall. The possibility of such a large block of stagnating ice is unique to this segment of the valley. However, the combination of high outwash sediment discharge, steepness of the valley walls (slope $= 0.5$ and the elevation is > 366 m from top to bottom), dip of the ice surface and the orientation of the valley axis are conditions that could have induced stagnation. Raised above the ice-stagnation features are descending flights of kame terraces on the valley wall that dip in an up-valley direction. The terraces have a washed bedrock surface above them and appear to have descended in elevation as the ice surface became reduced. Glacial lake shorelines are also found in this area, meaning some the older kame terraces may have been reworked by glaciolacustrine wave-action.

Immediately north of kame delta 31 (Fig. 14, pp. 59), kame delta 32 (321 m, although there are lower levels) on the northern valley bank, is highly kettled and has adjacent kame deltas. It was an ice-contact delta that was also fed by a lateral meltwater channel on the north valley wall. Kame deltas retreat in a down-valley direction away from this position.

4.3.3 Kame Terraces

Kame terraces are commonly found near the tops of the northbank tributary valley walls. In the three most northeasterly northbank tributary valleys, elevated kame terraces are nearly exclusively restricted to the western sides of the valley. This may have been due to differential melting and increased meltwater flowing along the western sides of ice tongues melting within the northern valleys. Kame delta terraces occur mostly in time-transgressive sequences that indicate ice-marginal retreat in a downvalley direction. The base of the kame delta terraces appear to be graded to a horizontally uniform elevation, probably a paleo-lake level indicator. Above many of the kame terraces are glaciofluvially washed bedrock surfaces. In places, the terraces were fed through deeply incised meltwater channels. Northern tributary kame terraces may either have smooth top surfaces or be indented with lateral ice-marginal drainage channels that dip up-valley. Descending flights of kame terraces, evident in the second most northeasterly valley (70 km upstream) indicate that there was a progressive lowering of the ice-surface elevation. In the same valley, many of the kame terraces align perfectly with linear meltwater features (probably lateral meltwater channels) that curve down from the western interfluve area. These meltwater features were ice-marginal because they were prevented from flowing directly downhill. Each one them may represent an ablation season. They suggest that the ice margin was crossing the interfluves, connecting the tongues of ice in adjacent valleys.

In the more western northbank tributaries there are large elevated kame terraces that appear smoother and have greater widths. The large terraces are more common in the larger valleys but two prominent kame terraces are found in smaller SW-NE to W-E

48

trending valleys. In some places they were fed by col gullies which connected them to adjacent valleys. For example, at elevation site #26 (524 m), in a tributary 41 km upstream, there is a col gully incised into fractured granite gneiss that is graded to the level of a kame terrace consisting of bouldery-cobbley gravel. This suggests that it may have been a meltwater overflow deposit from either ice or a proglacial lake in the adjacent valley or from ice within the same valley. Meltwater channels incised into the surface of this terrace all appear to dip in an up-valley direction. No terraces are present on the southern sides of these valleys.

Beginning in the Upper Ravn Valley, near the Ravn-Quernbiter spillway (Fig. 8) and moving south, kame terraces are almost exclusively found on the north bank valley walls. Further down-valley, the situation is reversed, with most of the kame terraces existing on the southern and eastern banks. Extended stretches of kame terraces, deeply incised ice-marginal drainage channels and washed bedrock surfaces are found at varying elevations on the northern valley wall running from km 86 to km 51. The meltwater channels dip up-valley and are found at decreasing elevations on the valley wall along with the associated kame terraces (Fig. 10, pp. 50). In some places they plunge deeply as though the channel acted as some sort of spillway. In several locations they are fed by kame terraces while in others, the lower meltwater channels appear to have spilled onto a sediment shoreline terrace slightly above the 310-320 m level. The fact that none of these features are seen on the southern walls of the upper valley confirms that this was not simply a valley glacier receding in a down-valley direction, otherwise, these features would have been found on both sides of the valley. As ice receded out of the valley in

the east, meltwater spilled along the ice margin from the west in an up-valley direction into a proglacial lake.
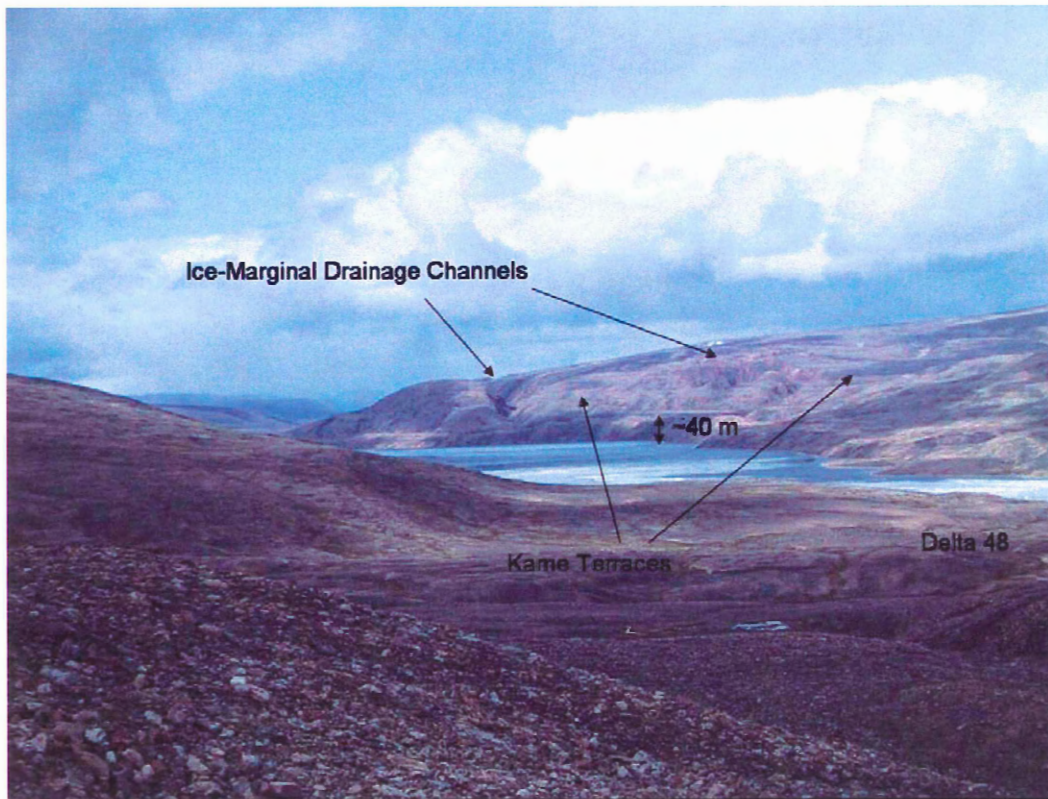
Figure 10: View looking west-northwest from a southern tributary valley at km 72. On the north bank, deeply incised ice-marginal drainage channels dip in an up-valley direction. Elevated kame terraces of varying elevations are found associated with these drainage channels. In the northeastern segment of the Ravn Valley, these features are almost exclusively confined to the north bank.

Upper Ravn southbank tributary valleys are more open and broad than those of their northbank counterparts. Like their northbank equivalents, they also contain kame terraces, but the southbank tributaries have a greater abundance of glaciofluvial/kame terraces which are associated with lateral meltwater channels (Fig. 15, pp. 61) that dip in a down-valley (northward) direction. These features are found on the valley bottoms and up their sides. Glaciofluvial terraces are stacked in an up-valley direction from a morainal position near delta 48 (km 72). Raised kame terrace surfaces are found near the

mouths of some of these valleys. The valley feeding delta 48 contains elevated kame terraces deposited when ice was probably still extending into the main valley. In these tributaries there are also highly elevated, kame terraces. The most prominent one is 3 km long and is situated south of delta 42 (km 55) and has an elevation of approximately 410 m. Below it there is a glaciofluvial terrace-barbed drainage channel system and above it is a washed bedrock surface with descending flights of kame terraces. It appears to represent a significant period in the deglacial history.

On the southbank valley wall to the west, above delta 31 (km 40), there are abundant descending flights of kame terraces that dip in an up-valley direction. Further to the west, kame delta 23 (km 33) is fed by a large upvalley dipping kame terrace with a washed bedrock surface above it. It was fed by the large col gully dipping from south to north that later fed valley delta # 22 (km 31). Kame terraces, once feeding kame deltas, are also found on the northbank valley wall. The presence of up-valley dipping terraces and meltwater channels on both valley sides represents a period when a large block of ice may have stagnated on the southbank or when a valley glacier started to recede in a down-valley direction.

Where the river bends towards the southwest (below km 30), kame terraces that once fed kame deltas are found on the westbank. However, the majority of them are found on the eastbank. One of the more elevated terraces, curling around the bend from the major eastern tributary at km 25.5, has a washed bedrock surface above it. Meltwater was flowing around this bend from coalescent ice in the eastern tributary valley and was entering a col gully that was feeding deltas 23 and 22 (km 33 and 31). Kame terraces then decrease in elevation showing that the ice surface in the valley was reducing its

height. This provides strong evidence for a valley glacier lobe that persisted as upland ice thinned and retreated southward.

In the large adjacent western tributary, there is a large terrace (~400 m long) surrounding the entrance to a large col gully trending to the NE into the Ravn Valley at km 27.5. The terrace appears to dip to the NW and there is a heavily washed bedrock surface above it, north of the gully. The presence of a valley delta at the opposite end of the col means that there was ice present in this valley, feeding the col, when the lake was in existence at the opposite end.

There are extensive kame terraces down the eastern valley sides of the Lower Ravn Valley. On the western side they are less abundant and include one 11 km upsteam, dipping towards kame delta # 6 (314 m), comprised of a boulder-cobble sand, on the west side of the valley. On the same side, 6-7 km upstream, a lengthy kame terrace slopes from kame delta # 2 (326 m) to near the level of kame delta 5 (318 m). A large kame delta is found on the opposite side of the valley to site #5 associated with flights of kame terraces, lateral meltwater channels and washed bedrock surfaces.

4.3.4 Glacial Lake Shorelines (Strandlines)

Glacial lake shorelines are well developed on the northbank of the Upper Ravn River Valley and near the mouths of the northern tributary valleys while they are virtually absent on the southbank valley walls. This was noted by Ives and Andrews (1963) and is thought to represent a time when a proglacial lake was dammed against the southward facing slopes in the north and the main ice-margin to the south. The main ice-margin was still shielding the northward facing slopes from glaciolacustrine activity and prevented a

52

shoreline from developing. Also, abundant glacigenic sediment deposited against the northbank may have served as an easier medium for a lake to etch in a prominent strandline.

Elevated, continuous to discontinuous proglacial-lake strandlines are present in a couple of the northern tributary valleys. In most places they are evident from a colour change boundary in the field and from air photos with light above dark. The longest of these strandlines is in the second most northeasterly valley (north of km 70) and is continuous for more than 3.6 km. The shoreline itself has an elevation of roughly 550 m, nearly the equivalent to the kame delta terraces on the opposite side. These elevated strandlines, in conjunction with the presence of glaciolacustrine and kame deltas, indicate that there were once proglacial lakes dammed in these valleys. Both Ives and Andrews (1963) and Hodgson and Haselton (1974) also mapped shorelines in these valleys.

Prominent shorelines in the Upper Ravn Valley range from 300-320 m in elevation. The strandlines are discontinuous and loop into northern tributary valleys (Fig 11). Delta 38 (301 m), at km 48, in one of the northern tributary valleys, has a prominent strandline associated with it that continues into the main valley (Fig. 37 in Appendix 1). The only evidence for paleo-lake levels on the southern valley wall is from glaciolacustrine deltas eminating from southern tributary valleys, kame deltas and a stretch of glacial lake strandlines in the vicinity of delta 27 (Fig. 12). The strandlines near delta 27 (km 34.5) have a washed bedrock surface above them with kame terraces. Most coincide with the paleo-lake strandlines on the northbank but some are higher.

Figure 11: Looking northwest from the southbank, across the Ravn River Valley at km 49. In the foreground are glaciolacustrine sediments that are composed of pebbly-coarse sands, either the remnants of dissected deltas or outwash. The sands are all found at a similar elevation, probably deposited at a paleo-lake shoreline. Behind the lacustrine sediments are the cross-valley/sublacustrine moraines. On the far valley wall, is a glacial lake shoreline at 302 m, traced from a prominent strandline above delta 38, just off the picture to the right. Backpack for scale.
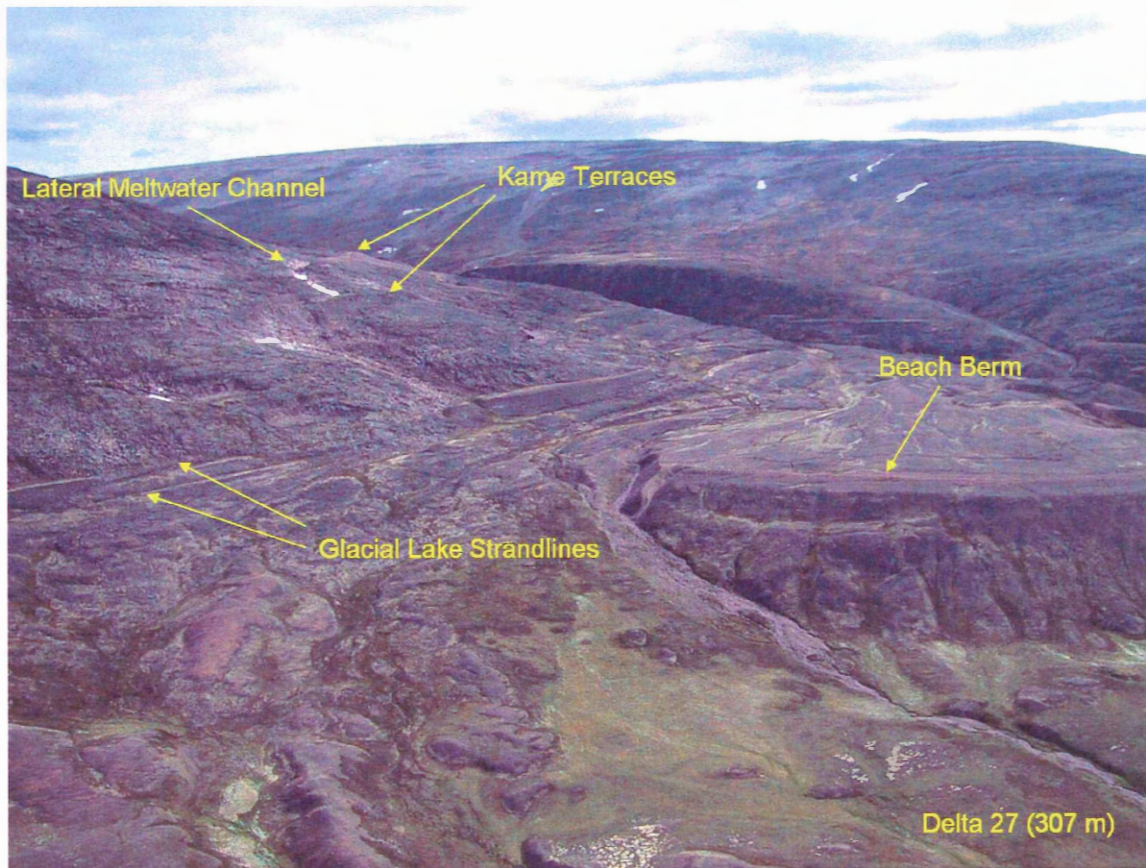
Figure 12: View looking south at lacustrine delta 27 (307 m) eminating from a southbank tributary at km 34.5. To the left and behind the delta is a flight of older prominent glacial lake strandlines. The strandlines are flat and have a uniform width (both uncharacteristic of kame terraces). The strandlines can be traced further east but eventually become difficult to distinguish from kame terraces. Each strandline represents a paleo-lake elevation, in this case, levels higher than the delta. Above the uppermost strandline in the foreground is a washed bedrock surface, probably created through glacio-fluvial activity. The washed bedrock surface contains kame terraces, one of which was fed by a lateral meltwater channel.

Landform Elevations in the Ravn River Valley
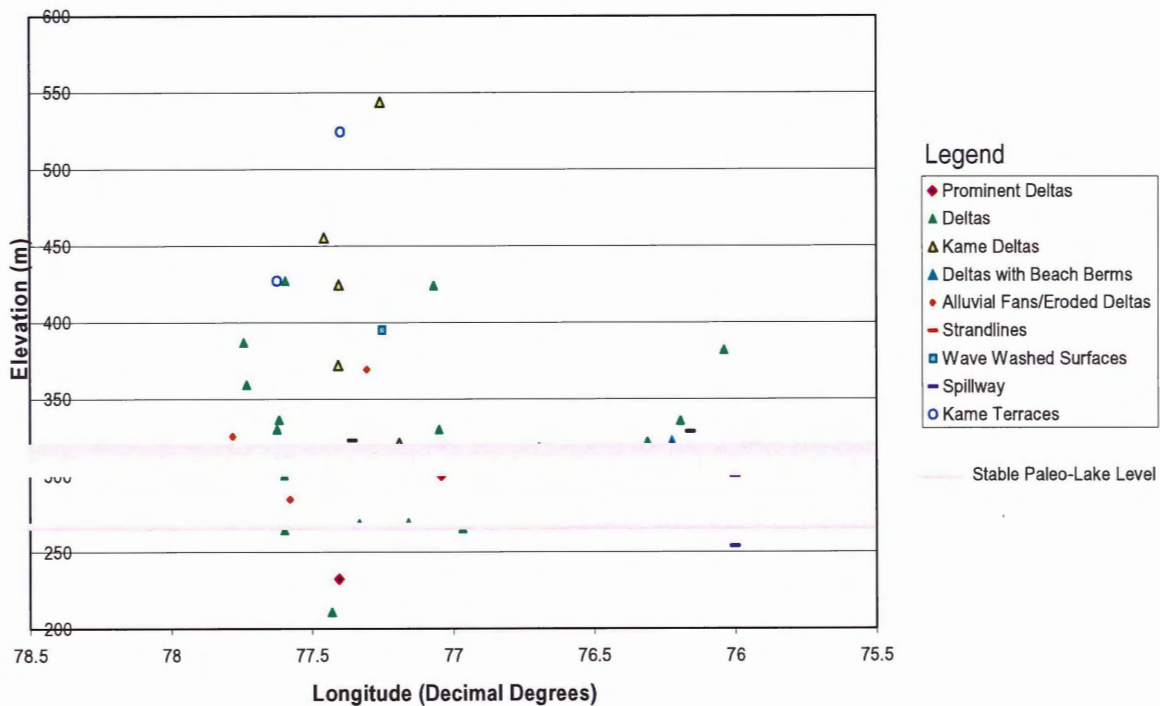
Figure 13: Plot of paleo-lake level indicator landforms vs. longitude. Eroded deltas were grouped with fans because neither provides an accurate paleo-lake level elevation. Prominent deltas carry the most weight and are followed by ordinary glaciolacustrine deltas, kame deltas, deltas with beach berms, strandlines and spillway strath elevations. Kame deltas have a broad elevation distribution, because they were probably deposited in smaller lakes dammed in by the ice and not in Glacial Lake Ravn itself. The lack of kame terraces below 320 m helps provide a relative timing for deglaciation (ie. Contemporaneous with the lakes). The kame terraces are indicative of a paleo-ice surface. Two prominent shorelines can be easily identified: one at 300-320 m and the other at 268 m. The higher ones were deposited in elevated lakes.

The 300-320 m shoreline is discontinuous along the valley to the west but it becomes highly visible once again on the westbank of the Ravn at the bend and continues south to the 20 km mark. The shoreline can be faintly traced north from delta 20 (305 m and 27.5 km upstream) for approximately 4 km. South of the delta 20, two prominent strandlines may easily be traced, one at ~ 305 m and the other possibly at ~300 m. A more elevated shoreline is visible to the south at approximately 315-320 m. The 305 m strandline is strongly visible on the westbank of the western tributary whose mouth is at

56

km 20. A 305 m strandline and one directly above it, can be traced from kame delta 12 (305 m at km 20) into the western valley. Further up the tributary valley there is what appears to be the remains of a dissected (eroded) glaciolacustrine delta at approximately the same level. There may also be a higher strandline in this valley, at approximately the level of delta 13 (427 m at km 19.5), but the feature was not visited and is difficult to distinguish from a kame terrace on air photos. Shorelines are not easily distinguished south of this point. Paleo-lake level indicator elevations are shown in Fig. 13.

4.3.5 Ice-Contact (Kame) Deltas

A possible kame delta was identified in one of the northern tributary valleys, once fed by a kame terrace with a washed bedrock surface above it. One of these terraces, in the most northeasterly tributary valley had an elevation of approximately 550 m. Delta 47 and 48 (km 64 and 71) were originally ice-contact deltas because they have large kettle holes. However, since they emanated from large southern tributary valleys, they will be considered as glaciolacustrine deltas. A large isolated kame delta (# 43) at 309 m and 52 km upstream lies in the centre of the valley. It was most likely fed by ice that was proximal, immediately to the west because the delta is not at the mouth of a tributary. Ice-contact deltas in the main valley become more abundant in the vicinity of delta 31 (km 40).

Kame delta 31 (308 m) is an ice contact delta with foresets dipping up-valley and was fed by meltwater winding its way around a large (stagnating?) ice mass in the valley bottom (Fig. 14 and Fig. 34 in Appendix 1). Kame delta 32 (km 40), on the northbank with its most northerly segment at 321 m also contains visible foresets and consists of

57

another segment nearer to the centre of the valley at a lower elevation (~310 m?) that was likely coeval with 31. Two other smaller kame deltas were deposited immediately to the west of this amongst more kettle holes. Farther along the northern valley wall to the west, are two larger raised ice-contact deltas, one being delta 29 (308 m) at km 35. These deltas are elongated along the valley axis, have curved geometries, and are not fed by tributary valleys but by kame terraces. The curved outer outline of delta 29 has the shape a former ice-contact position when ice was in position down-valley. The delta is graded to the level of a west to east dipping col gully that fed the delta when either ice and/or a lake were present in the adjacent tributary valley. Delta 29, contains lateral meltwater channels above it that dip in an up-valley direction (Fig. 33 in Appendix 1). A strandline is also graded to just above the delta surface.
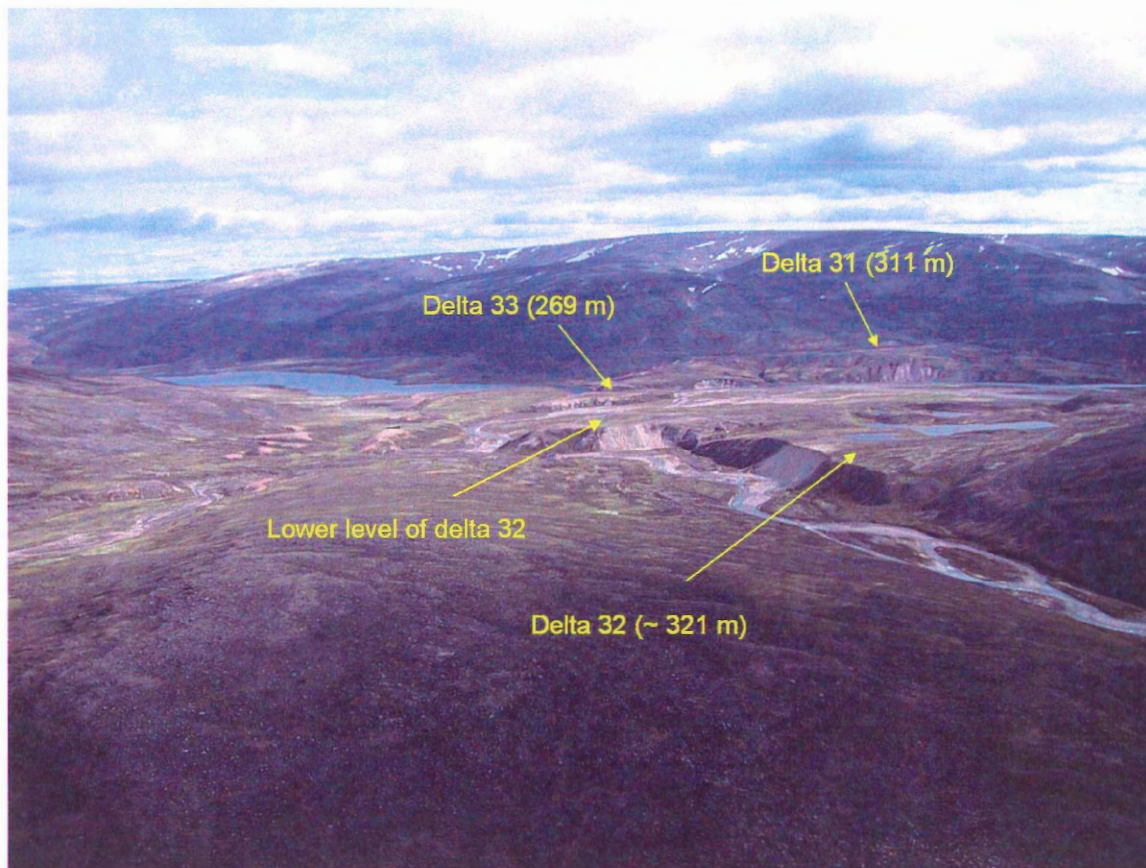
Figure 14: View looking south from northbank tributary towards delta 31 at km 40. Delta 32 exhibits kettle holes and is interpreted to represent a former ice-contact position. The delta pad beyond the kettles is lower and probably coeval with delta 31 across the river. The shape of delta 31 reveals that an ice lobe to the west may have obstructed its sedimentation. Delta 33 is situated at the mouth of a southern tributary valley.

Kame delta #23 (323 m) at km 32, was once fed by a kame terrace with a washed bedrock surface above it. The kame terrace was fed by a large col gully that also later fed glaciolacustrine delta 22 (313 m). Delta 21(310 m) at km 29, is an ice-contact delta on the eastern valley wall. Above it and to the south, there is a washed bedrock surface that aligns with kame terraces further down-valley. Across the valley, above delta 20 (305 m), there is a washed bedrock surface overlying up-valley dipping kame terraces that once fed several westbank kame deltas. Kame delta 15 (424 m) at km 23.5, was probably fed into a smaller pinned in lake. On the west bank, kame deltas 9 and 6 (300 m and 316

m respectively) both have kame terraces feeding them that are dipping up-valley. Delta 2 (325 m) of km 6, fed by a small col gully, and is part of the same kame terrace that feeds delta 6 and may have been deposited in a pool dammed in against the lateral ice margin.

4.3.6 Glaciolacustrine and Perched Deltas

Any raised deltaic landform with a flat surface, emanating from a tributary valley or smaller drainage that was fed either directly or indirectly by meltwater was considered as a glaciolacustrine valley delta to distinguish them from glaciolacustrine ice-contact (kame) deltas. The topset/foreset contact of a delta, represents the paleo-lake level when the delta was deposited. Since the topsets are thinner than the altitudinal precision (± 4-5 m), the elevation of the delta surface is a good approximation for the former lake level. There were well defined beach berms / ice-push ridges on several of the glaciolacustrine deltas, giving a definite elevation for the paleo-lake level at the time of delta deposition (Fig. 12, pp. 55). Southern tributary deltas of the Upper Ravn are the largest and most well developed, more than likely because they were proximal to the ice margin for a longer period of time.

Glaciolacustrine Deltas

Glaciolacustrine delta elevations show that there were two prominent paleo-lake levels found at 300-320 m and 268 m. Of these deltas, those in the 300-320 m category are the most ubiquitous and are found throughout length of the valley. Beginning in the northeast, delta 50 (322 m) at km 79, has a beach ridge, a kettled surface and was fed by a col gully that dips from the adjacent tributary valley to the west that fed delta 49 (322 m).

60

The only possible source of meltwater to delta 50 would have been from ice in the adjacent valley. All flow to this delta would have ceased before the ice reached the morainal position in that valley (Fig. 15). Delta 49 was being deposited isochronously with delta 50. Delta 53 (353 m) at km 86, found on the southern side of the river near the kettled outwash zone did not have its elevation corrected and may have been from a lower lake level.
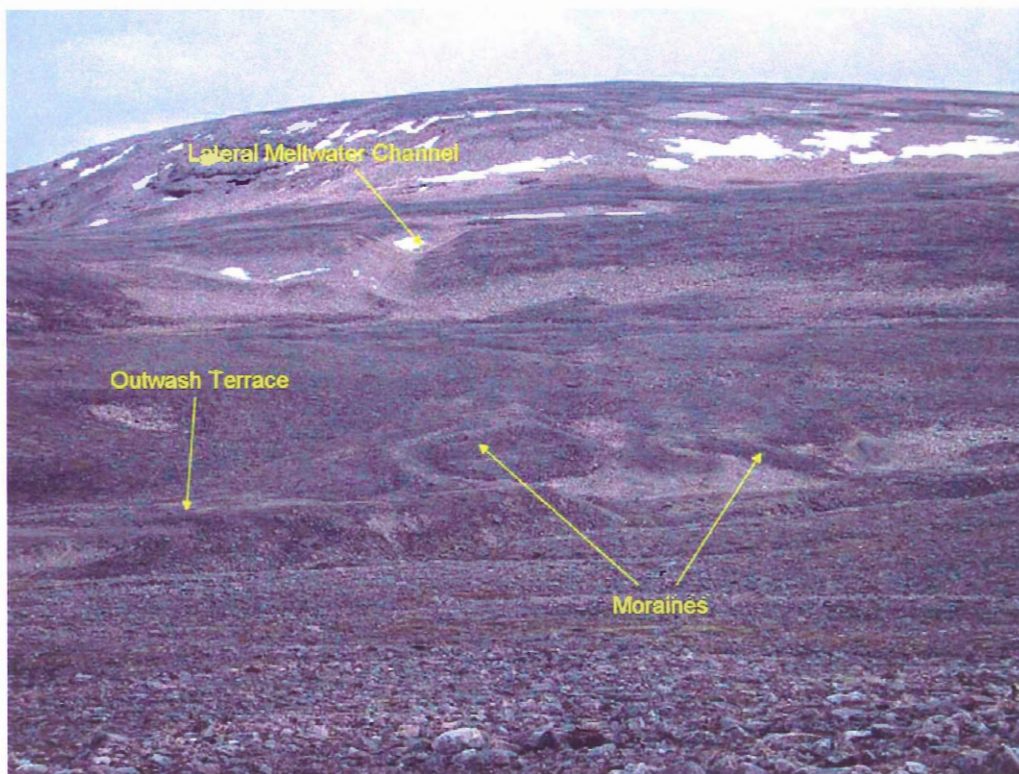
Figure 15: Looking east across a major southern tributary valley, leading to glaciolacustrine delta 49. In the foreground are two morainal segments, oriented perpendicular to the valley axis. This position probably represents an ice still-stand position within this valley with ice positioned to the right. Down-valley, immediately infront of the moraines are glacial outwash terraces. These terraces occur in flights in an up-valley direction behind the moraines. Above the moraines is a lateral meltwater channel that appears to be winding its way around an ice-frontal position.

Delta 48 (306 m at km 72), comprised of a pebbly gravel and delta 47 (308 m at km 64), were both initially deposited proximally to ice due to the presence of large kettle

holes. Large blocks of ice persisted in these large deltas as ice receded up the southern valleys. This may either signify rapid retreat of the ice margin or massive sediment influx over a short period of time. Other major southbank glaciolacustrine deltas before the bend in the river are deltas 42 (307 m), 27 (307 m) and 22 (313 m). Delta 42 at km 55, has a large kettle hole in its frontal edge, was comprised of a cobbly-gravel and was fed from ice that was in a southern tributary valley. Delta 27 at km 34.5, was comprised of a pebbly-gravel and was fed by a long col gully (4.8 km long) that runs from the major eastern tributary valley to the south. Delta 22 was fed by cols emanating from the southern uplands and from the col that may have fed kame delta 23. At this point, ice on the uplands may have separated from a valley glacier to the west in the main valley, allowing meltwater to flow into the col and then out to feed delta 22.

In the Upper Ravn Valley, glaciolacustrine valley deltas also occur in the longer, more prominent northern tributary valleys but they are more dissected and elongated along the central valley axes. They are not as prominent as those on the southbank because the shores of Glacial Lake Ravn penetrated significantly up the mouths of some of these valleys. Most of them are coeval with the 300-320 m level and have prominent strandlines associated with them. An example is delta 38 (301 m) at km 48 that has a strandline that is traceable well out into the main valley (Fig. 37 in Appendix 1, pp. 107). At the mouth of the same valley is delta 39 (265 m), composed of a pebbly-gravel sand. Deltas 33 (269 m) and 25 (265 m) at km 41 and 32.5 respectively, were deposited in a similar fashion. These northern tributary deltas gradually prograded out as the lake level decreased unlike those of the southern tributary valleys which were primarily deposited when the lake was at 300-320 m.

Delta 17 (232 m) at km 24.5 is found at the mouth of the major eastern tributary and its foresets dip into the main valley. Delta pads appear to systematically increase in elevation up the tributary valley and decrease in elevation further down. Delta 16 (210 m) at 24 km, emanated from the same valley and must have been deposited as the lake level dropped. The major western tributary at km 20 also contains highly dissected deltaic sediment deposited up-valley when the ice was at the 300-320 m level. As the ice receded either up or down-valley and the lake level fell, the delta gradually prograded out to meet the shoreline. The deposition of kame delta #6 (314 m) and valley deltas 10 (264 m) and 7 (284 m) further down-valley than km 25 prove that delta 17 (232 m at km 24.5) and other deltas were not deposited until later on.

Perched Deltas

Perched deltas are found throughout the Ravn River Valley. Perched deltas were either formed in larger tributary valleys or in smaller pockets of water that were pinned against the main valley wall by a glacier. They occur in northern tributary valleys and were likely deposited by remnant upland ice persisting between adjacent valleys. In several places, deltas were proximally fed by deeply incised meltwater channels flowing west to east from ice that was in adjacent valleys to the west. The majority of these perched deltas were formed near the mouths of the tributary valleys. Meltwater in eastward dipping cols also deposited small deltas into these valleys that were later dissected (Ives and Andrews, 1963). As ice was receding from the northern tributary valleys from east to west, meltwater was being discharged into freshly deglaciated valleys. Deltas continued to be deposited in the northern valleys as the lake level

63

continued to fall, until ice pulled away and allowed the lakes to equilibrate with Glacial Lake Ravn.

In the Upper Ravn, perched deltas also formed in smaller lakes that were pooled between the retreating frontal main ice margin and the northern valley wall. Perched deltas are also commonly found in the Lower Ravn, likely deposited in small lakes pinned in against the sides of a retreating valley glacier. An example is delta 18 (372 m) at km 25 that is found within the main valley against the eastern wall. Delta 18, as well as an adjacent delta were fed by meltwater from cols emanating from the eastern tributary and could have only been deposited when ice was at the height of the col heads in the nearby valley. Further south, on the western side of the main valley, delta 8 (336 m) at km 18 and one above it were probably formed in a lake that was jammed against the valley sides by ice. Several others were deposited in this manner in the south towards the uplands mouth of the Ravn. Deltas also formed in the eastern tributary at km 4 including delta #1 at 330 m. This suggests that ice had at least partially receded up the valley to the east (as indicated by meltwater channels) when there was still a large valley glacier damming Glacial Lake Ravn.

4.3.7 Alluvial Fans

The Ravn River Valley exhibits many alluvial fans emanating from drainages throughout the extent of its uplands segment. The majority of these fans were deposited into the valley bottom from large-small drainages in a neo-glacial river-lacustrine setting near the current river level. There are however, a couple of large raised fans present in the Upper Ravn Valley. A large fan at site 40 (306 m) at km 52, composed of a

bouldery-gravel and was fed from two deeply incised meltwater channels, one of which was fed by a large col gully cut through the uplands with its head in the northeast of the large eastern tributary valley to the south. Due to the size of the clastic material, the fan probably had most of its sediment deposited when ice was in an upland proximal position at the same time when meltwater was depositing delta 42 (306 m). The fan also has a beach ridge around its outer rim. Site 45 (312 m and km 61) is also a raised fan composed of a bouldery-gravel that eminates from a smaller south bank drainage.

4.3.8 Ice-Marginal Drainage Channels

Ice-marginal drainage channels are ubiquitous throughout the study area and include lateral meltwater channels and other incised channels that transported meltwater in a proglacial/ice-contact environment. In the northern tributary valleys, primarily on their western banks, there are meltwater channels dipping up-valley that were cut into bedrock and once fed elevated kame terraces. Meltwater channels are also found descending from interfluve areas into the northern valleys, in places dissecting previously deposited kame terraces. Deeply incised col gullies that dip from east to west are found near the mouths of some of these northern valleys, where they enter the Ravn Valley.

Descending flights of up-valley dipping lateral meltwater channels that were incised into bedrock are abundantly found on the northbank of the Upper Ravn River Valley (Fig. 10, pp. 50). Many of these channels are deeply cut and as described earlier, are associated with kame terraces. In some places, the southbank valley walls have drainages that slope directly down their sides towards the main valley.

South bank tributaries contain descending flights of lateral meltwater channels on both valley sides, some incised into sediment, others into bedrock. These lateral meltwater channels dip slightly in towards the centre of the valley in a down-valley direction (Fig. 15, pp. 61). Several of the southern tributary valleys were fed by meltwater in deeply incised col gullies from ice that must have been resting at their heads.

In the Lower Ravn River Valley, ice-marginal drainage channels are found on both valley walls, however, they are most plentiful on the eastbank. The eastbank also contains deeply incised drainage channels that slope directly down from the valley wall tops and partway down the valley walls.

4.3.9 Moraines

A series of sublacustrine/cross-valley morainal features were observed in many of the northern tributary valleys. In most cases, the moraines are perpendicular to the axis of the tributary valleys. Only a few of them appear to have extended across the bottom widths of some of the valleys to be subsequently dissected by tributary drainages. None of the moraines appear above the highest observed paleo-lake level. Some of them are narrow and wispy while others just look like linear, crested piles of sediment.

Several moraines were also found in the southern tributary valleys of the Upper Ravn. One set of two moraines was found in the tributary valley to the south of delta 49 (Fig. 15, pp. 61). The moraines were only found on the east side of the tributary and were perpendicular to the valley axis. They had large glacial outwash terraces infront of

them that were dipping in a down-valley direction. The glaciofluvial terraces and drainage channels continued up-valley as the ice receded south-southwest.
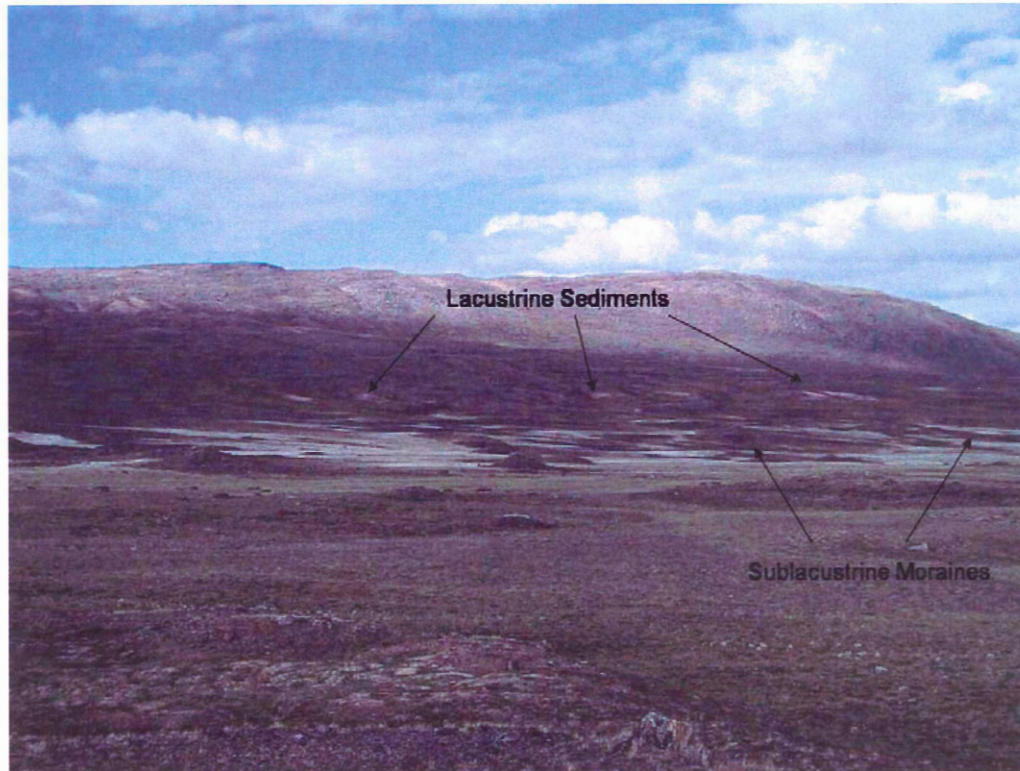
Figure 16: View looking south at sublacustrine moraines in the Ravn Valley. The moraines, are comprised of sandy till. The ridges have variable sizes and shapes and most are oriented ~ perpendicularly to the valley axis. Above the moraines in the valley bottom are isolated lenses of glacial lacustrine sediments, indicating the elevation of a former lake level.

Moraines were only observed in one small segment of the main valley (Fig. 16). All of them were found on the southbank and the majority of them were oriented subperpendicular to the valley axis. Most of them were slightly curved and a morainal feature beside the river was parallel to the valley axis. The longest segment is approximately 360 m long and the shortest is less than 100 m. Several of the moraines appear to extend above the highest estimated paleo-lake level. It is difficult to say whether or not they were all actually formed in an ice-marginal sublacustrine

67

environment. However, due to the fact that many of them are wavy and not all perpendicular to the valley axis, they may have been formed from the injection of displacement of liquefied till as described by Andrews and Smithson (1966). A couple of moraines in the southern tributary valleys were not discernable on aerial photographs and could only be identified on foot traverses. If more foot traverses had been conducted in these valleys, more morainal positions would likely have been identified.

4.3.10 Glaciolacustrine Sediments

Glaciolacustrine sediments are found throughout the Ravn River Valley and in places, help define the paleo-lake shorelines (Fig. 16). Glacial lake sediments are also found in one of the northern tributary valleys at a highly elevated level. The facies consists of linear patches of a light (white) coloured material (probably coarse sand) that rest at an elevation of 550 m. In the valley bottoms, there is a lighter material but it is hard to tell whether or not it is glaciolacustrine in origin.

In the main valley, glaciolacustrine sediment occurs in small to large patches and clearly defines paleo-shorelines if traced from measured delta surfaces. None of the glaciolacustrine clastic material is found above the highest paleo-shoreline elevation. The lacustrine sediment was made-up of a pebbly-coarse sand. A likely explanation for the provenance of these sediments is that they were either ice-proximal outwash deposits or the remnants of dissected deltas.

4.4 Cosmogenic Exposure Dating of Deltas

Eight deltas were sampled for cosmogenic nuclide exposure dating within the Ravn River Valley (see Table 1, or Appendix 1 for a more detailed description and Fig. 17 for sample locations). Three kame deltas were sampled, two in the bottom of the valley at the 310 m elevation while the third was perched at 425 m. The rest of the samples were taken from glaciolacustrine deltas eminating from tributary valleys that flowed into Glacial Lake Ravn with the exception of delta 53, that was likely deposited into a smaller pinned in lake. For an example of a sample pit see Fig. 18.
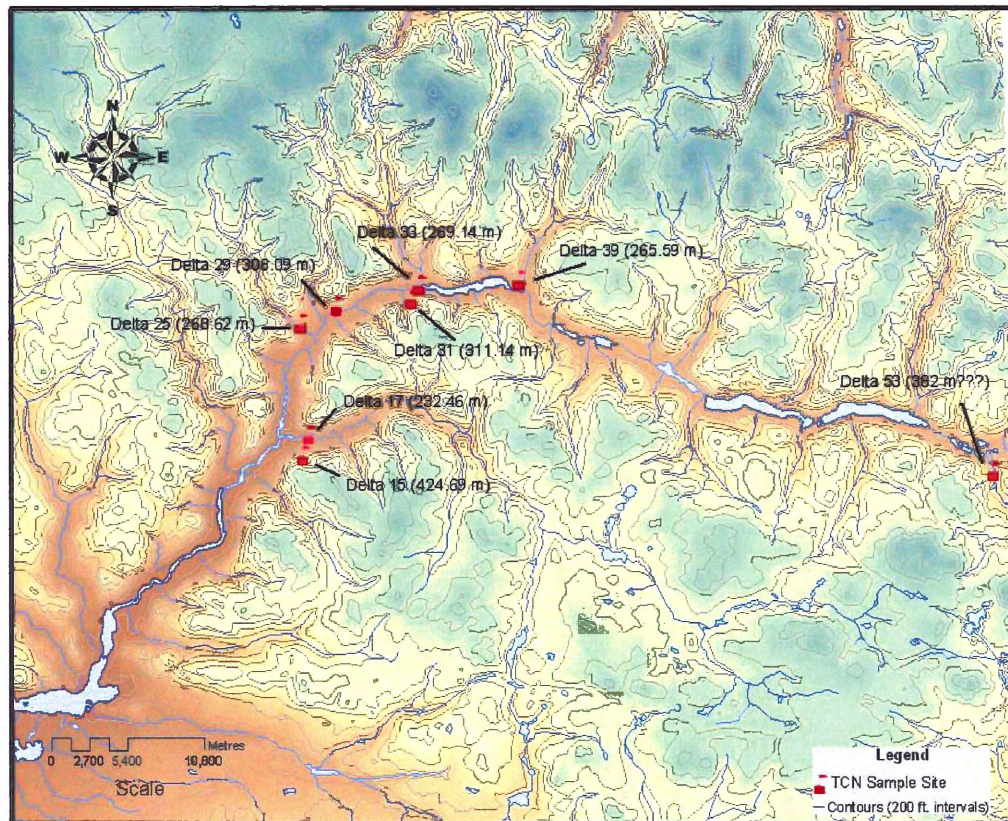
Figure 17: Locations of TCN sample sites within the Ravn River Valley. Delta 15 was a boulder sample from a kame delta. Samples 17, 25, 33 and 39 were taken from glaciolacustrine valley deltas and delta 53 was interpreted to have been deposited into a smaller pinned-in lake. Deltas 31 and 29 were sampled kame deltas.

69
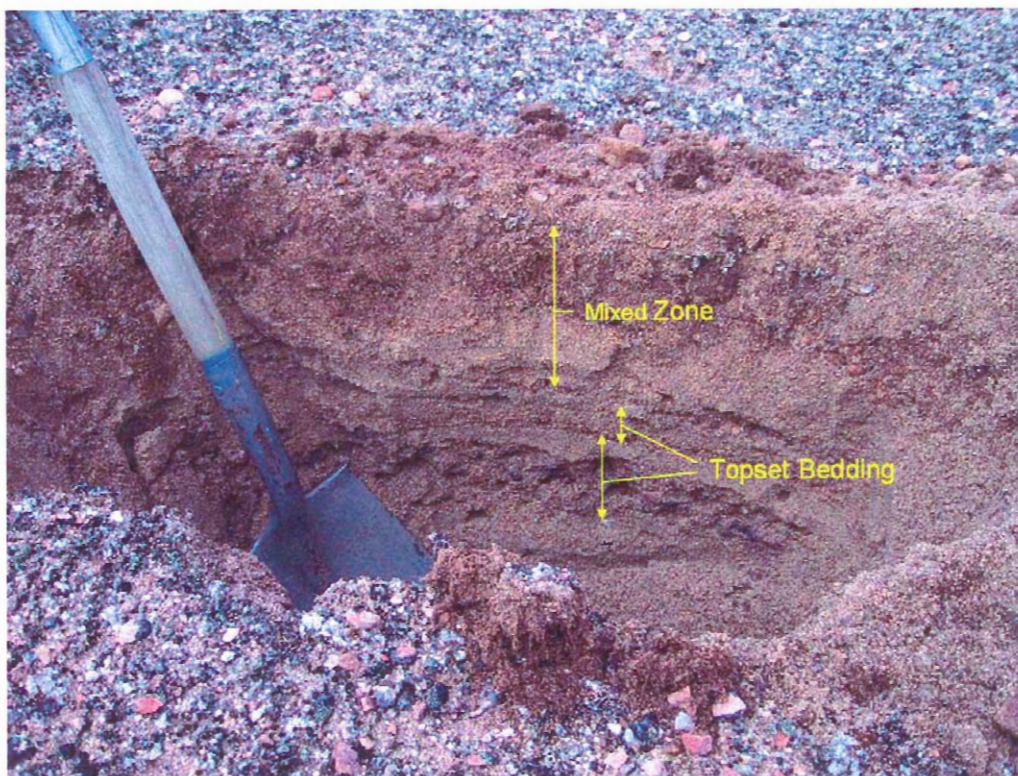
Figure 18: Sample pit in north bank glaciolacustrine delta 25 at km 32.5. Diameter of the shovel handle is 4.5 cm. The pebble lag on the surface resembles an immature desert pavement. The deflated clasts have a good lichen cover, indicating stability. The mixed zone is approximately 20 cm thick and contains rootlets. Below the mixed zone are well preserved horizontal topset beds. Each topset contains a fining upwards sequence that grades from a pebbly sand to massive sand. TCN samples were collected from these undisturbed topset layers, to avoid the undesirable affects of mixing. Mixing is most likely from cryoturbation and shallow bioturbation from burrowing animals.

The sample blank used was 3 X 10^{-14} ^{10}Be atoms/^{9}Be atoms. This value is approximately 4X higher than the usual value of 0.8 X 10^{-14} ^{10}Be/^{9}Be but does not cause a significant adjustment to the measured $R_{\frac{10}{9}}$ because the ratios of the unknown are of an order of magnitude higher. Delta 53 reported an exposure age of 8.3 ± 0.3 ka while the next youngest dates were obtained from deltas 29, 15 and 25 that had exposure ages of 19 ± 0.7 ka, 21 ± 0.9 ka and 25 ± 0.6 ka respectively. Delta 15 was the only boulder sample site. The next cluster of ^{10}Be ages included deltas 17, 31, 33 and 39 that had their

corresponding exposure ages calculated out to be 37 ± 1.0 ka, 33 ± 0.8 ka, 34 ± 0.8 ka and 32 ± 0.9 ka.

Delta #	Sample I.D. #	Lab I.D. #	Elevation (m)	Sample Depth (cm)	Sample Thickness (cm)	Material Sampled	Event	Age ^{10}Be Exposure Age (ka)	Uncertainties (± ka)
15	3088	1372	425			Boulder	Age of Kame delta	21	0.9
17	3087	1371	232	27	3	Delta Topsets	Age of 232 m lake level from glacial lacustrine delta	37	1.0
25	3089	1373	269	26	4	Delta Topsets	Age of 268 m lake level from glacial lacustrine delta	25	0.6
29	3090	1374	308	30	4	Delta Topsets	Age of 310 m lake level from kame delta	19	0.7
31	3091	1375	311	22	5	Delta Topsets	Age of 310 m lake level from kame delta	33	0.8
33	3092	1376	269	26	5	Delta Topsets	Age of 268 m lake level from glacial lacustrine delta	34	0.8
39	3093	1377	266	30	5	Delta Topsets	Age of 268 m lake level from glacial lacustrine delta	32	0.9
53	3094	1378	382	29	5	Delta Topsets	Age of pinned in lake from glacial lacustrine delta	8.3	0.3

Table 1: TCN delta exposure ages.

Chapter 5: Interpretations

5.1 Deglacial History of the Ravn River Valley

The deglacial history of the Ravn River Valley is complex and challenging to decipher. Using the mapped features discussed earlier, the author constructed a series of maps showing former ice-marginal positions during the progressive deglaciation of the Ravn River Valley. Some of the features mapped by Ives and Andrews (1963) and Hodgson and Haselton (1974) were also used.

When the main ice margin receded over the regional watershed divide (Stage 1), tongues of ice resting in the northern tributary valleys created a series of proglacial ice-dammed lakes that spilled north into Eclipse Sound and Baffin Bay as described by Ives and Andrews (1963) (Fig. 21, pp. 79). The ice-margin was receding in a south-southwesterly direction, progressively deglaciating the northern tributaries from east to west. As the tongues of ice receded, a series of sublacustrine/cross-valley moraines were deposited along with elevated kame terraces and lateral meltwater channels. It is difficult to distinguish whether the moraines indicate active ice or whether they were deposited from the ice-frontal liquefaction of till during the ablation season. The northern tributary kame terraces were mostly restricted to the western valley walls, possibly due some sort of differential melting between the western and eastern sides of the ice tongues. During Stage 2, as the ice receded further south and the proglacial lakes in the northern tributaries became larger, deltas were deposited by meltwater derived from ice in the west and from ice remaining in the upland interfluve areas (Fig. 22, pp. 80).

The most northeasterly segment of the Ravn River Valley was the first to become ice-free, marking the beginning of Glacial Lake Ravn (Phase 1) (Fig. 23, pp. 81). The

lake basin opened as the ice-margin had receded to the south-southwest down the south facing valley walls. Flights of descending kame terraces mark this retreat down the valley wall north of the Ravn-Quernbiter spillway. These terraces were likely deposited when meltwater was flowing between the northern margin of the Paleo-Barnes Ice Cap and the south facing valley wall, into the Quernbiter Valley (similarly described by Ives (1962) in the Isortoq Valley). When the headwaters of the Quernbiter River became ice-free, this bedrock gorge spillway served as the main outlet for water leaving Glacial Lake Ravn. As ice began calving into Glacial Lake Ravn, large icebergs began flowing up-valley towards the spillway outlet where they were later buried and surrounded by a large influx of outwash sediment being discharged from the ice-margin to the south and west. Another possible mode of transportation for the large blocks of ice that stagnated to form the kettles was from a catastrophic flood (jokulhlaup) that may have been caused when ice damming any one of the major northern tributaries was breached, delivering all the ice blocks and sediment during a single event. This may explain the large size of the kettle holes. Glacial Lake Ravn was dammed in the west by the retreating margin of the Paleo-Barnes Ice Cap. Delta 53 (382 m) of km 86, located near the spillway was probably deposited into a small lake pooled in by ice.

As the main ice-margin, with its northward dipping surface, receded into the Ravn River Valley from the uplands and was oriented with its margin sub-parallel to the valley axis, small lakes were dammed between the main ice margin and the northern valley wall. Abundant meltwater spilled in an up-valley direction along the Paleo-Barnes margin, and created kame terraces and upsteam dipping ice-marginal drainage channels. The meltwater continued along the ice margin until it spilled into Glacial Lake Ravn to the

east. This ice configuration resulted in large amounts of glaciofluvial sediments being deposited on the northern valley wall while little was deposited on its southern equivalent.

By the time that the ice-margin had receded to the position of delta 48 at km 72, the lake level was completely controlled by the incision into the Quernbiter bedrock spillway at 300-320 m. Ice that was receding up the southern tributary valleys left stagnating blocks of ice in the Ravn River Valley that obstructed the flow of sediment to their respective deltas and fans. In the majority of the southern tributary valleys, down-valley dipping, ice-marginal meltwater channels were incised, showing the paleo-contours of the southerly receding ice lobes. Minor glacial advances were marked in the southern tributary valleys by the deposition of subaerial moraines. Ice lobes occupying the southern tributary valleys, deposited progressively stacked sequences of outwash terraces in an up-stream direction. The prominent shorelines of Glacial Lake Ravn are primarily confined to northern bank walls and tributaries. This was likely because the lake was initially dammed between the ice-margin and the northern valley walls (as hypothesized by Ives and Andrews (1963)), as well as from the abundant sediments deposited against the northbank allowing prominent glacial lake shorelines to be well developed. The glacial lake shorelines remained at a constant elevation of between 300 and 320 m. This range in elevations signifies the time period when the majority of deltas were deposited into Glacial Lake Ravn due to the close proximity of the Paleo-Barnes ice margin and the probable persistence of uplands ice, and hence, abundant sediment supply. In places where there were no tributary valleys, the main ice margin gradually receded up the southbank walls to the south-southwest as was described by Ives and

Andrews (1963). Large deltas, decreasing in age from east to west were deposited into the lake from southbank tributaries.

Glacial Lake Ravn (Phase 2) was initiated when nearly the entire eastern segment of the Upper Ravn Valley had become ice-free (Fig. 24, pp. 82). The ice margin had thinned to the point that it could no longer recede up the steeper valley walls. A large block of ice may have then detached from the main ice-margin and began to stagnate in situ (also interpretation of Ives and Andrews (1963). At this point, it is proposed that a valley glacier began depositing kame deltas, kame terraces and washed bedrock surfaces as it systematically receded in a down-valley direction. A model for its recession can be seen in Figs. 19 and 20.
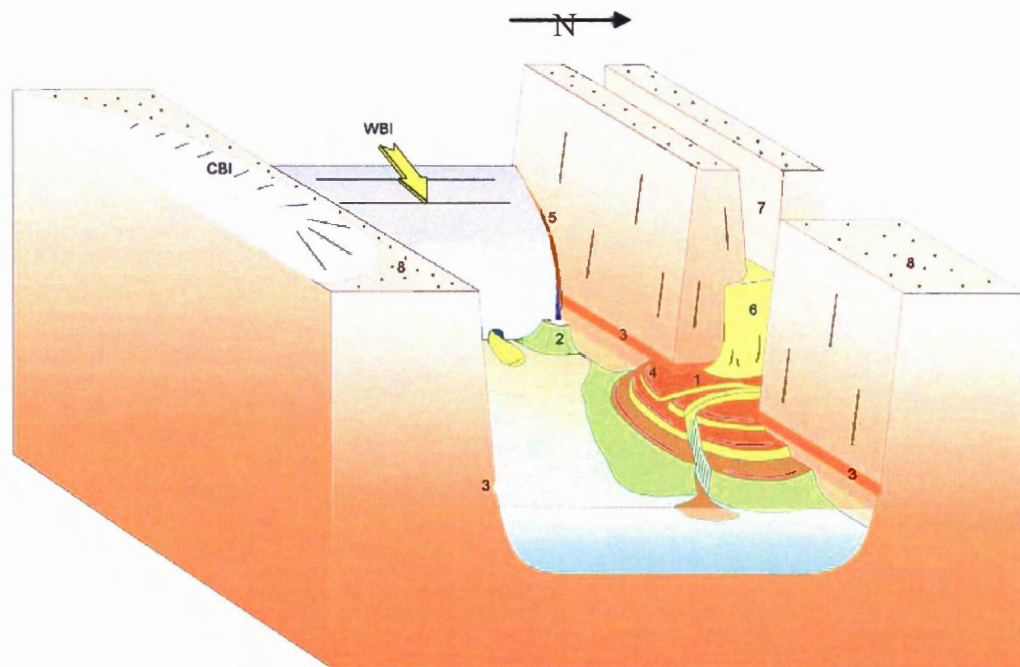
Figure 19: Conceptual model of ice recession in the Ravn River Valley after the inception of a valley glacier retreating systematically down-valley: 1) delta pad with 3 tiers, each reflecting a paleo-lake level; 2) kame delta; 3) glacial lake strandline; 4) beach berm on delta surface; 5) lateral meltwater channel; 6) kame terrace in northern tributary valley; 7) col gully (deeply incised meltwater channel); 8) Uplands surface containing weathered rock felsenmeer; WBI – warm-based ice; CBI - cold-based ice; arrow represents ice-movement direction.
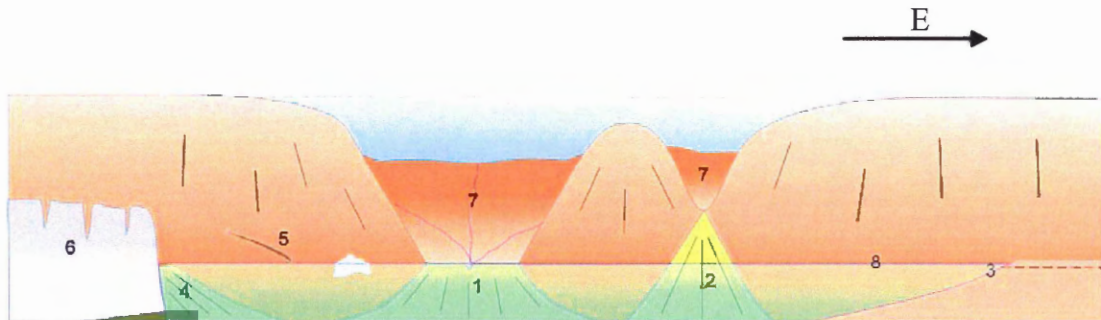
Figure 20: Latitudinal section of the Ravn River Valley after inception of valley glacier: 1) glaciolacustrine delta; 2) alluvial fan; 3) spillway (~310 m); 4) kame delta; 5) lateral meltwater channel; 6) down-valley retreating glacier; 7) northern tributary valley; 8) glacial lake strandline.

As the valley glacier receded to the southwest, the paleo-lake level remained at approximately the 300-320 m level and is shown by long continuous stretches of glacial lake shoreline (although confined to the westbank) and several ice-contact deltas. Small lakes developed against the sides of the valley glacier and perched deltas were deposited within them. As the valley glacier was receding south during Glacial Lake Ravn Phase 3 (Fig. 25, pp. 83), ice in the uplands was receding east as is indicated by glaciofluvial terraces and meltwater channels. Abundant meltwater drainage channels running down eastbank slopes suggest that ice may have remained in the uplands for a significant period of time. The maximal extent of Glacial Lake Ravn at the 300-320 m level was approximately 75 km. As ice continued to dam the lake to the south, the next relatively stable lake level to be formed was at the 268 m level (Fig. 26, pp. 84). Only one delta (282 m), with a possibly eroded slope, was found with an intermediate elevation between 268 and 300 m, suggesting that part of the bedrock spillway may have catastrophically given way and significantly lowered the lake level to 268 m. The period when the lake level was stable at 268 m is Glacial Lake Ravn Phase 4 (Fig. 26). Once the lake level

dropped to below approximately 268 m the Ravn-Quernbiter spillway was abandoned. It is likely that the spillway had subsequently incised to 255 m in a post-lake setting. When the spillway was abandoned during Glacial Lake Ravn Phase 5, the flow of water would have then been directed in a down-valley direction instead of towards the northeast (Fig. 27, pp. 85). An incised bedrock gorge located on the eastbank near the uplands mouth of the Ravn River Valley may then have served as the new glacial lake spillway. The spillway occupied an elevation of approximately 232 m. The elevation for this spillway was chosen because prominent delta 17 was also found at the same elevation. When the Paleo-Barnes Ice Cap receded from the uplands mouth of the Ravn River Valley, Glacial Lake Ravn was subsequently drained.
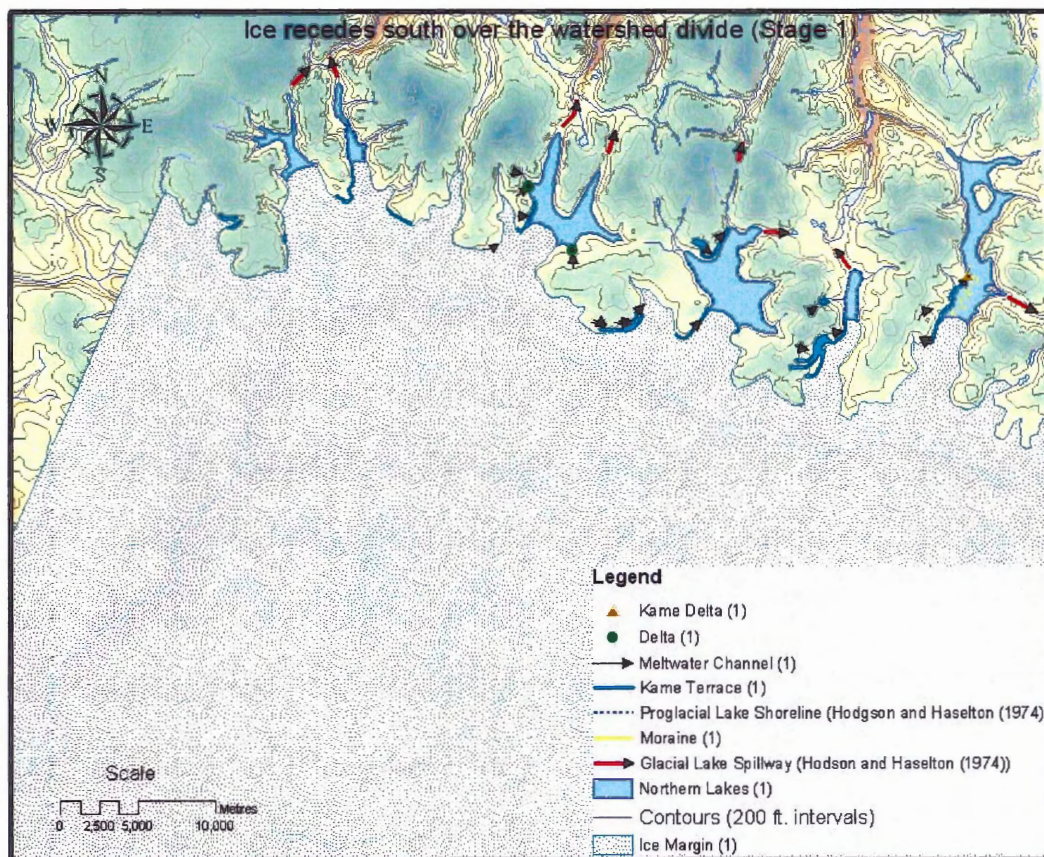
Figure 21: Ice-recession (Stage 1) Conceptual sequential geometry of Paleo-Barnes ice during deglaciation of the Ravn River Valley. As the ice receded over the watershed divide tongues of ice began to stagnate in the northern tributaries of the Ravn River Valley. Meltwater flowing north along the margins of these tongues of ice deposited kame terraces and ultimately deltas into proglacial lakes. The lakes were emptied via spillways noted by Hodgson and Haselton (1974) northwards into Baffin Bay and Eclipse Sound (Ives and Andrews, 1963). Up-valley dipping ice-marginal drainage channels had also been formed by meltwater flowing north during this period. A series of glacial lake shorelines were also observed by Hodgson and Haselton (1974) to have formed during this period. Sublacustrine/cross-valley moraines were deposited in some of the northern valleys. The kame terraces were mostly restricted to the western valley walls.

79
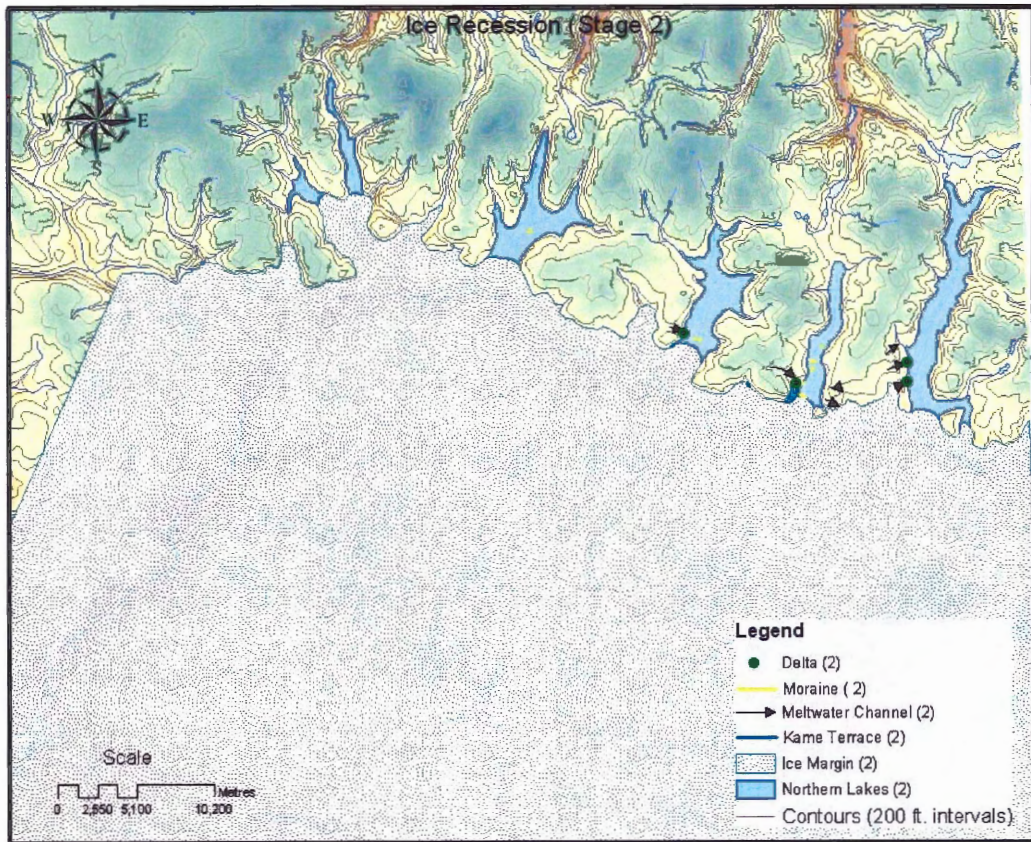
Figure 22: Ice-recession (Stage 2). As the tongues of ice receded south, the northern tributary lakes became larger and deltas were deposited within them. Most of the deltas were deposited on the western sides of the valleys.
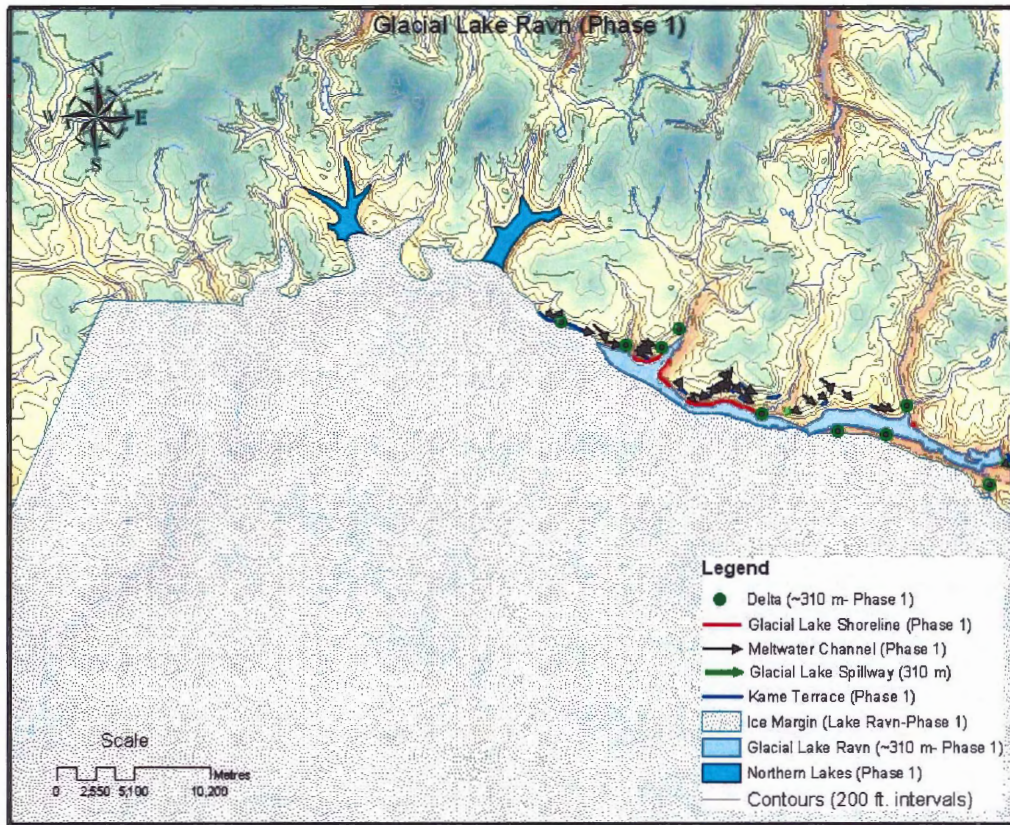
Figure 23: Glacial Lake Ravn (Phase 1). The genesis of Glacial Lake Ravn began as the ice-margin retreated south from the Ravn/Quernbiter spillway at the 300-320 m level. As the Paleo-Barnes ice-margin receded down the Ravn River Valley, small lakes were pooled between it and the northbank valley wall. Meltwater flowed between the ice margin and the northern valley wall, depositing upvalley dipping incised meltwater channels and kame terraces. The water spilled east into Glacial Lake Ravn.
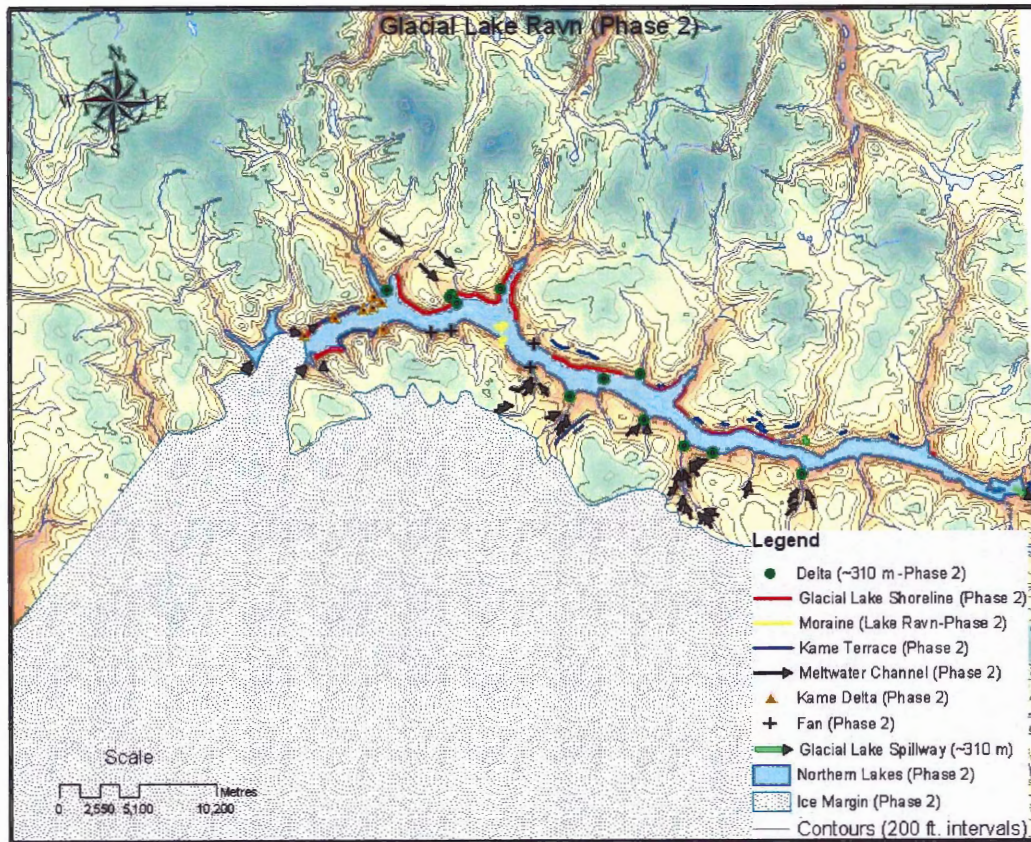
Figure 24: Glacial Lake Ravn (Phase 2). During Phase 2 (lake level 300-320 m), a valley glacier had formed and began to systematically retreat in a down-valley direction. The first evidence for this happening may be at the position of the sublacustrine moraines. Down-valley of kame delta 31 and 32 at 40 km, ice contact deltas and up-valley dipping kame terraces were deposited on both sides of the valley along with the formation of up-valley dipping meltwater channels. A small ice tongue at this time was depositing proglacial delta 29. Areas with one or more large kettle holes are notes on the map.
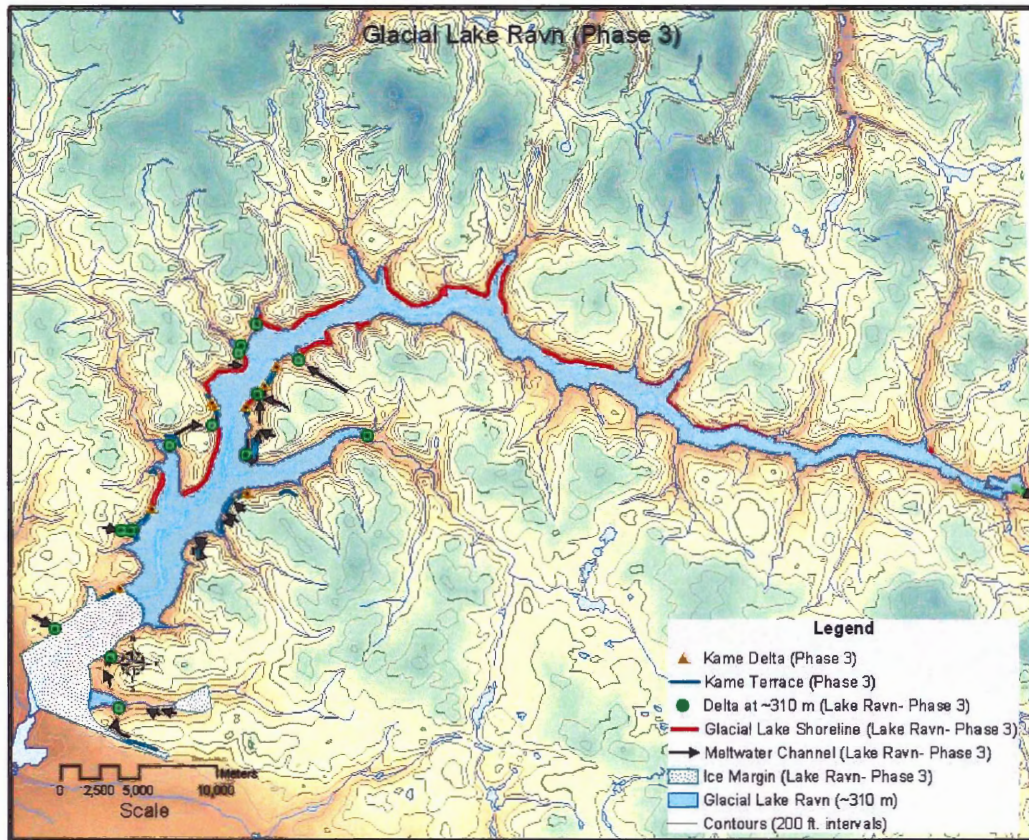
Figure 25: Glacial Lake Ravn (Phase 3). Glacial Lake Ravn has nearly reached its maximum extent of 75 km at the 300-320 m elevation. Perched deltas were deposited in lakes pooled against the sides of the retreating valley-glacier. It is uncertain what the ice configurations were outside of the Ravn River Valley so they were left out of this model.
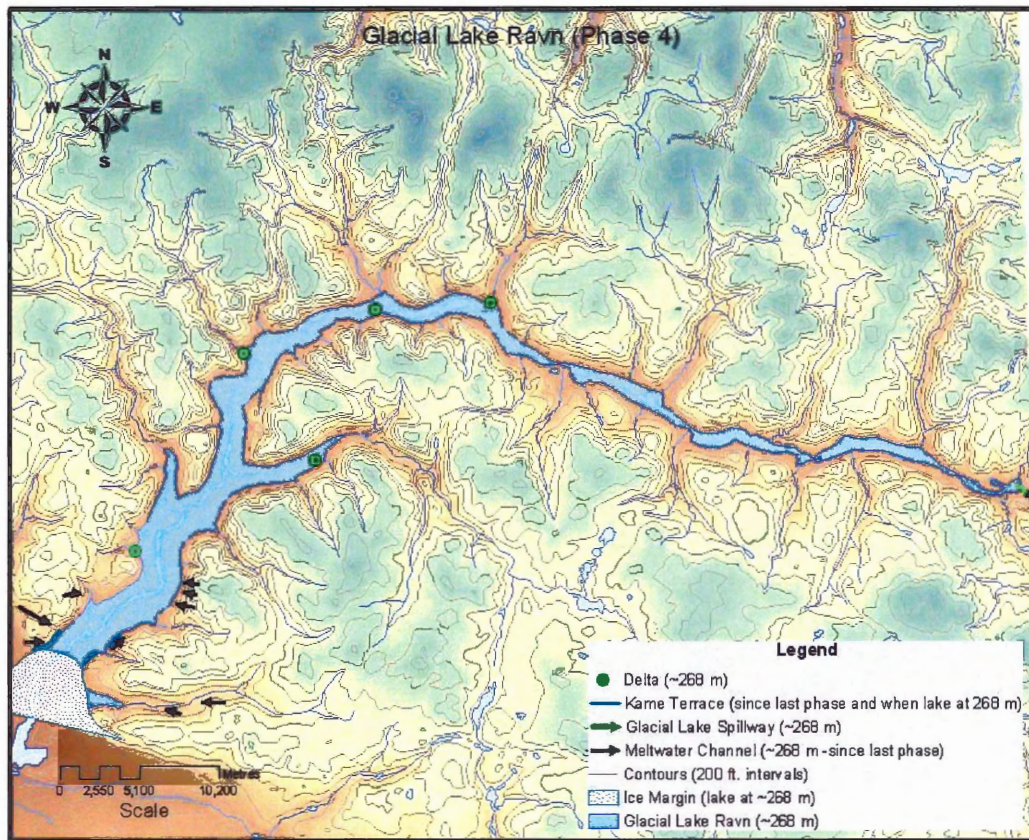
Figure 26: Glacial Lake Ravn (Phase 4). Glacial Lake Ravn is still dammed by ice to the southwest and is still utilizing the Quernbiter spillway as an outlet, however, the lake level has dropped to 268 m. To attain such rapid incision (46 m), this may have been the result of something catastrophically giving way in the spillway. Meltwater channels were deeply incised directly down the eastern valley walls by ice that may have been persisting in the uplands area. It is uncertain what the ice configurations were outside of the Ravn River Valley so they were left out of this model.
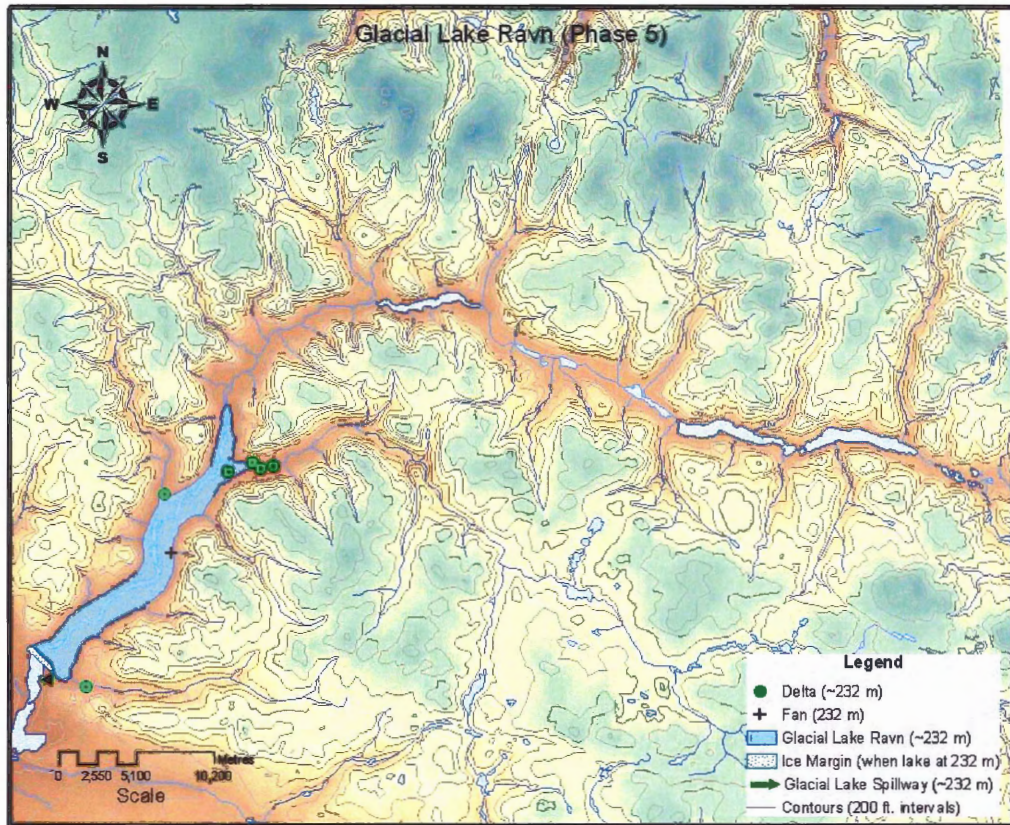
Figure 27: Glacial Lake Ravn (Phase 5). The final stage of Glacial Lake Ravn. The Quernbiter spillway was abandoned once the lake level fell below 268 m in favour of a spillway to the southwest. The new spillway maintained a lake level of approximately 232 m while ice continued to dam the lake to the west. Once ice withdrew from the Lancaster Plateau in the south, Glacial Lake Ravn was subsequently drained. It is uncertain what the ice configurations were outside of the Ravn River Valley so they were left out of this model.

5.2 Delta Cosmogenic Exposure Ages

Based on several criteria, the [10]Be exposure ages (Table 1) obtained for the deltas cannot be correct. Previous studies have shown that the Ravn River Valley area became deglaciated approximately 5.5 to 4.5 ^{14}C ka B.P. (Dyke, 1974). If the exposure ages of this study are considered correct then they are greater than 1 order of magnitude older than what they were originally believed to be. Also, the topography has a fresh appearance and if the surface were in fact 30-40 ka then it would be expected to have been more subdued. Delta 53 is an exception to this and its exposure date of 8.3 ka ± 0.3 ka is interpreted to be the delta's maximum age of deposition. This age may be a little higher than the actual delta age due to a small amount of previous inheritance.

There are three possible reasons why the other exposure dates do not represent the actual delta age of deposition:

1) The sediment samples may have inherited large amounts of [10]Be from previous exposures.

2) Human induced systematic error during the chemical preparation of the samples may have been a factor. One of the possible mistakes may have been from adding tap water to all of the samples, artificially increasing their [10]Be concentrations. If this were the case, the blank should also show a large increase in [10]Be, but it does not.

3) There may have been a systematic AMS problem. The only way for this to be tested is by a reanalysis at a later date. The run after the first batch of samples (3087-3093 + blank) contained sample 3094 (delta 53). 3094 ran well and it was

run on the same wheel immediately after the other samples were done. Therefore, it should have also been affected and it was not.

The preferred interpretation is that inheritance caused the high [10]Be concentrations. If this is the case then the results may prove an advantage for insight into the glaciological processes that have occurred on the Baffin Uplands in the past. By using the estimated time of deglaciation from previous work (~6 ka), the amount of [10]Be that would have been produced in deltas of that age can be subtracted from the amount of measured [10]Be, allowing the amount of pre-depositional inheritance to be calculated for each sediment sample. If the delta ages are taken to be approximately 6 ka, and only the samples taken from topsets are utilized, then the previous inheritance values are as follows (listed in Table 2):

Sample I.D.	Field I.D.	Delta #	Elevation	Feature	Measured [10]Be conc. atoms/g qtz	Inheritance for 6 ka deltas
			(m)			X10[5] atoms/g
1371	Ravn 03-3087-01	17	232	Glaciolacustrine Delta	176318	1.48
1373	Ravn 03-3089-01	25	269	Glaciolacustrine Delta	125098	0.953
1374	Ravn 03-3090-01	29	308	Kame Delta	92247	0.625
1375	Ravn 03-3091-01	31	311	Kame Delta	177154	1.45
1376	Ravn 03-3092-01	33	269	Glacioacustrine Delta	165324	1.36
1377	Ravn 03-3093-01	39	266	Glaciolacustrine Delta	150498	1.22
1378	Ravn 03-3094-01	53	382	Pinned in Lake Delta	44240	0.123

Table 2: Delta topset sample sites. Amount of [10]Be that would have been produced in 6 ka deltas at this latitude and elevation were subtracted from the measured amount of [10]Be in order to obtain the previous inheritance.

When the inheritance is plotted against delta elevation (Fig. 28, pp. 88), the inheritance concentrations appear to decrease with altitude. This trend is counterintuitive since cold-based ice is usually found in the higher elevation upland areas, meaning less erosion and hence, more inheritance. Lower inheritance values should be found at lower elevations where there has been active ice and more erosion and in this case, they are not.

87

If inheritance is plotted against relative age, a weaker trend is also evident (Fig. 29, pp. 89). The relative age represents the order in which the sampled deltas were believed to have been deposited in relation to one other. The oldest delta was assumed to be # 53, followed by the two kame deltas and then the four glaciolacustrine deltas with delta #17 being deposited last. The data show that the inheritance may increase with decreasing relative age. There are too few data points to draw any real conclusions. Also, the source of the deltaic sediments was ultimately from the erosion of the upland areas.

Inheritance vs Elevation
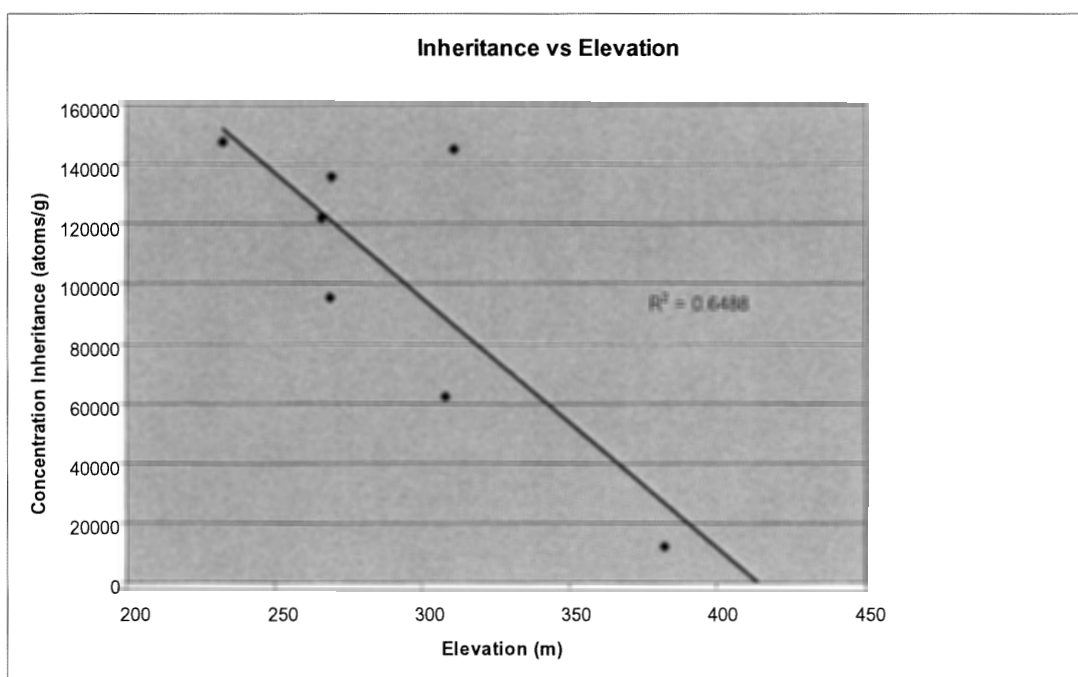
Figure 28: The inherited concentration of ^{10}Be vs. elevation if the estimated concentration for 6 ka deltas is subtracted from the actual values. Concentration is decreasing with elevation.
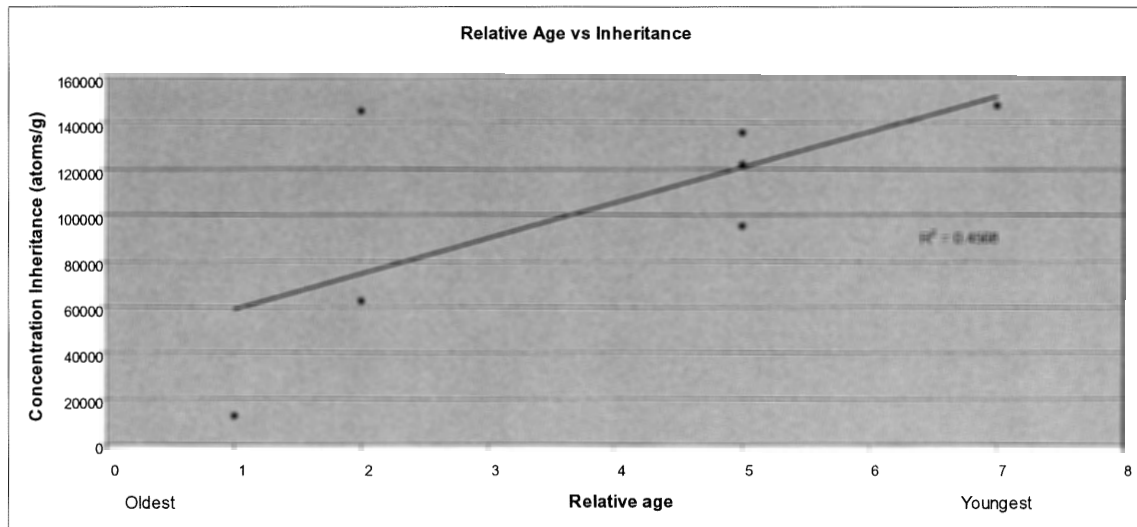
Figure 29: This is a graph showing the inheritance of ^{10}Be in atoms $\cdot g^{-1}$ *vs* relative delta age. A weak trend is evident showing inheritance increasing from left to right with increasing relative delta age. Delta 53 is the oldest, followed by the kame deltas at the 300-320 m lake level, then the glaciolacustrine deltas deposited into the 268 m level and finally the 232 m delta.

5.3 Age of Glacial Lake Ravn

Delta 53 (sample 1378) has an unrealistically high erosion rate and since its exposure age of 8.3 ka ± 0.3 ka is close to the previously hypothesized age of deglaciation for the study area, it will be interpreted to be the age of the delta (lake). Sample 1378 may have had some inheritance, so 8.3 ± 0.3 ka is likely to be a maximum age for Glacial Lake Ravn.

5.4 Erosion Rates for the Baffin Uplands

The provenance of the deltaic sediments was from the glacially eroded upland areas. Therefore, the erosion rates (Table 3 and Fig. 30) will be representative of the average long term steady state erosion of the North Baffin Uplands.

| CNEF ID | Sample ID | Delta # | Plateau | | Production Rate | Meas Concentration | Inherited Conc [10]Be | Erosion Rate | |
			Lat (deg)	Elev (km)	at/g/yr	10Be in qtz	adj for 6ka	cm/yr	m/Myr
1371	Ravn 03-3087-01	17	71	0.67	9.2	176318	147586	0.0038	38
1373	Ravn 03-3089-01	25	71	0.67	9.2	125098	95276	0.0060	60
1374	Ravn 03-3090-01	29	71	0.67	9.2	92247	62490	0.0091	91
1375	Ravn 03-3091-01	31	71	0.67	9.2	177154	145141	0.0039	39
1376	Ravn 03-3092-01	33	71	0.67	9.2	165324	135627	0.0042	42
1377	Ravn 03-3093-01	39	71	0.67	9.2	150498	121985	0.0046	46
1378	Ravn 03-3094-01	53	71	0.67	9.2	44240	12306	0.0461	461

Table 3: Erosion rates for 7 of the 8 delta sample sites. The average elevation of the uplands plateau was estimated to be 670 m. Sample 1378 is believed to have had little inheritance and its [10]Be concentration is thought to represent the maximum exposure age of the delta. The other erosion rates are reasonable estimates for bedrock that is affected by zones of both cold and wet-based ice that have been known to frequently occur on Baffin Island.
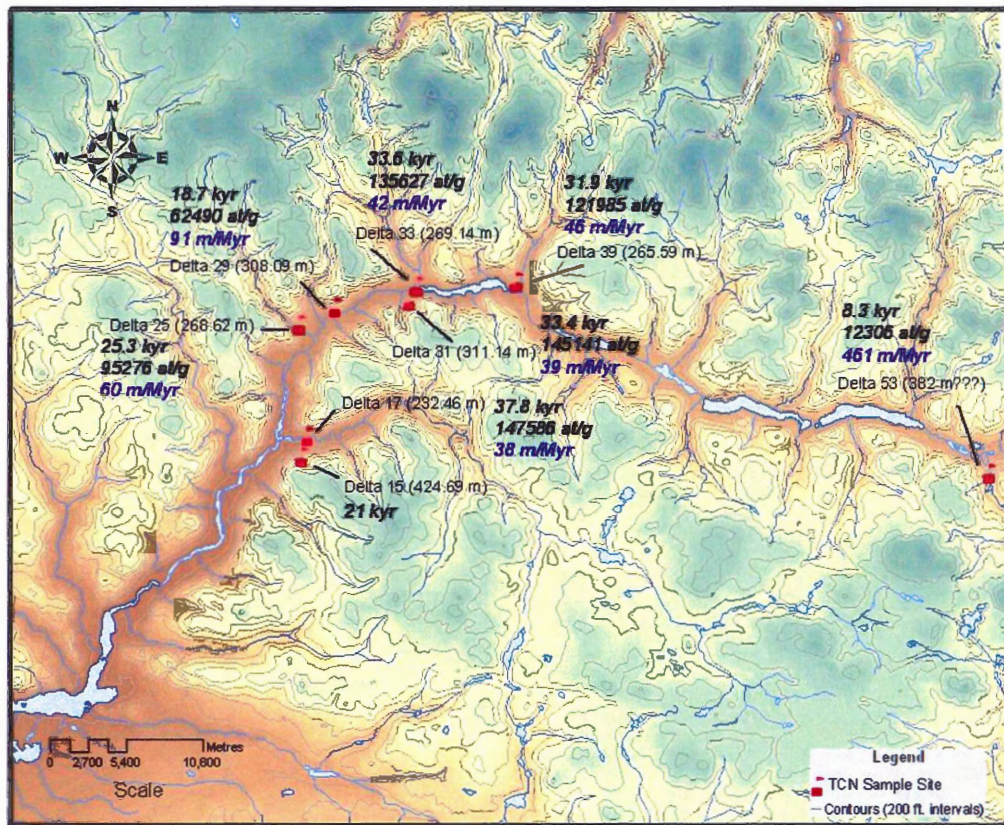
Figure 30: Delta topset sample site locations (with the exception of the boulder) with their corresponding; exposure ages (kyr), estimated previous inheritance (atoms/g) and erosion rates (metres / million years). The mean erosion rate for the uplands plateau ranges from 38 to 91 m/Myr. Delta 53 does not give an erosion rate but the time that the delta was deposited.

The erosion rates are slow to intermediate and range from 38 to 91 m/Myr. This makes sense because the North Baffin Uplands was previously known to have been frequently covered by both cold-based (non-erosive) and warm-based (erosive) ice. Cold-based ice was protecting the underlying uplands surface, preventing it from losing a substantial amount of its accumulated inheritance while active ice was periodically eroding it. Samples 1373 and 1374 (from deltas 25 and 29 respectively), have relatively high erosion rates. Delta 25 is glaciolacustrine and # 29 is ice-contact. They are both

91

found on the northbank of the Ravn River Valley and have lower amounts of ^{10}Be inheritance in their sediments. There are several possible reasons for these anomalies:

1) The sediments that fed into deltas 29 and 25 were eroded from bedrock that was at a lower elevation than the rest of the samples, causing them to have lower production rates and less inheritance. However, this is not the case for delta 25 because its catchment reaches to a high upland area. For delta 29 it is difficult to judge whether or not this is the case because it was a kame delta, with no indication of original sediment provinance.

2) The catchment for delta 25 and the original sediment source(s) (non-glacial) of delta 29 were more highly eroded than the other areas, erasing much of their previous inheritances. It is inconclusive of whether or not this is the case for either delta.

5.5 Erosion Rate into the Ravn-Quernbiter Spillway

A minimum estimate for the erosion rate into the Ravn-Quernbiter spillway can also be calculated. We can assume that the spillway was first activated during the existence of Glacial Lake Ravn (8.3 ka ± 0.3 ka). The upper spillway strath is found at 301 m while the spillway bottom is found at 255 m, meaning that the spillway has incised a minimum of 46 m since its inception. A minimum average incision rate estimate of 5.5 m/ka is obtained. This is a minimum estimate because the spillway would have been incising at a more rapid rate when it served as the outlet for a Glacial Lake Ravn. There is also a possibility that the spillway may have catastrophically given way during an instantaneous event between the 301 m and 268 m lake levels. Also, the 8.3 ka ± 0.3 ka delta has had

some previous inheritance, meaning that the lake is slightly younger than 8.3 ka ± 0.3 ka, which would increase the incision rate.

Chapter 6: Conclusions

The deglacial history for the Ravn River Valley began when the Paleo-Barnes Ice Cap receded south from the regional watershed divide, allowing tongues of ice to melt and recede from the northern tributary valleys. As the Paleo-Barnes margin receded to the south-southwest, the Ravn River Valley was deglaciated from east to west. Glacial Lake Ravn was initially dammed between the Paleo-Barnes ice-margin and the northern valley wall. A valley glacier later developed and began to systematically retreat in a down-valley direction. Glacial Lake Ravn was maintained at the level of the Ravn-Quernbiter spillway (300-320 m) until it gave way and a new 268 m stillstand was established. Once the spillway dropped to below approximately 268 m, a new spillway was utilized to the southwest and remained as the main outlet until the valley was completely ice-free, allowing the lake to drain.

My hypothesis was that the concentrations of [10]Be within delta topset beds represented the age of a former ice-dammed lake within the Ravn River Valley and the time that the Paleo-Barnes ice-margin was receding from the North Baffin Upland area. Seven of the eight samples were not representative of delta exposure ages because it is believed they had high inheritance levels of [10]Be. This study demonstrates the difficulty in TCN exposure dating of sediments and boulders derived from surfaces that have been covered with (and protected by) cold-based ice. Felsenmeer was observed elsewhere in the uplands and is also an indication of cold-based glaciation. Six of the topsets sampled likely represent an average erosion rate for the Baffin Uplands area that ranged from 38 to 91 m/Myr. The range in erosion rates can be explained by the temporal and spatial variations of both warm and cold-based ice throughout the ancient history Baffin

94

Upland's, creating differential (patchy) rates of erosion. One of the deltas yielded a maximum age of 8.3 ka ± 0.3 ka for Glacial Lake Ravn and it is consistent with Dyke et al. (2003), considering a small amount of inheritence. So, the possibility exists that TCN exposure dating of deltas in environments dominated by warm-based ice conditions will be successful. However, when dating deltas in areas that were once host to cold-based ice, high inheritance values must be taken into account. Using the maximum age of the lake, the Ravn-Quernbiter spillway has been incising a minimum of 5.5 m/ka since the existence of Glacial Lake Ravn.

Future Work

The surficial mapping component of this study was a success and the results may be incorporated into and/or used for other mapping projects conducted in the North Baffin Region. In future research it will also be important to verify whether or not the TCN values for the Baffin Uplands are in fact inheritance values. This can be done by reprocessing some of the remaining samples by following the same chemical procedures and then running them through the AMS. If they do represent inheritance values then this will have large implications for the way TCN dating is conducted in the Arctic.

References

- Anderson, R.S., Repka, J.L., and Dick, G.S., 1996. Explicit treatment of inheritance in dating depositional surfaces using in situ ^{10}Be and ^{26}Al: Geology, v. 24, p. 47-51.

- Andrews, J.T., 1989. Quaternary geology of the northeastern Canadian Shield (see Dyke et al., 1989).

- Andrews, J.T., 1982b. Holocene glacier variations in the eastern Canadian Arctic: A review; Striae, v.18, p. 9-14.

- Andrews, J.T., Barnett, D.M., 1979. Holocene (Neoglacial) moraine and proglacial lake chronology, Barnes Ice Cap, Canada. Boreas (8) 341-358.

- Andrews, J.T., and Smithson, B.B., 1966. Till fabrics of the cross-valley moraines of north-central Baffin Island, N.W.T., Canada; Geological Society of America, Bulletin, v. 77, p. 271-290.

- Andrews, J.T.,1963. Cross-valley moraines of the Rimrock and Isortoq River Valleys, Baffin Island, N.W.T.: a descriptive analysis; Geographical Bulletin, 19. p. 49-76.

- Barnett, D.M. and Holdsworth, G., 1974. Origin, morphology, and chronology of sublacustrine moraines, Generator Lake, Baffin Island, Northwest Territories, Canada; Canadian Journal of Earth Sciences, v. 11, p. 380-408.

- Benn, D., Evans, D.J., 1998. Glaciers and Glaciation. Arnold, London, U.K.

- Bierman, P.R., Marsella, K.A., Patterson, C., Davis, P.T., Caffee, M., 1999. Mid-Pleistocene cosmogenic minimum-age limits for pre-Wisconsinan glacial surfaces in southwestern Minnesota and southern Baffin Island: a multiple nuclide approach. Geomorphology 27, 25-39.

- Blake, W., Jr., 1966. End moraines and deglaciation chronology in northern Canada with special reference to southern Baffin Island; Geological Survey of Canada, Paper 66-26, 31 p.

- Briner, J.P., Miller, G.H., Davis, P.T., Bierman, P.R., Caffee, M., 2003. Last Glacial Maximum ice sheet dynamics in Arctic Canada inferred from young erratics perched on ancient tors; Quaternary Science Reviews, no.22, p. 437-444.

- Davis, P.T., Briner, J.P., Miller, G.H., Coulthard, R.D., Bierman, P., Finkel, R.W., 2002. Huge >54 000 Yr old glaciomarine delta on northern Baffin Island overlain by boulders with <20 000 Yr old cosmogenic exposure ages: implications for non-erosive cold-based ice on Baffin Island during the LGM. (Abstract) Geological Society of America, Annual Meeting (October 27-30, 2002) Denver, Colorado.

- Dyke, A.S. (compiler); Moore, A (compiler); Robertson, L (compiler). 2003. Deglaciation of North America. Open-File Report - Geological Survey of Canada, Report: 1574, 1 disc.

- Dyke, A.S., Prest, V.K., 1987. Late-Wisconsinan and Holocene history of the Laurentide Ice Sheet; Geographie physique et Quaternaire 41, 237-263.

- Dyke, A.S., Andrews, J.T., Clark, P.U., England, J.H., Miller, G.H., Shaw, J., Veillette, J.J., 2002. The Laurentide and Innuitian Ice Sheets during the last glacial maximum; Quaternary Science Reviews, 21 9-31.

- Dyke, A.S., Hooper, J., 2001. Deglaciation of northwestern Baffin Island, Nunavut, Canada, Map 1999A, scale 1: 500 000.

- Dyke, A.S., 2000. Surficial Geology, Navy Board Inlet, Baffin Island, Nunavut, Canada. Geological Survey of Canada, Map 1965A, scale 1: 250 000.

- Dyke, A.S., Vincent, J-S., Andrews, J.T., Dredge, L.A., Cowan, W.R., 1989. The Laurentide Ice Sheet and an introduction to the Quaternary Geology of the Canadian Shield. Chapter 3 in Quaternary Geology of Canada and Greenland, R.J. Fulton (Ed); Geological Survey of Canada, Geology of Canada, no. 1.

- Dyke, A.S., 1977, Quaternary geomorphology, glacial chronology, and climatic and sea-level history of southwestern Cumberland Peninsula, Baffin Island, Northwest Territories, Canada [Phd. Dissert.]: Boulder, University of Colorado, 184 p.

- Dyke, A.S., 1974. Deglacial chronology and uplift history: northeastern sector, Laurentide Ice Sheet; institute of Arctic and Alpine Research, University of Colorado, Occasional Paper, v.12, 73p.

- Eyles, N., Eyles, C.H., Glacial depositional systems. In Facies Models by Walker, R.G. and James, N.P.: Terrigenous clastic facies models. Geological Association of Canada, June 1992.

- Flint, R.F., 1943. Growth of the North American Ice Sheet during the Wisconsinan Age; Geological Society of America, Bulletin, v.54, p.39-53.

- Goldthwait, R.P., 1951: Development of end-moraines in east-central Baffin Island. J. Geol. 70. 737-753.

- Gosse, J.C., 1994. Alpine glacial history reconstruction: 1. Application of the cosmogenic 10Be exposure age method to determine the glacial chronology of the Wind River Mountains, Wyoming, USA; 2. Relative dating of Quaternary deposits in the Rio Atuel Valley, Mendoza, Argentina. Dissertation Thesis, Lehigh University.

- Gosse, J.C., Klein, J., Evenson, E B., Lawn, B., Middleton, R. 1995. Beryllium-10 dating of the duration and retreat of the last Pinedale glacial sequence. Science, vol.268, no.5215, pp.1329-1333.

- Gosse, J.C. and F. M. Phillips, 2001. Terrestrial in situ cosmogenic nuclides: theory and application. Quaternary Science Reviews (20) 1475-1560.

- Hodgson, D.A., Haselton, G.M., 1974. Reconnaissance glacial geology, northeastern Baffin Island; Geological Survey of Canada, Paper 74-20, 10p.

- Holden, N.E., 1990. Total half-lives for selected nuclides. Pure and applied chemistry 62 (5), 941-958.

- IPCC Intergovernmental Panel on Climate Change 2001. Climate Change 2000 –Third Assessment Report, Cambridge University Press.

- Institute of Arctic and Alpine Research. DEM Map of Baffin Island. (INSTAAR: http://instaar.colorado. edu/cosmolab/BI_CE_database /maps/map.html).

- Ives, J.D., Andrews, J.T., 1963. Studies in the physical geography of north-central Baffin Island, N.W.T.; Geographical Bulletin 19, 5-48

- Ives, J., 1962. Indications of recent extensive glacierization in north-central Baffin Island, N.W.T. Journal of Glaciology, vol.4, no.32, pp.197-205.

- Jennings, A.E., Tedesco, K.A., Andrews, J.T., Kirby, M.E., 1996. Shelf erosion and glacial ice proximity in the Labrador Sea during Heinrich events (H-3 or 4 to H-O) as shown by foraminifera. In: Andrews, J.T., Austin, W.E.N., Bergsten, H., Jennings, A.E. (Eds), Late Quaternary Paleoceanography of the North Atlantic Margins. Geological Society Special Publications, London, pp. 29-49.

- Jennings, A.E.,1993. The Quaternary history of Cumberland Sound, Southeastern Baffin Island: the marine evidence; Geographie physique et Quaternaire 47, 21-42.

- Johannessen, Ola., Bengtsson, L., Miles, M.W., Kuzmina, S.I., Semenov, V.A., Alekseev, G.V., Nagurnyi, A.P., Zakharov, V.F., Bobylev, L., Pettersson, L.H., Hasselmann, K., Cattle, H.P., 2002. Arctic climate change- observed and modeled temperature and sea ice variability. Nansen Environmental and Remote Sensing Centre, Technical report No. 218 Bergen, http://www.nersc.no/AICSEX/rep218.pdf.

- Kaplan, M.R., Miller, G.H., Steig, E.J., 2001. Low-gradient outlet glaciers (ice-streams?) drained the Laurentide ice sheet; Geology; vol. 29; no. 4; p. 343-346.

- Kim, J., Englert, P.A.J., Finkel, R., Krofcheck, D., 1999. Cosmic-ray-induced [10]Be and 26Al in subsurface samples from Macraes Flat, East Otago, New Zealand. EOS, Transactions American Geophysical Union 80 (17), F1166-F1167.

- Lingenfelter, R.E., and Flamm, E.J., 1964. Solar neutrons and the earth radiation belts. Science 144, 292-294.

- Little, Edward C., Phillip J. Holme., Andrew C. Hilchey., and Mike Young. 2004. Glacial Geology, Ice-Movement Chronology and Drift Prospecting in the Vicinity of Icebound Lakes (NTS 37G), Northern Baffin Island, Nunavut. GSC Current Research Paper (In Press).

- Loken, O.H., 1966. Baffin Island refugia older than 54,000 years. Science 153, 1378-1380.

- Maclean, B., Williams, G.L., Jennings, A.E., Blakeney, C., 1986. Bedrock and surficial geology of Cumberland Sound, N.W.T. Geological Survey of Canada, Ottawa.

- Miller, G.H., Alexander, P.W., Steig, E.J., Sauer, P.E., Kaplan, M.R., Briner, J.P., 2002 The Goldilocks dilemma: big ice, little ice, or "just-right" ice in the Eastern Canadian Arctic. Quaternary Science Reviews 21 (2002) 33-48.

- Miller, G.H., Mode, W.N., Wolfe, A.P., Sauer, P.E., Bennike, O., Forman, S.L., Short, S.K., Stafford Jr., T.W., 1999. Stratified interglacial lacustrine sediments from Baffin Island, Arctic Canada: chronology and paleoenvironmental implications. Quaternary Science Reviews, 789-810.

- Marsalla, K.A., Bierman, P.R., Davis, P.T., Caffee, M.W., 2000. Cosmogenic 10Be and 26Al ages for the last glacial maximum, eastern Baffin Island, Arctic Canada. Geological Society of America Bulletin 112, 1296-1312.

- Praeg, D.B., MacLean, B., Hardy, I.A., Mudie, P.J., 1986. Quaternary geology of the southeast Baffin Island continental shelf, N.W.T. Geological Society of Canada Special Paper 85-1.

- Smart, D.F. and Shea, M.A. (Ed.), 1985. Galactic cosmic radiation and solar energetic particles. Handbook of Geophysics and the Space Environment. Air Force Geophysics Laboratory, 6-1-6-29 pp.

- Stone, J.O., 1999. A consistant Be-10 production rate in quartz-muons and altitude scaling. AMS-8 Proceedings Abstract Volume, Vienna, Austria.

- Wolfe, Alexander P and King, Roger H., 1999. A paleolimnological constraint to the extent of the last glaciation on northern Devon Island, Canadian High Arctic. Quaternary Science Reviews, vol.18, no.14, pp.1563-1568.

- Zentmire, K.N., Gosse, J.C., Baker, C., McDonald, E., and Wells, S., 1999. The problem of inheritance when dating alluvial fans and terraces with TCN: Insight from the Matanuska Glacier. GSA Abstracts and Programs, 31.

Appendix 1: Sampled Delta Observations

Delta 15 (424.69 m) is situated on the southern valley wall at the mouth of the large western tributary draining into the Ravn Valley (see figure 31). As discussed earlier this delta was deposited into a smaller lake pinned in between the side of a glacier in the valley and the valley wall. This may also have been a kame delta fed by a kame terrace because it has elongated irregular outline. There was a cobble beach berm on the delta surface that had a large boulder of granite gneiss resting on top of it.

The boulder was resting 30 m from the nearest colluvial apron so a colluvial source cannot be rules out. The boulder's dimensions were 60-120 cm and it is too large to suggest that it was emplaced by frost heave. Snow cover and neutron leakage is likely a factor since it is less than 2 m tall. A sample that was 5 cm thick was trimmed of the top of the boulder more than 10 cm from any of the boulder edges.
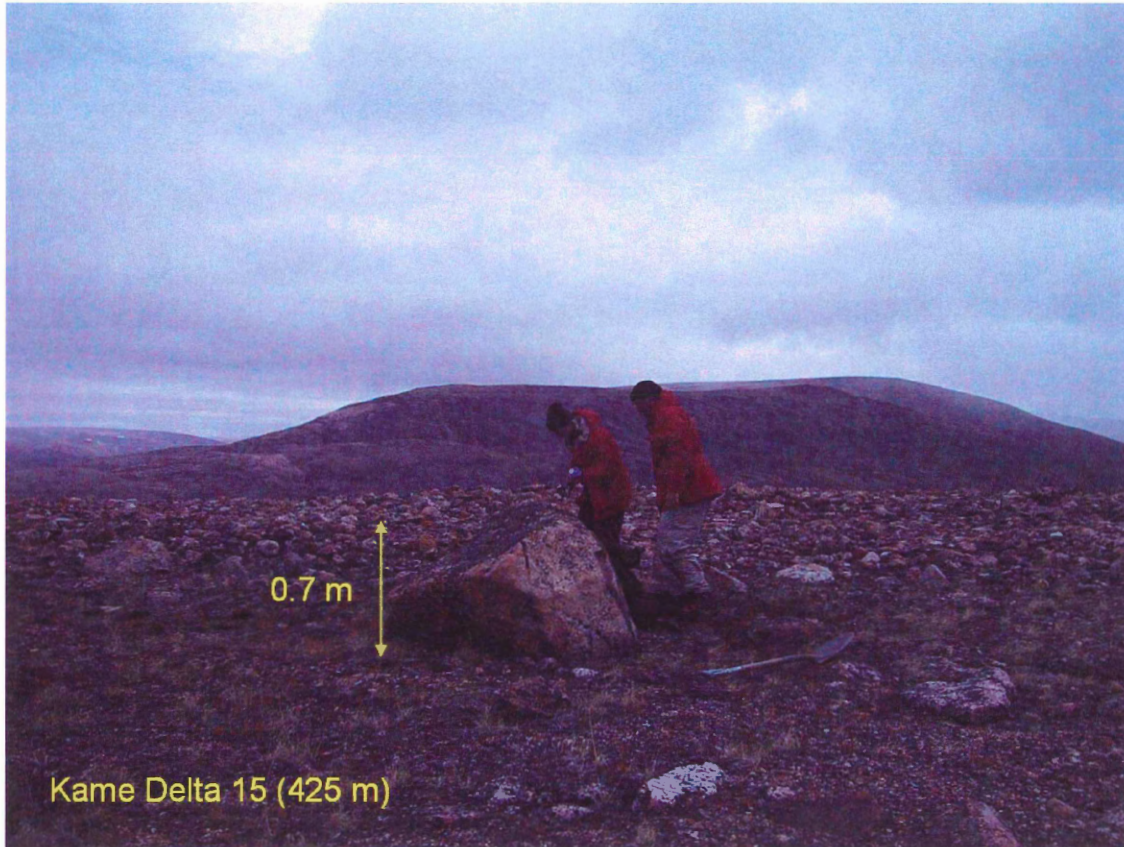
Figure 31: View at km 24 looking north from kame delta 15 (425 m). It is associated with nearby kame terraces and was probably deposited in a smaller lake pinned-in by ice occupying the Ravn Valley. This picture shows a granite gneiss boulder sampled for cosmogenic exposure dating. It was 30 m away from the nearest colluvial apron.

Delta 17 (232.47 m) is found at the mouth of the large western tributary north of delta 15, in the valley bottom. The surface of the delta was comprised of a pebble-gravel sand. A sample was taken 15 m from the nearest delta cut and in the centre of a large 12 m wide polygon. Horizontal fining upwards topset layers were identified below the surface along with 1.5 cm thick heavy mineral laminations. The depth to the top of the sample layer was 27 cm and its thickness was 3 cm.

Delta 25 (269 m) eminated from a northern tributary just east of the major SW bend in the Ravn Valley. The surface of the delta was covered by a deflated pebbly-gravel. Horizontal topset layers were identified and sampled (see figures 32 and 18).

101

The depth to the top of the sample zone was 26 cm and its thickness was 4 cm. Above, the delta to the northwest there were two more delta pads eminating from the same tribuatary. Delta 24 has an elevation of 311 m and the other delta pad to the east across the tributary has an elevation that is slightly lower. The delta pad between deltas 24 and 25 had its foresets dipping in an upstream direction.

Figure 32: Figure showing the extensive lichen cover on the surface of delta 25. A stable environment shows that little erosion has taken place on the delta surface, increasing its potential for TCN exposure dating.

Delta 29 (310 m) has a surface comprised of a deflated cobbly lag. The sand underneath with matrix supported gravel and cobble clasts is medium to coarse grained and has fining upwards sequences. A sample was taken from a horizontal topset layer. The depth to the top of the sample is 30 cm and the sample zone itself is approximately 4

102

cm thick. The sample site is located 10 m from the edge of the nearest polygon. The
surface of the delta contains a beach berm and elevated lateral meltwater channel above it
that dips 2-3 degrees upstream (see figure 33). Above the lateral meltwater channel there
is a washed bedrock surface.

Figure 33: Kame delta 29 (308 m) is located on a north bank valley wall at km 35. Ice was
resting in a downvalley position when the delta was deposited. A col gully also fed the kame
delta from an adjacent tributary valley. Above the delta surface there is a near-horizontal and
flat glacial lake strandline and up-valley dipping lateral meltwater channels. Above the upper
channel there is a glaciofluvially washed bedrock surface.

Delta 31 (311 m) is found on the south bank and is comprised of a pebbly –gravel

sand. The sand is medium to coarse and is well sorted. Clasts (pebble size and greater)

comprise 25 % of the sediment and are angular to subrounded in shape with the average

being subrounded. A sample was taken 4 m from the nearest polygon edge. The depth to

the top of the sample was 22 cm and its thickness was 5 cm. Above the delta top is a

lateral meltwater channel that is dipping 2-3 degrees upstream (figure 34).

103

Figure 34: Looking south across kame delta 31 at km 40. Kame delta 31 had its sediment obstructed by ice that was resting downvalley in the depression to the right of Dr. Gosse. The horizontal strandline in the distance was probably also a kame-terrace like feature that was graded to the level of the lake. As water flowed around the ice mass or lobe it was deposited infront, as delta 31 with foresets dipping up-valley.

Delta 33 (269.14 m) is located in the centre of the valley. It was approximately 150 m wide from west to east and foresets and underlying bottomsets (lake bottom sediments- Fig. 36) were easily identified. There was an eolian veneer on the downwind western side of the valley that was comprised of structureless sand (Fig. 35). The eastern side of the delta had no eolian veneer and has probably remained this way since it was exposed. Sediment suspended by wind coming down the valley would have been deflected up by the delta and deposited on the downwind side. The delta surface was comprised of a deflated pebble gravel. There was good to very good lichen cover on the

104

clasts indicating stability. A sample was taken on the eastern end, 3 m from the nearest frost crack. Topset layers below the mixed zone were comprised of a medium to coarse sand. The depth to the sample top was 26 cm and the thickness was 5 cm.
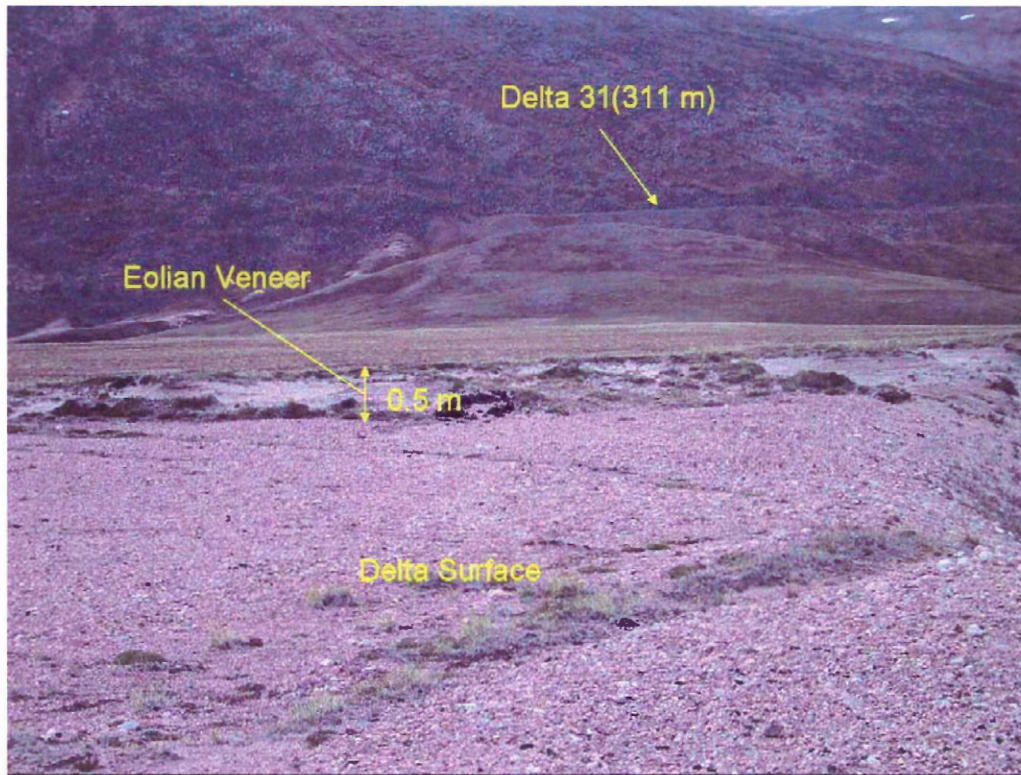
Figure 35: Looking south from delta 33 (269 m), towards delta 31. The down-valley side of the delta was capped by a structureless eolian veneer of fine sand. It was only deposited on this side because as the prevailing wind swept down-valley it blew over the top of the up-valley side of the delta, depositing its bedload on the downwind side of the delta. It was estimated that the upwind side of the delta had always remained uncovered. Places with evidence of having had an eolian veneer were avoided when TCN sampling.

Figure 36: Bottomsets deposited at the base of delta 33. They appear comprise a darker, silty mud.

Delta 39 (282 m) has a surface composed of a deflated pebble gravel with lichen cover. The sample was taken from topset layers that were comprised of medium to coarse grained sand with approximately 20 % clasts (>=pebble). The depth to the top of the sample was 30 cm and its thickness was 5 cm. There is also a prominent strandline associated with it.

Figure 37: View looking north towards deltas 38 and 39 from the top of a sublacustrine moraine at the bottom of the Ravn Valley at km 48.5. A prominent strandline can be traced from the surface of delta 38 in a westerly direction to the left.

Delta 53 is located just to the southwest of the entrance to the former Quernbiter spillway in a small tributary that is highly kettled. The surface is comprised of a pebbly-gravel deflation lag. The underlying sand is medium to coarse and it is well sorted. The clasts comprise 10% of the sediment and they were subrounded to subangular. The clasts on the surface contained lichen cover. A sample was taken 1 m from the nearest frost crack below the mixed zone at a depth of 29 cm and had a thickness of 5 cm.

Appendix 2: Background for Cosmogenic Nuclide Exposure Dating

Galactic cosmic rays (GCR) are highly energetic particles derived mostly from outside our solar system, mainly from within the Milky Way Galaxy (Lingenfelter and Flamm (1964) in Gosse and Phillips (2001)). These rays are comprised of several different types of particles that include 83% protons (nucleons), 13% α-particles, 1% heavy nuclei and 3% electrons (Smart and Shea, 1985). When GCR reach the Earth's geomagnetic field and enter the atmosphere they interact with target nuclei, producing a series of secondary particles that progressively decrease in energy and eventually penetrate up to tens of metres (muon particles) into the Earth's surface. Many of the cosmic rays, after interacting with the atmosphere, are reflected back into outer-space (Gosse and Phillips, 2001). When the primaries or secondaries interact with a target nucleus, a spallation reaction occurs. The collision shatters the target nucleus and it may release several kinds of lighter particles, one being a smaller nucleus (cosmogenic nuclide) and if the atom was large, several nuclei. Secondary particles produced from these atomic impacts are primarily neutrons but also include π +/- and κ +/- mesons (Gosse and Phillips, 2001). Mesons can then decay into muons with masses 207 times smaller than that of an electron and half lives of 10^{-6}s. As the secondary nucleons spall with target nuclei, their energy is dissipated through the transfer of momentum to the shattered particles (Gosse and Phillips, 2001). As the nucleons gradually lose their energy, they pass from the epithermal neutron state (~ 0.1 MeV and 0.5 eV) to the thermal neutron energy state (~ 0.025 eV). The thermal neutrons may then be captured by the nuclei of other atoms, producing a cosmogenic nuclide. ^{10}Be tends to be primarily

produced from spallation reactions while ^{36}Cl has a large proportion of its nuclides produced from thermal neutron absorption (Gosse and Phillips, 2001).

Terrestrial cosmogenic nuclides (TCN) are atomic species that are produced *in situ* within minerals at and below the Earth's surface (Gosse and Phillips, 2001). TCN are generated by a series of interactions between GCR, the atmosphere and subsequently, rock material. When a secondary high energy particle shatters a target nucleus through spallation, it is most likely that a nucleus with a smaller but similar atomic number will be produced along with a nucleus with a much smaller atomic number. Gosse and Phillips (2001) noted that with ^{28}Si as a target atom, nuclei with atomic numbers between 27-25 and 1-3 will be favoured, increasing the amounts of ^{26}Al generated over ^{10}Be. This process is biased towards the creation of ^{26}Al because the chances are greater for the nucleon to chip off tiny particles from the target nucleus during collision than to split it in half. Muons are less reactive and can penetrate more deeply into the earth's surface than spallation reactions. Negative muons can produce TCN through being absorbed into a positively charged nuclei producing ^{10}Be, ^{26}Al, ^{36}Cl and other cosmogenic isotopes (Gosse and Phillips, 2001). Spallation reactions and muonic interactions with Si and O atoms are the most common producers of ^{10}Be in quartz. High energy muons may also induce spallogenic reactions to occur. The attenuation length for muons is approximately 1500 g cm^{-2}.

The production rate of a nuclide is the rate at which a certain nuclide is generated within a specific mineral phase and is measured in atoms per gram of matter per year. This study is only interested in cosmogenic ^{10}Be produced in quartz with a half-life of approximately 1.52 Myr (Holden, 1990 in Gosse and Phillips, 2001). The average ^{10}Be

production rate in quartz is approximately 5.1 +/-3 [10]Be atoms g^{-1} yr^{-1} (Stone, 1999 in Gosse and Phillips, 2001).). The following equation given in Gosse and Phillips (2001) is used to calculate the production rate due to spallation for a given nuclide:

$$P^{(Z)}_{s,m} = \psi^{(0)}_{m,k} C_k \, e^{\left[\frac{[-z]}{A_f}\right]}$$

P is the spallation production rate of nuclide m at depth z. $\psi_{m,k}$ is the production rate of the nuclide from the spallation of target element k at the reference position (0, often the surface) and is given in atoms (g target element)$^{-1}$ yr^{-1}. C_k is the concentration of element k whose units are given in g of k (g material)$^{-1}$. A_f is the particle attenuation length in g cm^{-2} and Z is the mass length of material that the particle passed through in g cm^{-2}, where z = Thickness (cm) (X) Bulk Density (g cm^{-3})

Appendix 3: Sample Processing Procedure

Prior to use, the crushing room was thoroughly cleaned with a shop-vac and broom. The equipment was also cleaned with an air hose and then had its surfaces wiped down with acetone. All samples but 1 were unconsolidated and were already for pulverization by the disk mill. The boulder sample of granitic gneiss had to be reduced into smaller fragments by a jaw crusher before it was a suitable size for the mill. Almost all of the samples, with the exception of the boulder, were pebbly-granule coarse sands and had to be sieved through a > 0.5 cm mesh to isolate the larger clasts. Clasts larger than 1 cm in diameter were removed from the sample and saved in a labeled zip-lock bag. The next step was to mill the samples while trying to obtain as much of the 250-355 μm and 355-500 μm grain size fractions as possible since these grain sizes are easily distinguished with the naked eye and the desirable quartz grains won't be completely dissolved away. In order to ensure that there was minimal sample loss to dust while pulverizing, the sediment was poured into the mill very slowly. Another strategy to reduce the amount of dust was to progressively decrease the spacing between the 2 ceramic plates. The initial spacing between the disks was approximately 2 mm to crush the granule sized clasts and was incrementally decreased until it was < 0.5 mm wide. Meanwhile, the samples were being manually sieved using the >500 μm, 500-355 μm, 355-250 μm sieves. These samples were then placed in separate labeled ziplock bags including everything <250 μm. Samples were then mechanically sieved in the Sedimentary Geology Lab (LSC 2010) of the Earth Sciences Department. All grain sizes of a given sample with the exception of the <250 μm size fraction were placed back in their respective sieves and placed in the box shaker for 20 minutes. This removed grains

stuck in the mesh and any residual dust. Between each sample, the sieves were cleaned using wire brushes and a dental pick to remove any leftover grains. They were then cleaned with acetone.

Each sample was given its own CNEF number and the amount of each grain size fraction was weighed. Approximately 800-1200 g of each sample was measured because the modal mineralogy was 30-40 % quartz. 400 ml of aqua regia solution, a mixture of 3HCl: 1 HNO$_3$ was added to each beaker and heated to 200 °C for 2 hours. Aqua regia is extremely oxidizing, allowing it to dissolve and weaken many of the non-quartz minerals and break up the aggregate grains. The samples were then etched a couple of times using a high ratio of HF. The etching process not only dissolved many of the unwanted mineral grains but it also stripped-off the outer layer from each quartz grain, removing atmospheric and meteoric cosmogenic [10]Be. Magnetic minerals were then removed from several samples using a strong bar magnet. Next, the samples were placed an ultrasonic bath with a ratio of 240 ml HF: 114 ml HNO$_3$: 4000 ml H$_2$O. Each sample was put through several ultrasonic cycles and a smaller HF ratio was added as the samples were reduced in size. This process removed most of the non-quartz minerals from the sample and left behind a quartz concentrate. The next step involved the fragmentation of the remnant aggregate grains and resistant feldspars. Fortunately, only 2 samples required this treatment and were placed in an air abraider that had 4 stainless steel containers capable of each carrying 20 g per cycle. Air under high pressure was forced into the canisters causing the grains to collide both with each other and the walls.

An aluminum test was then conducted on each sample to ensure that they had less than 100 ppm of Al but optimally, less than 50 ppm. In order to do this, 1.0 g of quartz

concentrate was weighed out and dissolved in HF and then redissolved in 0.5 N HCl. A Quant-EM stick Al test strip kit was then used and the Al concentration for each sample was calculated. All samples had Al concentrations <50 ppm meaning that they were ready for the next phase.

Preparation of ^{10}Be oxides from quartz

Approximately 120 g of quartz concentrate was measured from each sample and placed into a 500 ml teflon acid digestion vessel. Roughly 0.5 ml of Be carrier, which is mostly ^{9}Be with a known amount of ^{10}Be, was then added to each sample. The purpose of a carrier was to give the AMS a larger target for analysis so that it can report back the amount of ^{10}Be to ^{9}Be counted. Also, we need to know the ^{9}Be abundance to 4 decimal places, and can only do this by adding a large amount gravimetrically. A sample blank vessel was added at this point that contained only carrier. 120 ml of HF, 12 ml $HClO_4$ and 25 ml of aqua regia was added to each sample and heated to 125 degrees C. Further amounts of HF, HNO_3 and $HClO_3$ and finally aqua regia were added to finally dissolve the samples. The samples then went through a series of dissolutions and evaporations until $BeNO_3$ remained.

Each sample was then redissolved and eventually placed in an anion exchange column that contained microscopic spheres of styrene resin with high ion exchange capacities. The anions in the sample solutions either adsorbed onto or were substituted into the spheres. The column pH is what dictated which anions were collected by the resin. The $BeCl_2$ and $AlCl_3$ passed through the column at a pH of 9 N HCl and were collected as eluant for the next step. A controlled precipitation was then conducted by

adding NH$_4$OH to each sample solution. Hydroxides were precipitated between the pH's of 6.5 and 9.5 and since Be(OH)$_2$ is insoluble at those pH's, it remained in solution. Each sample was then placed in a pH regulated cation column. Unwanted cations were removed from the sample solution and Be and Al eluants were concentrated and collected separately. The final process of converting the Be eluant to BeO involved a series of more dissolutions and evaporations followed by a precipitation using ammonia gas bubbles. Samples were then placed in quartz vials and baked at 120 ^{o}C then at 850°C.

Appendix 4: Chemistry Data

WS4_QtzDissolution

This worksheet outlines the steps for dissolving quartz and adding Be carrier.

JG/GY

Chemist: AH   **Date:** 11/20/03   form:mm/dd/yy

	1	2	3	4	5	6	7	8	examples
CNEF ID	1371	1372	1373	1374	1375	1376	1377	1386	105
Sample ID	Ravn 03-3087-01	Ravn-03-3088-01	Ravn-03-3089-01	Ravn-03-3090-01	Ravn-03-3091-01	Ravn-03-3092-01	Ravn-03-3093-01	Blank	WY-96-001
300 ml vessel ID	A1	A2	A3	A4	A5	A6	A7	A8	AA
Beryl Carrier ID	Bottle 5	Bottle 5	Bottle 5	Bottle 5	Bottle 5	Bottle 5	Bottle 5	Bottle 5	BeI-Carrier
(tare balance after each measurement)									
Mass 300 ml vessel									148.7188 g
Mass 40g quartz	119.9996	119.9895	120.0156	120.0299	119.9915	119.9696	120.0581	0.0000	20.0000 g
Mass Be carrier	0.4441	0.3538	0.3456	0.3462	0.3604	0.3542	0.3528	0.3448	1.0147 g

SAVE AS: C:/Chemistry/CHEM_WK YYMMDD   .xls   **then PRINT**

- $_1$ Add 20 ml conc. HF and 2 ml $HClO_4$ per 5 g of quartz
- $_2$ Add 5 ml Aqua Regia
- $_3$ Heat at 100-125° C until quartz dissolves, add HF if needed
- $_4$ Raise to 200° C and evaporate to dryness
- $_5$ Add 5 ml $HClO_4$ and evaporate to dryness
- $_6$ Add 8 to 10 ml conc. HNO_3, swirl, and evaporate to dryness
- $_7$ Dissolved dried sample in 20 ml of 2% HNO_3.

Comments

Nov-19	250 ml HF	16 ml perc	10 ml A.R.
Nov-20	40 ml HF		
Nov-24	40 ml HF		20 ml nitr
Nov-25			20 ml nitr
Nov-28		20 ml A.R.	
	50 ml HF	8 ml perc	
Dec-01		6 ml perc	
Dec-02			15 ml nitr
		10	

WS5_ICP Aliquot and Al spiking

This worksheet outlines the steps for collecting ICP aliquots and adding Al carrier.

AH

Chemist: | AH |

form: 02/17/01

Date: | 12/04/03 |

- 1 **Label one 10 ml volumetric flasks per sample (8)**

- 2 **Label one ICP vial with CNEF ID per sample (8)**

	1	2	3	4	5	6	7	8	examples
CNEF ID	1371	1372	1373	1374	1375	1376	1377	1386	105
Sample ID	Ravn 03-3087-01	Ravn-03-3088-01	Ravn-03-3089-01	Ravn-03-3090-01	Ravn-03-3091-01	Ravn-03-3092-01	Ravn-03-3093-01	Blank	WY-96-001
Al carrier ID									ALI-carrier
Quant-EM est. Al in qtz									ppm
Volume carrier to add to smpl									ml
Volume carrier to add to vol A									ml
Volume carrier to add to vol. B									ml
				Tare between mass measurements					
Mass100 ml volumetric	68.2938	67.7938	67.3563	66.9334	66.7112	66.4910	67.0055	66.5899	66.9239 g
100ml volumetric+sample+2%HCl	101.0514	100.9602	100.8810	100.9890	100.9499	100.9042	101.0791	100.9406	166.9875 g
Mass 5 ml smpl pipetted to vol A	10.0878	10.0686	10.0948	10.0783	10.0651	10.0929	10.0716	10.0732	5.0000 g
Final Mass of 100 ml vol and smpl	159.2512	158.6804	158.1368	157.8397	157.5477	157.2909	157.9540	157.4068	1.0100 g
Mass Al carrier to remaining (row18)									1.0100 g
Unaccounted mass									0.0100 g

PRINT this form

- 3 Get digestion vessel and cover ready, Do not wipe now.

- 4 Transfer the 90 ml sample back into vessel

- 5 Bring contents of volumetrics A and B to 10 ml

- 6 Transfer contents volumetrics to ICP vials with same number

116

WS6_Anion Column Chemistry

This worksheet outlines the steps for the Anion Column Chemistry

Print this page

- 1   Evaporate 80 ml to dryness at 100-120°C (will take at least 3 hrs)

- 2   Dissolve in 10 ml 9N HCl (let stand for several hours)

- 3   Transfer to 15 ml centrifuge tubes, rinse digestion vessels
  with 9N HCl to bring volume in tube to 10 ml

- 4   Centrifuge at 1500 rpm or higher for minimum of 10 minutes

- 5   Allow any 9 N HCl in columns to drain out; discard

Vessel	B9	B10	B11	B12	B13	B14	B15	B16	
Column ID	**A**	**B**	**C**	**D**	**E**	**F**	**G**	**H**	AnionColumnID
CNEF ID	1371	1372	1373	1374	1375	1376	1377	1386	105
Sample ID	yn 03-3087	yn-03-3088	yn-03-3089	yn-03-3090	yn-03-3091	yn-03-3092	yn-03-3093	Blank	WY-96-001

- 6   With stopcock closed, pipet sample (avoid residue)onto columns.

- 7   Collect sample in same (wiped)120 ml teflon vessel

- 8   Elute with 30 ml 9 N HCl, and collect that, close stopcock

- 9   5 ml 4.5 N HCl, collect Anion Supernate in labeled 100 ml bottle

- 10   100 ml 1 N HCl, collect Anion Supernate

- 11   50 ml deionized water. Discard.

- 12   **CONDITION ANION COLUMN**

  (bottle A1) 50 ml 1N HCl, discard
  (bottle A2) 50 ml 4.5 N HCl, discard
  (bottle A3) 100 ml 9 N HCl, discard, but retain acid approx. 2 mm above resin

Comments

Done be 6:00 pm Dec. 5/03. All vessels on hotplate to evaporate.

WS7_Controlled Precipitate

This worksheet outlines the steps for the controlled precipitation chemistry

AH

Chemist: | AH |

form: MM/DD/YY

Date: | 12/09/03 |

Print this page

- 1 Evaporate "anion" elute to dryness at $125^{\circ}C$
- 2 Dissolve in 10 ml of a 1:1 solution of 0.5N HCl and 2% NH_4Cl
- 3 Transfer to 15 ml centrifuge, centrifuge for 10 minutes
- 4 Decant into clean test tube, heat in water bath at $60^{\circ}C$
- 5 Add drops of 1:1 $NH_4OH:H_2O$ to pH=9.2 (5 drops first then single)
- 6 Centrifuge for 15 minutes
- 7 Check pH of liquid, if less than pH=7, redo step • 5
- 8 Decant, save with Anion Supernate
- 9 Wash with deionized water, vortex, centrifuge, decant
- 10 Wash with deionized water, vortex, centrifuge, decant
- 11 Wash with deionized water, vortex, centrifuge, decant

CNEF ID	1371	1372	1373	1374	1375	1376	1377	1386	#
Sample ID	vn 03-3087	vn-03-3088	vn-03-3089	vn-03-3090	vn-03-3091	vn-03-3092	vn-03-3093	Blank	
Approx. vol. Ptte	1.2	0.6	1.1	1	0.6	1.1	0.9	0.2	

WS8_Cation Column Chemistry

This worksheet outlines the steps for the Cation Column Chemistry

GY/JG

Chemist: | AH |

mm/dd/yy

Date: | 12/10/03 |

Print this page

- 1   Dissolve in 5 ml conc. HCl and evaporate to dryness at 125°C

- 2   Redissolve in 2.5 ml 1N HCl and 2.5 ml 0.5 N HCl

- 3   Transfer to centrifuge tube, rinse with 1 ml 0.5N, and centrifuge

Column ID	1	2	3	4	5	6	7	8	examples
CNEF ID	1371	1372	1373	1374	1375	1376	1377	1386	105
Sample ID	Ravn 03-3087-01	Ravn-03-3088-01	Ravn-03-3089-01	Ravn-03-3090-01	Ravn-03-3091-01	Ravn-03-3092-01	Ravn-03-3093-01	Blank	WY-96-001

- 4   Pipette all of the sample into designated conditioned cation column

- 5   Discard the eluant. Add 220 ml 0.5 N HCL (bottle C6)

- 6   Collect eluant as Cation Supernate, add 200 ml 0.5 N HCl (bottle C7)

- 7   Collect eluant as Be-Sample into vessels.

- 8   Add 30 ml 1N HCl (bottle8)

- 9   Save this as Be-sample as well.

- 10   Add 100 ml 4.5 N HCl, save as Al sample.

- 11

- 12

- 13   **CONDITION CATION COLUMN**

  (bottle C1) 100 ml 9N HCl
  (bottle C2) 50 ml 4.5 N HCl
  (bottle C3) 50 ml 1 N HCl
  (bottle C4) 50 ml water
  (bottle C5) 100 ml 0.5 N HCl

WS9_Be Sample Chemistry

This worksheet outlines the steps to prepare the BeO sample

Chemist: AH

AH

Date: 12/15/03

form: mm/dd/yy

Print this page

- 1 Evaporate Be Sample from column in wiped digestion vessels at $125^{\circ}C$

- 2 Add 2-5 ml 20% perchloric and evaporate at 200oC

- 3 Again, add 2-5 ml 20% perchloric and evaporate at $200^{\circ}C$

- 4 Dissolve sample in 10 ml of 0.5 N HCl (optima grade)

- 5 Transfer to 15 ml centrifuge tube

- 6 Centrifuge and decant into clean centrifuge tube

- 7 Heat centrifuge tubes in water bath at $60^{\circ}C$

- 8 Precipitate $Be(OH)_2$ using Matheson ultimate grade ammonia gas

    Gently bubble NH_3 with clean pipet tip on hose

    for ca.15 bubbles, or ca. 8-12 sec until ptte forms

    Optimum pH=9.2; 1N HCl may be added

- 9 Centrifuge 15 min., decant (save and redo • 8 if pH of liquid is < 8)

- 10 Wash with water, vortex, centrifuge for 10 min, and decant

- 11 Record mass quartz vials, label, and place them in furnace holder

CNEF ID	1371	1372	1373	1374	1375	1376	1377	1386	105
Sample ID	Ravn 03-3087-01	Ravn-03-3088-01	Ravn-03-3089-01	Ravn-03-3090-01	Ravn-03-3091-01	Ravn-03-3092-01	Ravn-03-3093-01	Blank	WY-96-001
Mass Qtz Vial	2.4655	2.4381	2.466	2.428	2.4713	2.5072	2.4333	2.4397	2.1400 g
Mass Vial+Spl	2.468	2.4389	2.4687	2.4311	2.473	2.5104	2.4361	2.4401	2.1410 g
Mass Spl	0.0025	0.0008	0.0027	0.0031	0.0017	0.0032	0.0028	0.0004	1 mg

- 12 Add 1 small drop of water with micropipet, slurry precipitate

- 13 Transfer sample into quartz vial, cover with alumina vial

- 14 Heat in oven at $120^{\circ}C$ for 2-3 hours

- 15 Let cool and scrape sample down from walls of quartz tube

- 18 Place in furnace. Convert to BeO in furnace at $850^{\circ}C$ for minimum 1 hr

- 19 Determine mass of vial + sample

WS10_Al Sample Chemistry

This worksheet outlines the steps to prepare the Al oxide sample

AH
Chemist: AH

form: mm/dd/yy
Date: 12/15/03

Print this page

- $_1$ Evaporate Al Sample from column in wiped teflon vessel at $125^{\circ}C$

- $_2$ Dissolve sample in 10 ml of 0.5 N HCl (optima grade)

- $_3$ Transfer to 15 ml centrifuge tube

- $_4$ Centrifuge and decant into clean centrifuge tube

- $_5$ Heat centrifuge tubes in water bath at $60^{\circ}C$

- $_6$ Precipitate $Al(OH)_3$ using 50% NH_3OH (drops: 25, 5, 5, 3, 2...)

  Optimum pH=6.3; 1N HCl may be added

- $_7$ Centrifuge 15 min., decant (save and redo • $_6$ if pH of liquid is < 8)

- $_8$ Wash with water, vortex, centrifuge for 10 min, and decant

- $_9$ Record mass quartz vials, label, and place them in furnace holder

CNEF ID	1371	1372	1373	1374	1375	1376	1377	1386	105
Sample ID	vn 03-3087	vn-03-3088	vn-03-3089	vn-03-3090	vn-03-3091	vn-03-3092	vn-03-3093	Blank	WY-96-001
Mass Qtz Vial	2.4655	2.4381	2.4660	2.4280	2.4713	2.5072	2.4333	2.4397	2.1400 g
Mass Vial+Spl	2.4680	2.4389	2.4687	2.4311	2.4730	2.5104	2.4361	2.4401	2.1410 g
Mass Spl	0.0025	0.0008	0.0027	0.0031	0.0017	0.0032	0.0028	0.0004	1 mg

- $_{10}$ Add 1 small drop of water with micropipet, slurry precipitate

- $_{11}$ Transfer sample into quartz vial, cover with alumina vial

- $_{12}$ Heat in oven at $120^{\circ}C$ for 2-3 hours

- $_{13}$ Let cool and scrape sample down from walls of quartz tube

- $_{14}$ Convert to Al_2O_3 in furnace at $950^{\circ}C$ for minimum of 1 hr

- $_{15}$ Determine mass of vial + sample

Appendix 5: AMS Data

Standard used for normalization: LLNL 3000
10/9 ratio for standard   3E-12
Carrier background for   2E-14
Boron correction facto   0.00017 ±   0.00005 of total events   0.00005
KNSTD549 has a carrier blank of 4E-14

	DATE	SAMPLE N	CAMS #	runs	r_to_rstd	interror	exterror	Truefrac	10Be/9Be RATIO (CORRECTED FOR E) RATIO	ERROR	10Be/9Be RATIO (SAMPLE BKGD) RATIO	ERROR	10Be/9Be RATIO (CORR. FOR BKGDS) RATIO	ERROR		
GOSSE	36588	JG1371	BE18736	3	0.25392	0.005195	0.006292	0.995468	7.62E-13	1.89E-14	1.04E-14	1.95E-15	7.56E-13	1.9E-14	0.02509	LLNL3000
GOSSE	36588	JG1372	BE18737	2	0.274036	0.00763	0.01193	0.99888	8.22E-13	3.58E-14	1.04E-14	1.95E-15	8.17E-13	3.58E-14	0.043868	LLNL3000
GOSSE	36588	JG1373	BE18738	2	0.232445	0.005663	0.005109	0.996465	6.97E-13	1.7E-14	1.04E-14	1.95E-15	6.91E-13	1.71E-14	0.024731	LLNL3000
GOSSE	36588	JG1374	BE18739	2	0.17385	0.005091	0.005908	0.991495	5.22E-13	1.77E-14	1.04E-14	1.95E-15	5.15E-13	1.78E-14	0.034654	LLNL3000
GOSSE	36588	JG1375	BE18740	2	0.311897	0.007656	0.006619	0.99613	9.36E-13	2.3E-14	1.04E-14	1.95E-15	9.31E-13	2.31E-14	0.024749	LLNL3000
GOSSE	36588	JG1376	BE18741	2	0.296632	0.007135	0.006617	0.996877	8.9E-13	2.14E-14	1.04E-14	1.95E-15	8.85E-13	2.15E-14	0.024278	LLNL3000
GOSSE	36588	JG1377	BE18742	2	0.272184	0.006994	0.004385	0.994722	8.17E-13	2.1E-14	1.04E-14	1.95E-15	8.11E-13	2.11E-14	0.025968	LLNL3000
GOSSE	36588	JG1378	BE18744	3	0.077635	0.002597	0.001774	0.983891	2.33E-13	7.79E-15	1.04E-14	1.95E-15	2.24E-13	8.03E-15	0.035858	LLNL3000

CNEF ID	Sample ID	Densities Sample (g/cm3)	Cover (intgtd) (g/cm3)	Location data latitude (deg)	altitude (km)	Sample Thickness (cm)	sample Depth (cm) to top	Initial Production Rate (atoms/g/yr)	Muonic Contribution (Be fraction)	Site Production Rate (atoms/g/yr) (calc lalprod macro)
1371	Ravn 03-3087-01	1.5	1.5	71.27553	0.23246	3	27	3.95949123	0.022	4.862986337
1372	Ravn 03-3088-01	1.5	1.5	71.26111	0.42469	5	0	5.1	0.022	7.435359098
1373	Ravn 03-3089-01	1.5	1.5	71.34829	0.26862	4	26	3.996786006	0.022	5.07098902
1374	Ravn 03-3090-01	1.5	1.5	71.35674	0.30809	4	30	3.84968197	0.022	5.060048414
1375	Ravn 03-3091-01	1.5	1.5	71.36287	0.31114	5	22	4.149511182	0.022	5.469042779
1376	Ravn 03-3092-01	1.5	1.5	71.3726	0.26914	5	26	3.996786006	0.022	5.073396048
1377	Ravn 03-3093-01	1.5	1.5	71.37156	0.26559	5	30	3.84968197	0.022	4.871129008
1386	Blank									
1378	Ravn 03-3094-01	1.5	1.5	71.2411	0.382	5	29	3.885942444	0.022	5.455047056

CNEF ID	Sample ID	Prod Rate Adjustments (1 = no effect) Thickness	Topo shielding	Topo Sloped	Snow	Final Production Rate (atoms/g/yr)	Qtz mass meas. (g)	Carrier Carrier-ID Be3-Carrier	Concentrat (mg/ml) from icp or 1.xxxx	Density (g/ml)
1371	Ravn 03-3087-01	0.986068	1	1	1	4.79523723	119.9996	Be3-Carrier	1015	1.013
1372	Ravn 03-3088-01	0.976924	1	1	1	7.26378417	119.9895	Be3-Carrier	1015	1.013
1373	Ravn 03-3089-01	0.981482	1	1	1	4.97708543	120.0156	Be3-Carrier	1015	1.013
1374	Ravn 03-3090-01	0.981482	1	1	1	4.96634742	120.0299	Be3-Carrier	1015	1.013
1375	Ravn 03-3091-01	0.976924	1	1	1	5.34284166	119.9915	Be3-Carrier	1015	1.013
1376	Ravn 03-3092-01	0.976924	1	1	1	4.95632469	119.9696	Be3-Carrier	1015	1.013
1377	Ravn 03-3093-01	0.976924	1	1	1	4.75872507	120.0581	Be3-Carrier	1015	1.013
1386	Blank						0	Be3-Carrier	1015	1.013
1378	Ravn 03-3094-01	0.976924	1	1	1	5.3291689	115.7908	Be3-Carrier	1015	1.013

CNEF ID	Sample ID	10Be/9Be Corr. for Bckgrnd & Boron	10Be/9Be Error	10Be concentration 10Be atoms counted	10Be conc. (atom/g qtz)	Calculated Age (yr)	Age (kyr)
1371	Ravn 03-3087-01	7.30796E-13	1.898E-14	21158076.86	176317.895	37081.13399	37.08113399
1372	Ravn 03-3088-01	7.91146E-13	3.584E-14	18247923.1	152079.333	21037.24055	21.03724055
1373	Ravn 03-3089-01	6.66372E-13	1.71E-14	15013766.96	125098.462	25280.04111	25.28004111
1374	Ravn 03-3090-01	4.90586E-13	1.783E-14	11072393.17	92246.9582	18653.51909	18.65351909
1375	Ravn 03-3091-01	9.04728E-13	2.305E-14	21256994.78	177154.172	33410.52427	33.41052427
1376	Ravn 03-3092-01	8.58934E-13	2.149E-14	19833871.57	165324.145	33612.49074	33.61249074
1377	Ravn 03-3093-01	7.85589E-13	2.107E-14	18068551.27	150498.394	31856.04932	31.85604932
1386	Blank						
1378	Ravn 03-3094-01	2.24311E-13	8.03E-15	5122584.496	44239.9957	8317.234171	8.317234171

CNEF ID	Sample ID	Comment	CNEL ID CNEF-ID	Sample ID Field ID	Chem_WK FILE NAME (CNEL)	Lake Elev	Feature	Relative Age	inhert for 6 ka at/g	
1371	Ravn 03-3087-01	topset	1371	Ravn 03-3087-01	CHEM_WK....	232.46	GLD	7	0.025971677	147585.7736
1372	Ravn 03-3088-01	boulder	1372	Ravn 03-3088-01	CHEM_WK....	424.69	KD		0.045301396	
1373	Ravn 03-3089-01	topset	1373	Ravn 03-3089-01	CHEM_WK....	268.62	GLD	5	0.025661342	95276.49734
1374	Ravn 03-3090-01	topset	1374	Ravn 03-3090-01	CHEM_WK....	308.09	KD	2	0.036344283	62489.59415
1375	Ravn 03-3091-01	topset	1375	Ravn 03-3091-01	CHEM_WK....	311.14	KD	2	0.025477279	145140.6612
1376	Ravn 03-3092-01	topset	1376	Ravn 03-3092-01	CHEM_WK....	269.14	GLD	5	0.025019387	135626.6751
1377	Ravn 03-3093-01	topset	1377	Ravn 03-3093-01	CHEM_WK....	265.59	GLD	5	0.02682063	121985.0222
1386	Blank	blank	1386	Blank	CHEM_WK....					
1378	Ravn 03-3094-01	topset	1378	Ravn 03-3094-01	CHEM_WK....	382	LGLD	1	0.035798576	12306.45544

Appendix 6: Elevation Data

Delta #	Longitude	1 Prominent Delta	2 Delta	3 Kame Delta	4 Delta with beach berm or ice-pushed ridge	5 Alluvial Fan /Eroded Delta	6 Strandlines	7 Wave Washed Surface	8 Spillway	9 Kame Terrace
1	77.62407		330.26							
2	77.77986					325.75				
3	77.74034			386.91						
4	77.73005			359.39						
5	77.72824		318.08							
6	77.63107		314.56							
7	77.57771					284.53				
8	77.61683		336.50							
9	77.59834		300.39							
10	77.59772		264.47							
11	77.59311		427.34							
12	77.57904		305.04							
13	77.62239		427.34							
14	77.45636			455.51						
15	77.40455			424.69						
16	77.43007		210.79							
17	77.40443	232.46								
18	77.40721			372.09						
19	77.4113					310.71				
20	77.44895					305.10				
21	77.41179			310.74						
22	77.33677		312.69							
23	77.35736						323.19			
24	77.40473		311.74							
25	77.33347		268.62							
25	77.33347			310						
26	77.39721									524.58
27	77.31451				307.37					
28	77.30524					369.47				
29	77.32063			308.09						

Delta #	Longitude	1 Prominent Delta	2 Delta	3 Kame Delta	4 Delta with beach	5 Alluvial Fan /Eroded Delta	6 Strandlines	7 Wave Washed Surface	8 Spillway	9 Kame Terrace
30	77.25149							395.3146694		
31	77.17963			311.1387596						
32	77.19215			321.1335814						
33	77.15995			269.1365334						
34	77.05747					309.4524935				
35	77.0416	300.1912178								
36	77.06906		424.2795							
37	77.05107		330.3882							
38	77.9877						301.838285			
39	76.96717		265.5892							
40	76.91751					306.0799613				
41	76.92446							307.359336		
42	76.83013				306.6224505					
43	76.77317				309.5847521					
44	76.72035	314.0389235								
45	76.70054					312.3020381				
46	76.69493		318.4391							
47	76.63336	308.1616005								
48	76.32432			306.140738						
49	76.30963			322.0568027						
50	76.22303				322.3503406					
51	76.15796						328.8349353			
52	76.19297		335.8886							
53	76.0399		382							
spillway	76								300	
spillway	76								254	

Latitude	Longitude	Location Site Number	L=left down	(km upstream)	Raw Elevation Wrist Computer	Altimeter	Helicopter	Calibrated at
		0		0	160	169	520	9:36
71.1426	77.62407	1	L	4	331	332	1080	
71.17217	77.77986	2	R	4.5	327	327	1070	
71.18257	77.74034	3	R	7	388	390	1270	
71.18709	77.73005	4	R	7.5	363	368	1180	
71.18351	77.72824	5	R	7.5	321	312	1050	
71.20498	77.63107	6	R	12.5	318	311	1040	
71.19017	77.57771	7	L	13	294	275	925	
71.2326	77.61683	8	R	16.5	341	332	1115	
71.2344	77.59834	9	R	17	305	305	999	
71.22847	77.59772	10	R	16.5	271	269	880	
71.24978	77.59311	11	R	18.5	434	433	1415	
71.25011	77.57904	12	R	18.5	312	310	1020	
71.23964	77.62239	13	R	17.5	423	421	1380	
71.23303	77.45636	14	L	20.5	462	465	1510	
71.26111	77.40455	15	L	24	434	431	1415	
71.2709	77.43007	16	L	23.5	221	219	710	
71.27553	77.40443	17	T	24.5	241	241	780	
71.27553	77.40443	17	T	24.5	233	233	765	
71.28476	77.40721	18	L	25	370	375	1220	
71.28389	77.4113	19	I	25	309	312	1025	
71.30376	77.44895	20	R	27	302	312	995	
71.31345	77.41179	21	L	28	309	315	1020	
71.32222	77.33677	22	L	28.5	310	319	1025	
71.33349	77.35736	23	L	32	321	328	1065	
71.34225	77.40473	24	R	32	311	315	1030	
71.34829	77.33347	25	R	32.5	268	272	890	
		25						
71.37541	77.39721	26	R	33.5	524	530	1725	
71.34642	77.31451	27	L	34.5	308	310	1020	
71.34036	77.30524	28	L	34.5	370	374	1220	
71.35674	77.32063	29	R	35	309	311	1025	
		29						

127

| Location | | TCN possi | Surface features | | | Bedrock | | Data collected | Corrected for atmospheric change | | | Duration |
Site Number			Grainsize	relief	sloping/flat	Washed a	Notes		Wrist	Altimeter	Helicopter	
0	Feature						Calibration	9:36	160	169	158.5366	
1	camp	N	coarse		f		near mouth	9:43	330.5037	331.5037	328.772	0:07
2	delta	N						9:50	326.0074	326.0074	325.2269	0:07
3		M						9:57	386.5111	388.5111	385.7062	0:07
4		N						10:04	361.0147	366.0147	357.7708	0:07
5		N						10:11	318.5184	309.5184	317.6404	0:07
6		N						10:18	315.0221	308.0221	314.0953	0:07
7		N						10:25	290.5258	271.5258	278.538	0:07
8		N						10:32	337.0295	328.0295	335.9685	0:07
9		Y						10:39	300.5332	300.5332	300.1064	0:07
10		Y						10:46	266.0369	264.0369	263.3296	0:07
11		N						10:53	428.5406	427.5406	425.943	0:07
12		N						11:00	306.0442	304.0442	305.0199	0:07
13		N						11:07	416.5479	414.5479	414.2796	0:07
14		N						11:14	455.0516	458.0516	453.4175	0:07
15		Y						11:21	426.5553	423.5553	423.9577	0:07
16		Y						11:28	213.059	211.059	208.5224	0:07
17		Y						11:30	232.9172	232.9172	229.7221	0:02
									0	0	0	
17		Y						12:23	233	233	233.2317	0
18		N						12:28	369.7711	374.7711	371.7223	0:05
19		N						12:33	308.5424	311.5424	312.0424	0:05
20		M						12:38	301.3136	311.3136	302.6673	0:05
21		N						12:43	308.0848	314.0848	310.0605	0:05
22		M						12:48	308.8561	317.8561	311.3561	0:05
23		N						12:53	319.6273	326.6273	323.3225	0:05
24		Y						12:58	309.3986	313.3986	312.423	0:05
25		Y						13:03	266.1698	270.1698	269.5113	0:05
25												
26		N						13:09	521.9411	527.9411	523.8557	0:05
27		Y						13:14	305.7123	307.7123	308.6879	0:05
28		N						13:19	367.4836	371.4836	369.4348	0:05
29		Y						13:25	306.2548	308.2548	309.7548	0:05
29												

Location	change (+)		mean	stdev	coefficient	check			Jul-31					
									John	Andrew	Jamie	Mean	Time	rates of chg
Site Number	ft	m		1 sigma	variation									m/min
0	0													
1	1.6279		330.26	1.38209	0.004185									
2	3.2558		325.75	0.450615	0.001383									
3	4.8837		386.91	1.444251	0.003733									
4	6.5116		359.39	2.293785	0.006382									
5	8.1395		318.08	0.620874	0.001952									
6	9.7674		314.56	0.655367	0.002083									
7	11.3953		284.53	8.476658	0.029792	bad								
8	13.0233		336.50	0.750223	0.002229									
9	14.6512		300.39	0.24643	0.00082									
10	16.2791		264.47	1.404152	0.005309									
11	17.9070		427.34	1.310186	0.003066									
12	19.5349		305.04	1.000099	0.003279									
13	21.1628		415.13	1.239431	0.002986									
14	22.7907		455.51	2.350381	0.00516									
15	24.4186		424.69	1.628357	0.003834									
16	26.0465		210.79	3.20785	0.015218	bad								
17	26.5116		231.85	1.844705	0.007956									
			0.00	0	#DIV/0!	#DIV/0!								
17		0	233.08	0.133776	0.000574									
18		0.23	372.09	2.519997	0.006773									
19		0.46	310.71	1.892969	0.006092									
20		0.69	305.10	5.425121	0.017782	bad								
21		0.92	310.74	3.057743	0.00984									
22		1.14	312.69	4.645787	0.014858	bad								
23		1.37	323.19	3.501813	0.010835	bad								
24		1.60	311.74	2.085615	0.00669									
25		1.83	268.62	2.144724	0.007984				275	270	274	273	11:40	
25									272	270	271	271		
26		2.06	524.58	3.064747	0.005842									
27		2.29	307.37	1.516908	0.004935									
28		2.52	369.47	2.000198	0.005414									
29		2.75	308.09	1.755942	0.005699				316	318	316	317	12:04	-0.047
29									317	309	319	315	12:39	

129

	FINAL		
Location	long	site	elevation
Site Number			
0			
1	77.62407	1	330.2598
2	77.77986	2	325.7472
3	77.74034	3	386.9094
4	77.73005	4	359.3928
5	77.72824	5	318.0794
6	77.63107	6	314.5587
7	77.57771	7	284.5319
8	77.61683	8	336.499
9	77.59834	9	300.3909
10	77.59772	10	264.4678
11	77.59311	11	427.3414
12	77.57904	12	305.0361
13	77.62239	13	415.1252
14	77.45636	14	455.5069
15	77.40455	15	424.6894
16	77.43007	16	210.7907
17	77.40443	17	232.4647
17	77.40443		
18	77.40721	18	372.0882
19	77.4113	19	310.709
20	77.44895	20	305.0982
21	77.41179	21	310.7434
22	77.33677	22	312.6894
23	77.35736	23	323.1924
24	77.40473	24	311.74
25	77.33347	25	268.617
25			
26	77.39721	26	524.5793
27	77.31451	27	307.3709
28	77.30524	28	369.4673
29	77.32063	29	308.0881
29			

Latitude	Longitude	Location Site Number	L=left down	(km upstream)	Raw Elevation Wrist Computer	Altimeter	Helicopter	Calibrated at
71.34546	77.25149	30	L	37.5	396	401	1305	
71.36287	77.17963	31	L	40.5	311	318	1030	
		31						
71.3797	77.19215	32	R	41	321	328	1065	
71.3726	77.15995	33	C	41	270	274	900	
		33						
71.35955	77.05747	34	L	43.5	311	315	1030	
71.37647	77.0416	35	R	46	304	301	1010	
71.38321	77.06906	36	R	46	427	429	1410	
71.37744	77.05107	37	R	46	333	335	1105	
71.37342	77.9877	38	R	47.5	307	305	1010	
71.37156	76.96717	39	R	48	269	270	895	
		39						
71.33872	76.91751	40	L	51.5	310	310	1030	
71.34706	76.92446	41	R	51.5	312	311	1035	
71.32783	76.83013	42	L	55	311	312	1030	
71.32609	76.77317	43	C	57	314	314	1045	
71.32724	76.72035	44	R	58.5	318	321	1055	
71.30848	76.70054	45	L	60	317	319	1050	
71.30753	76.69493	46	L	60	324	325	1070	
71.29742	76.63336	47	L	63	314	314	1040	
71.27486	76.32432	48	L	71	312	313	1035	
71.27486	76.32432	48	L	71	312	314	1035	
71.2798	76.30963	49	L	74	328	332	1085	
71.27497	76.22303	50	L	78	329	331	1090	
71.27389	76.15796	51	R	79.5	336	338	1110	
71.28881	76.19297	52	R	78	355	353	1070	
71.2411	76.0399	53						
		53						
71.27553	77.40443	17	T	24.5	245	242	810	
		0			172	174	575	
71.4666	77.25849	539						
71.25	76	spillway						

Location	Raw Elevation						Surface features			Bedrock
Site Number	Wrist Computer	Altimeter	Helicopter	Calibrated	Feature	TCN possi	Grainsize	relief	sloping/flat	Washed above
30	396	401	1305			N				
31	311	318	1030			Y				
31										
32	321	328	1065			Y				
33	270	274	900			Y				
33										
34	311	315	1030			N				
35	304	301	1010			N				
36	427	429	1410			N				
37	333	335	1105			N				
38	307	305	1010			N				
39	269	270	895			Y				
39										
40	310	310	1030			N				
41	312	311	1035			N				
42	311	312	1030			N				
43	314	314	1045			N				
44	318	321	1055			N				
45	317	319	1050			N				
46	324	325	1070			N				
47	314	314	1040			N				
48	312	313	1035			M				
48	312	314	1035			M				
49	328	332	1085			Y				
50	329	331	1090			N				
51	336	338	1110			N				
52	355	353	1070			Y				
53										
53										
17	245	242	810							
0	172	174	575							
539										
spillway										

Location	Data collected	Corrected for atmospheric change			Duration		change (+)		mean	stdev	coefficient	check
Site Number		Wrist	Altimeter	Helicopter			ft	m		1 sigma	variation	
30	13:30	393.03	398.03	394.89	0:05			2.97	395.31	2.526667	0.006392	
31	13:35	307.80	314.80	310.82	0:05			3.20	311.14	3.510755	0.011284	bad
31												
32	13:40	317.57	324.57	321.26	0:05			3.43	321.13	3.501813	0.010905	bad
33	13:45	266.34	270.34	270.73	0:05			3.66	269.14	2.429902	0.009029	
33												
34	13:50	307.11	311.11	310.14	0:05			3.89	309.45	2.085615	0.00674	
35	13:55	299.88	296.88	303.81	0:05			4.12	300.19	3.473734	0.011572	bad
36	14:00	422.65	424.65	425.53	0:05			4.35	424.28	1.475022	0.003477	
37	14:05	328.42	330.42	332.32	0:05			4.58	330.39	1.94538	0.005888	
38	14:10	302.20	300.20	303.12	0:05			4.80	301.84	1.495847	0.004956	
39	14:14	263.97	264.97	267.83	0:04			5.03	265.59	2.00657	0.007555	
39												
40	14:19	304.74	304.74	308.76	0:05			5.26	306.08	2.323483	0.007591	
41	14:23	306.51	305.51	310.06	0:04			5.49	307.36	2.390441	0.007777	
42	14:28	305.28	306.28	308.31	0:05			5.72	306.62	1.540838	0.005025	
43	14:32	308.05	308.05	312.65	0:04			5.95	309.58	2.654403	0.008574	
44	14:37	311.82	314.82	315.47	0:05			6.18	314.04	1.94566	0.006196	
45	14:41	310.59	312.59	313.72	0:04			6.41	312.30	1.581421	0.005064	
46	14:45	317.37	318.37	319.59	0:04			6.63	318.44	1.111564	0.003491	
47	14:50	307.14	307.14	310.21	0:05			6.86	308.16	1.774296	0.005758	
48	14:54	304.91	305.91	308.46	0:04			7.09	306.42	1.829851	0.005972	
		0.00	0.00	0.00					0.00	0	#DIV/0!	#DIV/0!
48	15:15	304.01	306.01	307.56	0:21			7.99	305.86	1.779165	0.005817	
49	15:20	319.79	323.79	322.59	0:05			8.21	322.06	2.051694	0.006371	
50	15:25	320.58	322.58	323.90	0:05			8.42	322.35	1.670212	0.005181	
51	15:30	327.36	329.36	329.78	0:05			8.64	328.83	1.291148	0.003926	
52	15:35	346.15	344.15	317.37	0:05			8.85	335.89	16.07022	0.047844	bad
53		0.00	0.00	0.00					0.00	0	#DIV/0!	#DIV/0!
53												
		0.00	0.00	0.00					0.00	0	#DIV/0!	#DIV/0!
17	15:53	235.38	232.38	237.33	0:18			9.62	235.03	2.494054	0.010612	bad
0	16:20	172.00	174.00	175.30								
539												
spillway												

	Jul-31									FINAL		
Location	John	Andrew	Jamie	Mean	Time	rates of chg				long	site	elevation
Site Number						m/min						
30										77.25149	30	
31	318	315	319	317	12:50	-0.0545085				77.17963	31	312
31	316			316	13:12							316
32	323	328	324.6951	325	13:17					77.19215	32	333
33	271	272	274.3902	272	13:29	-0.141651				77.15995	33	273
33	267	264	269.8171	267	14:08							261
34										77.05747	34	
35										77.0416	35	
36										77.06906	36	
37										77.05107	37	
38										77.9877	38	
39	265	261	265.2439	264	14:12	0.01587302				76.96717	39	257
39	266	261	265.2439	264	14:33							256
40										76.91751	40	
41										76.92446	41	
42										76.83013	42	
43										76.77317	43	
44										76.72035	44	
45										76.70054	45	
46										76.69493	46	
47										76.63336	47	
48	308			308	16:10					76.32432	48	308
48										76.32432		
49	324	331	326.2195	327	14:47					76.30963	49	338
50										76.22303	50	
51										76.15796	51	
52										76.19297	52	
53	380	379	382.622	381	15:02	0.06080623				76.0399	53	378
53	382			382	15:26							382
17	222	218	221.0366	220								214
0												
539	543	559	545.7317	549						77.25849	539	575
spillway	301	298	301.8293	300						76	spillway	295
	255	250	256.0976	254						76	spillway-lov	245